universität wien

# MASTERARBEIT

Titel der Masterarbeit

## Engineering Spectrally Pure Quantum States with SPDC using Periodically Poled Crystals and Pulsed Laser Sources


verfasst von

Fabian Laudenbach BSc


angestrebter akademischer Grad

Master of Science (MSc)

Wien, 2015

| | |
|---|---|
| Studienkennzahl lt. Studienblatt: | A 066 876 |
| Studienrichtung lt. Studienblatt: | Masterstudium Physik |
| Betreut von: | Assoz. Prof. Dr. Philip Walther |

# Abstract

Pair creation by spontaneous parametric down-conversion (SPDC) has become a reliable source for single photon states, used in many kinds of quantum-related experiments and real-life applications. In order to be spectrally pure, the two photons within a generated pair should be as frequency-uncorrelated as possible. For this purpose most experiments use narrow bandpass filters, having to put up with a drastic decrease in count rates. This thesis discusses (theoretically and by numerical evaluation) how to engineer a setup such that the SPDC-generated quantum states are intrinsically pure. Using pulsed pump lasers and periodically poled crystals this approach makes bandpass filtering obsolete and allows for significantly higher output intensities and therefore count rates in the detectors.

Die Paarerzeugung mittels spontaner parametrischer Downconversion (SPDC) hat sich zu einer verlässlichen Quelle für Single-Photon-Zustände entwickelt, die in zahlreichen Quanten-basierten Experimenten und Anwendungen zum Einsatz kommt. Um spektrale Reinheit zu gewährleisten, sollten die beiden Photonen eines Paares möglichst Frequenz-unkorreliert sein. Zu diesem Zweck setzen die meisten Experimente schmale Bandpassfilter ein, nehmen dafür aber eine drastische Verminderung der Zählraten in Kauf. Die vorliegende Arbeit untersucht (sowohl theoretisch als auch durch numerische Berechnungen) wie ein Aufbau beschaffen sein muss, sodass die durch SPDC erzeugten Quantenzustände an sich rein sind. Unter Verwendung von gepulsten Pumplasern und periodisch gepolten Kristallen macht dieser Zugang den Einsatz von Bandpassfiltern obsolet und ermöglicht dadurch deutlich höhere Output-Intensitäten, also Zählraten in den Detektoren.

# Acknowledgements

There is a long list of people who contributed to this thesis. To begin with, my gratitude goes to my very kind and helpful colleagues at the Austrian Institute of Technology, Department Digital Safety and Security (AIT, DSS). First to mention is certainly my mentor and friend Andreas Poppe who not only supervised my research and this thesis but has been serving as an inexhaustible source of knowledge and advice. Furthermore I owe many thanks to Martin Stierle, Alexander Shurupov, Mike Hentschel, Bernhard Schrenk, Christoph Pacher, Florian Hipp, Ian Glendinning, Momtchil Peev, Agi Karyda and Mario Klima not only for precious scientific advices but also for many intriguing and pleasurable discussions beyond science.

Special thanks need to be addressed to Professor Philip Walther who kindly agreed to sponsor this thesis. Furthermore I want to thank my fellow students at the University of Vienna, Chiara Greganti and Max Tillmann, for fruitful discussions on the physics of down-conversion and phase-matching as well as for their very helpful support related to my numerical calculations.

Particular thanks are owed my dear parents, Erna and Toni, who have always been providing me with the necessary confidence and support which were absolutely required in order to tackle a task as complex and demanding as the studies of physics. Last but not least, I want to express my endless gratitude to my partner Christine whose patience and support over the last years have been making up a crucial contribution to my educational advancement.

This thesis is dedicated to my son and best friend Maximilian. His persistent questions on the nature of our world have been a huge motivation to profoundly understand the intriguing phenomena of natural science.

# Contents

# Introduction

The last decades have brought up a number of intriguing quantum mysteries which accomplished their transition from thought experiments to actual phenomena successfully observed in a lab. Now, at the dawn of the 21st century, we are about to submit these quantum phenomena to a second transition by exporting them from scientific labs to actual real-life applications. The concepts of quantum superposition, uncertainty principle, entanglement, no-cloning theorem and others have opened a wide range of possible applications challenging human creativity and ingenuity. These range from quantum information and computation (teleportation [4], entanglement swapping [22], dense coding [3], Deutsch-Jozsa algorithm [7] etc.) to—certainly most developed in the sense of industrial usability—quantum key distribution (QKD) which underwent a fast development from its theoretical birth [2] to experimental proof [24, 27].

No matter whether the setup relies on quantum entanglement, single-photon heralding or quantum interference—for successful realisation of quantum based experiments and applications the generation of indistinguishable single photons is a crucial task in any quantum lab. Quantum entanglement is undermined by any distinguishing information that the photons carry; at heralding, when a photon pair is spectrally correlated, the detection of one twin will project the other one into a mixed state, making it useless for almost any kind of further quantum processing; also quantum interference is intrinsically related to state purity and indistinguishability of the photons arriving at a beamsplitter.

For generation of single photon states *spontaneous parametric down-conversion* (SPDC) has become the method of choice. A non-linear crystal is impinged by a pump laser whereupon a certain portion of pump photons (usually between $10^{-10}$ to $10^{-6}$) decays into two daughter photons, usually referred to as *signal* and *idler*. The three photons, pump, signal and idler, obey energy conservation

$$\omega_p = \omega_s + \omega_i$$

and can, depending on the type of down-conversion, be polarisation-degenerate or polarised orthogonally to each other. The production of single photons in pairs offers major advantages; firstly it is the most common way to create entangled quanta, secondly it allows for heralding single photons by detection of their respective twins.

In order to allow for a positive energy transfer from pump to daughter fields throughout the crystal, thus to prevent the three waves to interfere destructively, pump, signal and idler have to meet the *phase-matching* condition

$$\mathbf{k}_p = \mathbf{k}_s + \mathbf{k}_i,$$

which in some cases can be achieved by tuning the impinging angle of the pump beam, a technique called *birefringent phase-matching* (BPM). Another method, already proposed in the early nineteen-sixties [1], uses a change of the crystal's non-linearity coefficient in multiples of a certain longitudinal constant $\Lambda$ in order to reset the phase mismatch periodically and permit the output intensity to increase together with the crystal length. This method is referred to as *quasi-phase-matching* (QPM). For any kind of collinear three-wave mixing it is possible to manufacture a non-linear crystal to meet the quasi-phase-match condition

$$k_p = k_s + k_i + \frac{2\pi}{\Lambda} m,$$

where $m$ may be a positive or negative odd integer. Even though both phase-matching techniques, BPM and QPM, will be discussed in detail, this thesis sets the focus on the latter.

The process of SPDC is in principle determined by two functions: the *pump envelope amplitude* $\mu(\omega_p)$ and the *phase-matching amplitude* $\psi(\omega_s, \omega_i)$. While $\mu$ describes the spectrum of the pump laser, $\psi$ determines which wavelength configurations are supported for a given SPDC type, non-linear crystal and temperature. The product of the two is the *joint spectral amplitude*

$$f(\omega_s, \omega_i) = \mu(\omega_s + \omega_i)\psi(\omega_s, \omega_i)$$

which uniquely determines the intensity, frequency spectrum and spectral purity of the output radiation. The quantum amplitude for SPDC can be represented as

$$|\Psi\rangle = \mathcal{N} \int_0^\infty \int_0^\infty f(\omega_s, \omega_i) a_s^\dagger a_i^\dagger \, d\omega_s \, d\omega_i \, |0\rangle \,,$$

where $\mathcal{N}$ is a normalisation constant and $a_{s/i}^\dagger$ are the quantum creation operators of the generated photons. As outlined in this thesis, signal and idler single photon states can be considered pure if the joint spectral amplitude is separable, i.e. if $f(\omega_s, \omega_i) = f_s(\omega_s) f_i(\omega_i)$, thus making the SPDC amplitude separable as well:

$$|\Psi\rangle = \mathcal{N} \int_0^\infty f_s(\omega_s) a_s^\dagger \, d\omega_s \int_0^\infty f_i(\omega_i) a_i^\dagger \, d\omega_i \, |0\rangle \,.$$

In order to achieve a separable SPDC amplitude (or in other words frequency-uncorrelated daughter photons) most experiments make use of narrow bandpass filters in both signal and idler channels but therefore have to tolerate a significant loss of output intensity, i.e. a decrease in single photon count rates. In recent years a new approach has come up which bypasses the need for spectral filtering by engineering *a priori* separable, i.e. intrinsically pure, single photon states. The degree of entanglement can be described by the Schmidt number $K$ whose inverse delivers the spectral purity $\mathcal{P}$ of the output single photon states. While the postulates of quantum mechanics, combined with numerical mathematics, show how to evaluate the degree of purity of down-converted photons [8, 21, 28], first experimental tests yielded promising results [15, 16, 12, 14]. This thesis investigates phase-matching conditions and state purity of all types of down-conversion in all common wavelength regimes and in two kinds of periodically poled crystals, lithium niobate (ppLN) and potassium titanyl phosphate (ppKTP).

This thesis is structured as follows: Chapter 1 introduces fundamental concepts of electromagnetism and optics, required to describe a non-linear process like SPDC; these include birefringence, optical dispersion and the non-linear polarisation vector. In Chapter 2 we derive the amplitude and intensity for SPDC in both a semi-classical and a fully quantum-mechanical way. Chapter 3 presents the basic concept and different techniques of phase-matching in a non-linear crystal. Chapter 4 introduces the quantum-mechanical concepts of entanglement and factorability and their implications on state mixedness and purity. Furthermore it shows how the degree of entanglement and state purity in an SPDC process can be investigated numerically. These methods were used for examination of a large number of SPDC setups, the results of which are presented in Chapter 5.

# Chapter 1

# Electrodynamical and Optical Prerequisites

For later examinations of non-linear processes and phase-matching it will be helpful to establish some basic concepts of linear and non-linear optics. After introducing Maxwell's equations in matter we investigate the wavelength-dependence of the refractive index $n$ (dispersion), determined by the Sellmeier equations. Furthermore we examine how the refractive index depends on the radiation's polarisation and its propagation direction (birefringence). Therefore we derive the angle-dependence of $n$ from Maxwell's equations. The chapter concludes with an introduction of the non-linear polarisation vector which holds responsible for any kind of non-linear process such as spontaneous parametric down-conversion.

## 1.1 Maxwell's Equations in Matter

In vacuum all electrodynamic phenomena can be described by the electric field $\mathbf{E}(\mathbf{r}, t)$ and magnetic field $\mathbf{B}(\mathbf{r}, t)$, which are related to each other by Maxwell's equation for vacuum. However, within matter the material's properties have to be taken into account, hence the definition of two additional fields, $\mathbf{D}$ and $\mathbf{H}$, where

$$\begin{aligned}\mathbf{D} &= \epsilon_0 \mathbf{E} + \mathbf{P} \\ &= \epsilon_0 \mathbf{E} + \epsilon_0 \chi \mathbf{E}\end{aligned} \tag{1.1}$$

is the electric displacement with $\epsilon_0$ being the vacuum permittivity constant, $\mathbf{P}$ the medium's polarisation and $\chi$ the electric susceptibility tensor and

$$\mathbf{H} = \frac{1}{\mu_0}\mathbf{B} - \mathbf{M} \tag{1.2}$$

is the magnetic field strength with $\mu_0$ being the magnetic permeability of free space and $\mathbf{M}$ representing the magnetisation vector of the medium. In this thesis we are dealing exclusively with non-magnetic media, which simplifies the magnetic field strength to

$$\mathbf{H} = \frac{1}{\mu_0}\mathbf{B}. \tag{1.3}$$

The four fields obey *Maxwell's equations in matter*:

$$\nabla \cdot \mathbf{D} = \rho_f, \tag{1.4a}$$

$$\nabla \times \mathbf{E} = -\frac{\partial \mathbf{B}}{\partial t}, \tag{1.4b}$$

$$\nabla \cdot \mathbf{B} = 0, \tag{1.4c}$$

$$\nabla \times \mathbf{H} = \mathbf{j}_f + \frac{\partial \mathbf{D}}{\partial t}, \tag{1.4d}$$

where $\rho_f$ and $\mathbf{j}_f$ are the free charge and current density, respectively.

All these fields can be described in the common way, by a real amplitude and a complex phase, e.g.:

$$\mathbf{E} = \mathbf{E}_0 e^{i(-\omega t + \mathbf{kr})}. \tag{1.5}$$

If we only consider the real part, then the above expression becomes

$$\mathbf{E} = \mathbf{E}_0 \cos(-\omega t + \mathbf{kr}). \tag{1.6}$$

For later use it will be convenient to describe the real electric field by the complex amplitude $\mathbf{A} = \mathbf{E}_0 e^{i\phi}$:

$$\begin{aligned} \mathbf{E} &= \frac{1}{2}\left(\mathbf{A}e^{i(-\omega t+\mathbf{kr})} + \mathbf{A}^* e^{-i(-\omega t+\mathbf{kr})}\right) \\ &= \frac{1}{2}\mathbf{A}e^{i(-\omega t+\mathbf{kr})} + \text{c.c.}, \end{aligned} \tag{1.7}$$

where we added the complex conjugate to ensure the field to remain real-valued.

## 1.2 Dispersion and Birefringence

The index of refraction of an optical medium is one its most crucial properties. It holds responsible for the refraction angle of a ray entering from one medium into another, as well as for a wave's group velocity and wavevector $\mathbf{k} = (2\pi n/\lambda)\hat{\mathbf{k}}$. Usually the refractive index inside a medium depends not only on the radiation's wavelength (dispersion) but also on its polarisation and the direction towards which it is propagating. The dispersion relation of a medium is described by the respective *Sellmeier equations*, which in their most common form look like follows:

$$n(\lambda) = A_0 + \frac{A_1\lambda^2}{\lambda^2 - B_1^2} + \frac{A_2\lambda^2}{\lambda^2 - B_2^2}. \tag{1.8}$$

The Sellmeier coefficients $A$ and $B$ are determined experimentally. Depending on the material that they are describing, the Sellmeier equations can have different representations than the one above, containing more (or less) coefficients and, as the case may be, temperature dependent terms. In non-isotropic optical media the Sellmeier coefficients themselves depend on the radiation's polarisation with respect to the medium's principal axes. In the most general case there is a different equation for $n_x$, $n_y$ and $n_z$ respectively. If a crystal has three different indices ($n_x \neq n_y \neq n_z$), it is referred to as a *biaxial* crystal. When two of the principal axes carry the same index for all $\lambda$ (by convention $n_x = n_y$) then we speak of a *uniaxial* crystal.

Using the definition $\mathbf{D} = \epsilon_0\mathbf{E} + \mathbf{P}$, the linear polarisation $\mathbf{P} = \epsilon_0\chi^{(1)}\mathbf{E}$ and the identity $n^2 = 1 + \chi^{(1)}$ we can write the electric displacement as*

$$\begin{aligned} \mathbf{D} &= \epsilon_0(1 + \chi^{(1)})\mathbf{E} \\ &= \epsilon_0 n^2 \mathbf{E} \end{aligned} \tag{1.9}$$

This relation is only true for isotropic media, where $n_x = n_y = n_z$. Since we have to allow for different indices with respect to the principal axes, we rewrite the above equation in matrix form:

$$\mathbf{D} = \epsilon_0 \begin{pmatrix} n_x^2 & 0 & 0 \\ 0 & n_y^2 & 0 \\ 0 & 0 & n_z^2 \end{pmatrix} \mathbf{E} \tag{1.10}$$

The definition of the permittivity tensor $\epsilon$

*For the following derivations cf. [25], p. 23 ff.

$$\epsilon = \epsilon_0 \begin{pmatrix} n_x^2 & 0 & 0 \\ 0 & n_y^2 & 0 \\ 0 & 0 & n_z^2 \end{pmatrix} \tag{1.11}$$

simplifies the expression for the electric displacement:

$$\mathbf{D} = \epsilon \mathbf{E}. \tag{1.12}$$

Since $\epsilon$ is a diagonal matrix, we can easily find its inverse in order to solve the above equation for $\mathbf{E}$:

$$\mathbf{E} = \frac{1}{\epsilon_0} \begin{pmatrix} n_x^{-2} & 0 & 0 \\ 0 & n_y^{-2} & 0 \\ 0 & 0 & n_z^{-2} \end{pmatrix} \mathbf{D}. \tag{1.13}$$

In component form this equation becomes:

$$E^i = \frac{1}{\epsilon_0 n_i^2} D^i. \tag{1.14}$$

When we take the curl of Maxwell's equation (1.4b) we obtain

$$\begin{aligned} \nabla \times (\nabla \times \mathbf{E}) &= -\frac{\partial}{\partial t} (\nabla \times \mathbf{B}) \\ &= -\frac{\partial}{\partial t} (\nabla \times \mu_0 \mathbf{H}) \\ &= -\mu_0 \frac{\partial^2 \mathbf{D}}{\partial t^2}, \end{aligned} \tag{1.15}$$

where we used (1.3) in the second and (1.4d) in the third line (assuming $\mathbf{j}_0 = 0$ in a dielectric). Straightforward calculation yield that $\nabla \times \mathbf{E} = i\mathbf{k} \times \mathbf{E}$ and that $\nabla \times (i\mathbf{k} \times \mathbf{E}) = i^2 \mathbf{k} \times (\mathbf{k} \times \mathbf{E})$. Moreover $\partial_t \mathbf{D} = -i\omega \mathbf{D}$, so we get

$$\mathbf{k} \times (\mathbf{k} \times \mathbf{E}) = -\omega^2 \mu_0 \mathbf{D}. \tag{1.16}$$

This equation can be simplified when we use the relation $\mathbf{k} = (n\omega/c)\hat{\mathbf{k}}$:

$$\frac{n^2}{c^2} \hat{\mathbf{k}} \times (\hat{\mathbf{k}} \times \mathbf{E}) = -\mu_0 \mathbf{D}. \tag{1.17}$$

Moreover, using the well known vector identity $\mathbf{a} \times (\mathbf{b} \times \mathbf{c}) = (\mathbf{a} \cdot \mathbf{c})\mathbf{b} - (\mathbf{a} \cdot \mathbf{b})\mathbf{c}$ we obtain

$$\frac{n^2}{c^2} \Big( (\hat{\mathbf{k}} \cdot \mathbf{E}) \hat{\mathbf{k}} - \mathbf{E} \Big) = -\mu_0 \mathbf{D}. \tag{1.18}$$

Rewriting this equation in component form yields

$$\frac{n^2}{c^2} \Big( (\hat{\mathbf{k}} \cdot \mathbf{E}) s^i - E^i \Big) = -\mu_0 D^i, \tag{1.19}$$

where $s^i$ are the components of the unit wavevector such that $\hat{\mathbf{k}} = s^x \hat{\mathbf{x}} + s^y \hat{\mathbf{y}} + s^z \hat{\mathbf{z}}$. We rearrange (1.19) and use (1.14) to replace $E^i$:

$$\begin{aligned} D^i &= \frac{n^2}{\mu_0 c^2}\left(E^i - (\hat{\mathbf{k}}\cdot\mathbf{E})s^i\right) \\ &= \frac{n^2}{\mu_0 c^2}\left(\frac{1}{\epsilon_0 n_i^2}D^i - (\hat{\mathbf{k}}\cdot\mathbf{E})s^i\right), \end{aligned} \tag{1.20}$$

where $n$ is the refractive index corresponding to a certain wave $\mathbf{k}$ and doesn't—in general—coincide with $n_i$, the index corresponding to a polarisation along one of the crystal's principal axes. We now solve the above expression for $D^i$ and get

$$\begin{aligned} D^i &= \frac{n^2/(\mu_0 c^2)(\hat{\mathbf{k}}\cdot\mathbf{E})s^i}{n^2/(\mu_0 c^2\epsilon_0 n_i^2) - 1} \\ &= \frac{(\hat{\mathbf{k}}\cdot\mathbf{E})s^i}{1/(\epsilon_0 n_i^2) - \mu_0 c^2/n^2} \\ &= \frac{(\hat{\mathbf{k}}\cdot\mathbf{E})s^i}{\mu_0 c^2(1/n_i^2 - 1/n^2)}, \end{aligned} \tag{1.21}$$

where we used $\mu_0\epsilon_0 c^2 = 1$ in the last line. Writing out all three components of $\mathbf{D}$ we obtain

$$\mathbf{D} = \frac{\hat{\mathbf{k}}\cdot\mathbf{E}}{\mu_0 c^2}\left(\frac{s^x}{1/n_x^2 - 1/n^2}\hat{\mathbf{x}} + \frac{s^y}{1/n_y^2 - 1/n^2}\hat{\mathbf{y}} + \frac{s^z}{1/n_z^2 - 1/n^2}\hat{\mathbf{z}}\right). \tag{1.22}$$

We multiply both sides of the above equation with the unit vector $\hat{\mathbf{k}}$ and use $\mathbf{k}\cdot\mathbf{D} = 0$ to arrive at the expression

$$\frac{(s^x)^2}{1/n_x^2 - 1/n^2} + \frac{(s^y)^2}{1/n_y^2 - 1/n^2} + \frac{(s^z)^2}{1/n_z^2 - 1/n^2} = 0. \tag{1.23}$$

The above equation is called *Fresnel's equation*, and it delivers the refractive index of any plane wave with respective polarisation inside a medium, provided the indices $n_x$, $n_y$ and $n_z$ are known by virtue of the Sellmeier equations. We can obtain a little more insight, when we multiply Fresnel's equation with $(1/n_x^2 - 1/n^2)(1/n_y^2 - 1/n^2)(1/n_z^2 - 1/n^2)$:

$$\left(\frac{1}{n_y^2} - \frac{1}{n^2}\right)\left(\frac{1}{n_z^2} - \frac{1}{n^2}\right)(s^x)^2 + \left(\frac{1}{n_x^2} - \frac{1}{n^2}\right)\left(\frac{1}{n_z^2} - \frac{1}{n^2}\right)(s^y)^2 + \left(\frac{1}{n_x^2} - \frac{1}{n^2}\right)\left(\frac{1}{n_y^2} - \frac{1}{n^2}\right)(s^z)^2 = 0. \tag{1.24}$$

Consider now a plane wave propagating, say, in the $xy$-plane. In this case $k^z = s^z = 0$ and Fresnel's equation simplifies to

$$\left(\frac{1}{n_z^2} - \frac{1}{n^2}\right)\left[\left(\frac{1}{n_y^2} - \frac{1}{n^2}\right)(s^x)^2 + \left(\frac{1}{n_x^2} - \frac{1}{n^2}\right)(s^y)^2\right] = 0. \tag{1.25}$$

An obvious solution to this equation is $n = n_z$. It is important to note that this solution satisfies Fresnel's equation regardless of the wave's orientation within the plane, i.e. for any $s_x$ and $s_y$. A second—non-trivial—solution can be found in

$$\begin{aligned} \left(\frac{1}{n_y^2} - \frac{1}{n^2}\right)(s^x)^2 + \left(\frac{1}{n_x^2} - \frac{1}{n^2}\right)(s^y)^2 &= 0 \\ \frac{(s^x)^2}{n_y^2} + \frac{(s^y)^2}{n_x^2} - \frac{(s^x)^2 + (s^y)^2}{n^2} &= 0 \\ \frac{(s^x)^2}{n_y^2} + \frac{(s^y)^2}{n_x^2} - \frac{1}{n^2} &= 0 \end{aligned} \tag{1.26}$$

In polar coordinates the unit vector components of $\mathbf{k}$ are described as follows:

$$s^x = \cos\varphi, \tag{1.27a}$$
$$s^y = \sin\varphi, \tag{1.27b}$$

where $\varphi$ is here the angle enclosed by $\mathbf{k}$ and the $x$-axis. Reinserting these expressions into (1.26) yields

$$\frac{1}{n^2} = \frac{\cos^2\varphi}{n_y^2} + \frac{\sin^2\varphi}{n_x^2}. \tag{1.28}$$

This equation is only valid in the special case of a plane wave propagating in the $xy$-plane. However, an analogous expression can be obtained for the other two principle planes. So we found that for propagation in any principle plane there are always two refractive indices $n$ which solve the Fresnel's equation: an angle-independent one and an angle-dependent one. The first one is usually referred to as the *ordinary* index $n_o$ whereas the latter—angle-dependent—one is called *extraordinary* index $n_e$. Coherently, a plane wave polarised along the the ordinary (extraordinary) axis is called ordinary (extraordinary) beam, or briefly o-ray (e-ray). Although in Equation (1.28) $n$ is written in terms of the angle with respect to the $x$-axis, it is common to express $n_e$ in terms of the angle with respect to the crystal's *optic axis* (by convention the $z$-axis):

$$\boxed{\frac{1}{n_e^2} = \frac{\cos^2\theta}{n_o^2} + \frac{\sin^2\theta}{n_z^2}.} \tag{1.29}$$

The optic axis is the axis along which o- and e-rays carry the same refractive index: As seen in the above equation, for a wave propagating along the optic axis $z$, i.e. $\theta = 0$, the ordinary and extraordinary index coincide. Since both, $n_o$ and $n_e$, are expressed in terms of the principal indices $n_x$, $n_y$ and $n_z$ which are evaluated by the (wavelength- and temperature-dependent) Sellmeier equations, they are of course still functions of $\lambda$ and $T$:

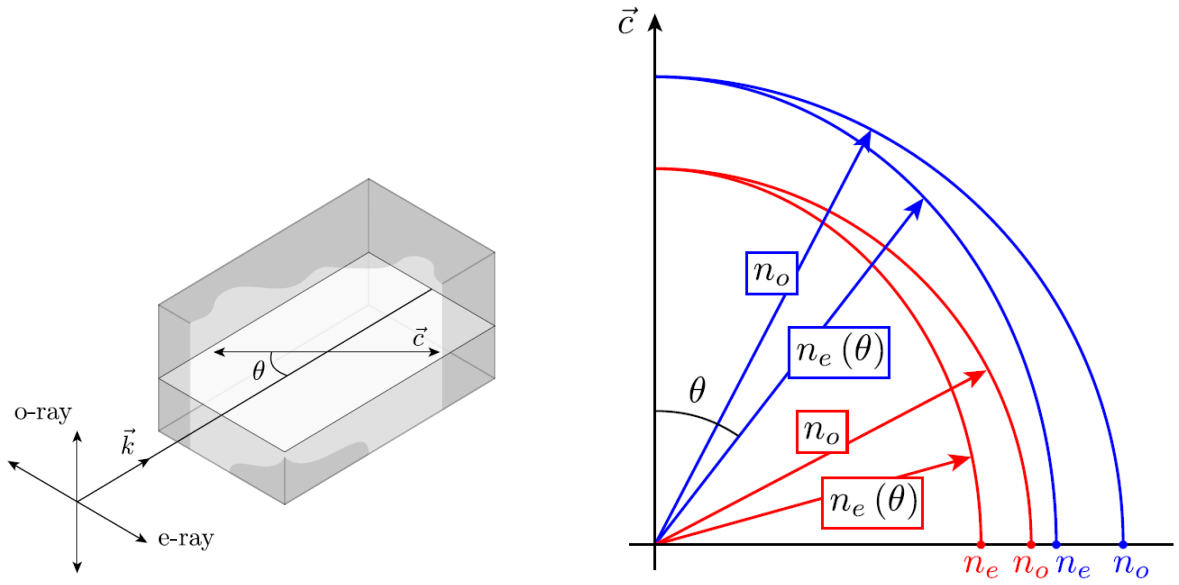


(a) (b)

Figure 1.1: Illustration of birefringence within a non-linear crystal. The light grey plane in Figure (a) is the plane spanned by the wavevector and the optic axis. When $\theta$ is varied the o-ray's polarisation remains orthogonal to the plane whereas the polarisation of the e-ray changes its orientation with respect to the optic axis, thus carrying an angle dependent refraction index, as depicted in Figure (b). Both figures from [20].

$$n_o = n_o(\lambda, T), \tag{1.30a}$$
$$n_e = n_e(\lambda, \theta, T). \tag{1.30b}$$

In order to determine ordinary and extraordinary polarisation we follow a simple procedure: Consider a plane spanned by the **k**-vector and the crystal's optic axis. Polarisation *orthogonal* to this plane will not change its orientation when the orientation of **k** within the plane varies, therefore it is ordinary; on the other hand polarisation *within* the plane will vary its orientation together with **k**, therefore it's angle-dependent and thus extraordinary (Figure 1.1).

Going back to Equation (1.10), we see that within anisotropic media **E** and **D** are in general not parallel. When the field's polarisation coincides with one of the principle axes, then $\mathbf{E} = E^i = \epsilon_0 n_i^2 D^i$ and **D** actually *are* parallel. This is the case for ordinary rays, where the polarisation—and thus the **E**-field—is oriented towards a principle axis, regardless of the direction of **k** within the plane (assuming propagation within one of the principle planes). For extraordinary waves however the direction of the **E**-field varies with the wave's propagation direction within the plane and therefore **E** can in general not be represented by a scalar any more. To summarise: In isotropic media ($n_x = n_y = n_z$) **E** and **D** are always parallel to each other; in birefringent media we distinguish between ordinary rays, where **E** and **D** are parallel, and extraordinary where they are not.

## 1.3 The Non-Linear Polarisation Vector

In its most general form the polarisation vector inside a medium which is excited by a field **E** is

$$\begin{aligned}\mathbf{P} &= \epsilon_0\chi^{(1)}\mathbf{E} + \epsilon_0\chi^{(2)}\mathbf{E}^2 + \epsilon_0\chi^{(3)}\mathbf{E}^3 \dots \\ &= \epsilon_0 \sum_{n=1,2,3,\dots} \chi^{(n)}\mathbf{E}^n,\end{aligned} \tag{1.31}$$

where $\chi^{(n)}$ are the terms of the non-linear electric susceptibility corresponding to the respective power of the electric field. This expression arises when we use the linear expression

$$\mathbf{P} = \epsilon_0\chi\mathbf{E}. \tag{1.32}$$

and expand the susceptibility tensor in powers of **E**:

$$\chi = \chi^{(1)} + \chi^{(2)}\mathbf{E} + \chi^{(3)}\mathbf{E}^2 + \chi^{(4)}\mathbf{E}^3 \dots \tag{1.33}$$

For small fields higher orders of **E** become negligible, therefore $\chi \approx \chi^{(1)}$, and we are left with a linear dependence of polarisation versus electric field:

$$\mathbf{P} = \epsilon_0\chi^{(1)}\mathbf{E}. \tag{1.34}$$

where $\chi^{(1)}$ is a scalar. The above relation is valid in all phenomena of linear optics. For sufficiently big fields however, the higher order terms come into play. The very most of relevant optical phenomena and applications involve susceptibilities up to $\chi^{(3)}$. In this thesis we focus on the non-linear process called *spontaneous parametric down-conversion* (SPDC), which is a $\chi^{(2)}$-process.

## 1.4 Summary

Electromagnetic radiation within a medium is subjected to a certain refractive index which not only depends on the radiation's wavelength and the temperature but—in case of extraordinary polarisation—also on its propagation direction with respect to the crystal's optic axis:

$$n_o = n_o(\lambda, T),$$
$$n_e = n_e(\lambda, \theta, T).$$

The polarisation $\mathbf{P}$ of a medium excited by an electric field depends on the electric field and on the material's susceptibility tensor $\chi$. Materials which carry a susceptibility of order higher than one are referred to as non-linear media. In this thesis we will neglect orders greater than two, so the polarisation vector reads

$$\mathbf{P} = \epsilon_0 \chi^{(1)} \mathbf{E} + \epsilon_0 \chi^{(2)} \mathbf{E}^2.$$

# Chapter 2

# Spontaneous Parametric Down-Conversion

After a brief qualitative description of spontaneous parametric down-conversion (SPDC) we derive the amplitude of this process as well as the intensity of the output radiation quantitatively in both a semi-classical and a quantum-mechanical way. In the semi-classical approach we will use Maxwell's equations to derive the amplitude and intensity of difference frequency generation (DFG) and then slightly adapt the result to the case of SPDC. In our quantum-mechanical derivation we will establish the Hamiltonian for SPDC and obtain the wavefunction by action of the time-evolution operator on a vacuum state. At the end we will compare the results of the two derivations and outline the most important properties of the derived expressions.

## 2.1 Fundamentals

At spontaneous parametric down-conversion a photon decays into two daughter photons by interaction with a non-linear optical medium (Figure 2.1). The frequencies of the three interacting photons have to obey energy conservation:

$$\omega_p = \omega_s + \omega_i, \tag{2.1}$$

where the subscripts $p$, $s$ and $i$ represent the traditional terminology *pump* for the initial photon, and *signal* and *idler* for the two daughter photons. Regarding the polarisation state (ordinary or extraordinary) of the three fields we distinguish three different types of down-conversion: type 0, I and II. In type 0 and type I down-conversion signal and idler are polarisation-degenerate:

$$\text{Type 0}: \; o \longrightarrow o + o, \quad e \longrightarrow e + e, \tag{2.2a}$$

$$\text{Type I}: \; o \longrightarrow e + e, \quad e \longrightarrow o + o, \tag{2.2b}$$

where at type II they are orthogonally polarised:

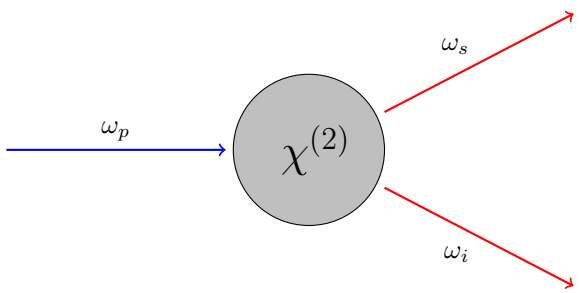


Figure 2.1: Schematic of SPDC. A photon with high energy $\omega_p$ decays into two lower-energetic photons $\omega_s$ and $\omega_i$ by interaction with a non-linear medium.

$$\text{Type II}: \; o \longrightarrow o + e, \quad e \longrightarrow o + e. \tag{2.3}$$

Type II down-conversion is the default method for production of polarisation-entangled photons.

The most common non-linear crystals used in the lab for SPDC are *barium borate* ($BaB_2O_4$, or briefly BBO), *potassium dihydrogen phosphate* ($KH_2PO_4$, KDP), *lithium niobate* ($LiNbO_3$, LN) and *potassium titanyl phosphate* ($KTiOPO_4$, KTP). Some properties of the latter two can be found in Appendix A.

## 2.2 Semi-Classical Description

SPDC is a quantum-mechanical process where there is only one input field present which decays spontaneously into two fields. Therefore it cannot be fully described by the classical arsenal of non-linear optics since a non-linear polarisation requires at least two inputs. This section provides a semi-classical derivation of the SPDC amplitude: First we will describe a slightly different $\chi^{(2)}$-process called *difference frequency generation* (DFG), a process which requires two input fields (say pump and idler). After derivation of the DFG intensity we will approximate the idler intensity by vacuum fluctuations inside the crystal, which shall imitate the required second input field in a quantum-mechanical way (Figure 2.2). A purely quantum-mechanical approach will be provided in the subsequent section.

### 2.2.1 Difference Frequency Generation

In DFG two input fields with frequencies $\omega_1$ and $\omega_2$ interact in a $\chi^{(2)}$-medium to create three photons in the output—two with frequency $\omega_2$ and one with $\omega_3 = \omega_1 - \omega_2$:

$$\hbar\omega_1 + \hbar\omega_2 \longrightarrow \hbar\omega_2 + \hbar\omega_2 + \hbar\omega_3, \tag{2.4}$$

where energy conservation is obviously implied: $\omega_1 = \omega_2 + \omega_3 = \omega_2 + (\omega_1 - \omega_2)$. So by DFG one of the input fields (with frequency $\omega_2$) is amplified, which we will here denote as the idler field. Accordingly we associate $\omega_1$ to the pump field and $\omega_3$ to the signal field. Say we use DFG with pump and idler as input fields in order to create a signal beam on the output, described by the electric field

$$\mathbf{E}(\omega_s) = \frac{1}{2}\mathbf{A}_s e^{i(-\omega_s t + \mathbf{k}_s \mathbf{r})} + \text{c.c.} \tag{2.5}$$

Without loss of generality we set the coordinate system such that the beam propagates along the $z$-axis, so we are able to omit the vectors and rewrite the above expression in terms of scalars:

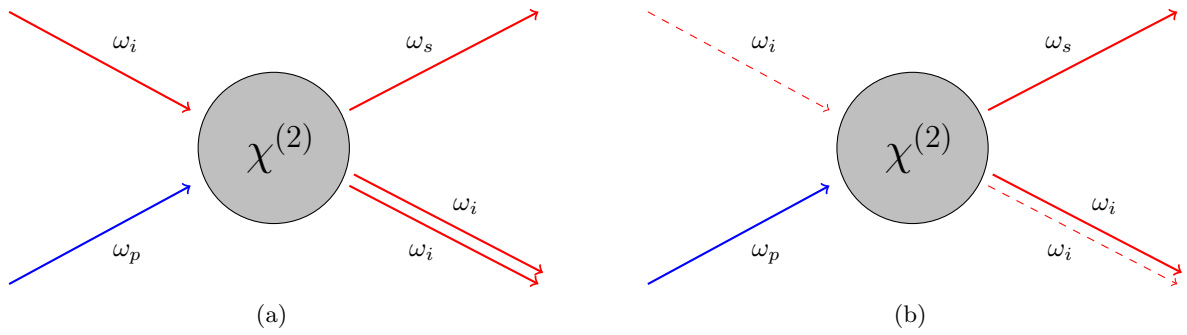


Figure 2.2: Comparison of difference frequency generation and spontaneous parametric down-conversion. At (a) DFG two (sufficiently strong) classical fields mix within a non-linear medium to amplify the lower-energetic input and create an additional field carrying the frequency difference of the input fields: $\omega_s = \omega_p - \omega_i$. After derivation of the DFG amplitude we will approximate the idler input with vacuum fluctuations (b) to obtain the amplitude for SPDC.

$$E(\omega_s) = \frac{1}{2} A_s e^{i(-\omega_s t + k_s z)} + \text{c.c.} \tag{2.6}$$

For DFG we consider a polarisation vector up to second order:

$$\mathbf{P} = \epsilon_0 \chi^{(1)} \mathbf{E} + \epsilon_0 \chi^{(2)} \mathbf{E}^2, \tag{2.7}$$

which is actually a composition of a linear and non-linear polarisation term:

$$\mathbf{P} = \mathbf{P}^{(1)} + \mathbf{P}^{(2)}. \tag{2.8}$$

The linear term can also be written as

$$\mathbf{P}^{(1)} = \frac{1}{2} \epsilon_0 \chi^{(1)} \mathbf{A} e^{i(-\omega t + \mathbf{kr})} + \text{c.c.} \tag{2.9}$$

Specified towards our process of interest, namely a difference frequency generation of a signal beam, the above expression reads

$$\mathbf{P}^{(1)}(\omega_s) = \frac{1}{2} \epsilon_0 \chi^{(1)} \mathbf{A}_s e^{i(-\omega_s t + \mathbf{k}_s \mathbf{r})} + \text{c.c.}, \tag{2.10}$$

or if we consider again propagation along the $z$-axis

$$P^{(1)}(\omega_s) = \frac{1}{2} \epsilon_0 \chi^{(1)} A_s e^{i(-\omega_s t + k_s z)} + \text{c.c.} \tag{2.11}$$

The total non-linear polarisation inside the crystal is

$$\mathbf{P}^{(2)}_{\text{tot}} = \epsilon_0 \chi^{(2)} \mathbf{E}^2_{\text{tot}}, \tag{2.12}$$

where $\mathbf{E}_{\text{tot}}$ is a superposition of all three involved fields:

$$\begin{aligned} \mathbf{E}_{\text{tot}} &= \mathbf{E}(\omega_p) + \mathbf{E}(\omega_s) + \mathbf{E}(\omega_i) \\ &= \frac{1}{2} \left( \mathbf{A}_p e^{i(-\omega_p t + \mathbf{k}_p \mathbf{r})} + \mathbf{A}_s e^{i(-\omega_s t + \mathbf{k}_s \mathbf{r})} + \mathbf{A}_i e^{i(-\omega_i t + \mathbf{k}_i \mathbf{r})} \right) + \text{c.c.} \end{aligned} \tag{2.13}$$

So (2.12) becomes

$$\mathbf{P}^{(2)}_{\text{tot}} = \epsilon_0 \chi^{(2)} \frac{1}{4} \left( \mathbf{A}_p e^{i(-\omega_p t + \mathbf{k}_p \mathbf{r})} + \mathbf{A}_s e^{i(-\omega_s t + \mathbf{k}_s \mathbf{r})} + \mathbf{A}_i e^{i(-\omega_i t + \mathbf{k}_i \mathbf{r})} + \text{c.c.} \right)^2. \tag{2.14}$$

We are interested in the non-linear polarisation of the signal field $\mathbf{P}^{(2)}(\omega_s)$. Squaring out the above equation we find the only terms corresponding to the frequency $\omega_s$ to be

$$\begin{aligned} &\mathbf{A}_p \mathbf{A}_i^* e^{i(-[\omega_p - \omega_i]t + [\mathbf{k}_p - \mathbf{k}_i]\mathbf{r})} + \mathbf{A}_p^* \mathbf{A}_i e^{-i(-[\omega_p - \omega_i]t + [\mathbf{k}_p - \mathbf{k}_i]\mathbf{r})} \\ =&\mathbf{A}_p \mathbf{A}_i^* e^{i(-\omega_s t + [\mathbf{k}_p - \mathbf{k}_i]\mathbf{r})} + \mathbf{A}_p^* \mathbf{A}_i e^{-i(-\omega_s t + [\mathbf{k}_p - \mathbf{k}_i]\mathbf{r})} \end{aligned} \tag{2.15}$$

Therefore, extracting $\mathbf{P}^{(2)}(\omega_s)$ out of $\mathbf{P}^{(2)}_{\text{tot}}$, we obtain

$$\mathbf{P}^{(2)}(\omega_s) = \frac{1}{4} \epsilon_0 \chi^{(2)} \mathbf{A}_p \mathbf{A}_i^* e^{i(-\omega_s t + [\mathbf{k}_p - \mathbf{k}_i]\mathbf{r})} + \text{c.c.} \tag{2.16}$$

This can be rewritten in terms of the *effective non-linear coefficient* $d_{\text{eff}}$ which is a scalar component of the susceptibility tensor depending on the crystal's properties and the angle of the field's polarisation with respect to the crystal. Replacement of $\chi^{(2)}/4$ with $d_{\text{eff}}$ yields

$$\mathbf{P}^{(2)}(\omega_s) = \epsilon_0 d_{\text{eff}} \mathbf{A}_p \mathbf{A}_i^* e^{i(-\omega_p t + [\mathbf{k}_p - \mathbf{k}_i]\mathbf{r})} + \text{c.c.} \tag{2.17}$$

If we assume the collinear case, where pump, signal and idler are propagating in the same (by convention in $z$-) direction we can again omit the vectors and obtain the scalar equation:

$$P^{(2)}(\omega_s) = \epsilon_0 d_{\text{eff}} A_p A_i^* e^{i(-\omega_p t + [k_p - k_i]z)} + \text{c.c.} \tag{2.18}$$

So the total signal polarisation is

$$P(\omega_s) = \frac{1}{2}\epsilon_0 \chi^{(1)} A_s e^{i(-\omega_s t + k_s z)} + \epsilon_0 d_{\text{eff}} A_p A_i^* e^{i(-\omega_s t + [k_p - k_i]z)} + \text{c.c.} \tag{2.19}$$

Like in Section 1.2 we take the curl of Maxwell's equation (1.4b):*

$$\nabla \times (\nabla \times \mathbf{E}) = -\mu_0 \frac{\partial^2 \mathbf{D}}{\partial t^2}, \tag{2.20}$$

and use a well known property of the rotation operator to write

$$\nabla(\nabla \cdot \mathbf{E}) - \nabla^2 \mathbf{E} = -\mu_0 \frac{\partial^2 \mathbf{D}}{\partial t^2}, \tag{2.21}$$

Since we are only considering non-conductive material, we can be sure that our optical medium doesn't carry free charges $\rho_f$, so by Maxwell's equation (1.4a) we see that $\nabla \cdot \mathbf{D} = 0$. Considering isotropic media and o-rays in birefringent materials, where $\mathbf{E}$ is by Equation (1.9) just a scalar multiple of $\mathbf{D}$, the $\mathbf{E}$-field is as well divergence free: $\nabla \cdot \mathbf{E} = 0$. In the following derivations we will assume weak birefringence, such that $\mathbf{E}$ and $\mathbf{D}$ are to a good approximation parallel and therefore $\nabla \cdot \mathbf{E} \approx 0$ even for e-rays. After these considerations what we are left with is

$$\nabla^2 \mathbf{E} = \mu_0 \frac{\partial^2 \mathbf{D}}{\partial t^2}. \tag{2.22}$$

When we replace $\mathbf{D}$ by its definition (1.1) we obtain

$$\nabla^2 \mathbf{E} = \mu_0 \epsilon_0 \frac{\partial^2 \mathbf{E}}{\partial t^2} + \mu_0 \frac{\partial^2 \mathbf{P}}{\partial t^2}, \tag{2.23}$$

or, since our process is assumed to be one-dimensional,

$$\frac{\partial^2}{\partial z^2} E = \mu_0 \epsilon_0 \frac{\partial^2 E}{\partial t^2} + \mu_0 \frac{\partial^2 P}{\partial t^2}. \tag{2.24}$$

Inserting Equation (2.6) the left hand side becomes

$$\frac{\partial^2}{\partial z^2} E(\omega_s) = \frac{1}{2}\left(-k_s^2 A_s + 2ik_s \frac{\partial A_s}{\partial z} + \frac{\partial^2 A_s}{\partial z^2}\right) e^{i(-\omega_s t + k_s z)}. \tag{2.25}$$

We use the *slowly varying envelope approximation* and assume a small change of $\mathbf{A}$ with respect to propagation in $\mathbf{k}$-direction. This implies that higher order derivatives can be neglected since $|\partial_z^2 A| \ll |k \partial_z A|$. So we are left with the simplified expression

*For the following derivations cf. [25], p. 86 ff.

$$\frac{\partial^2}{\partial z^2}E(\omega_s) = \frac{1}{2}\left(-k_s^2 A_s + 2ik_s\frac{\partial A_s}{\partial z}\right)e^{i(-\omega_s t + k_s z)}. \tag{2.26}$$

Using (2.6) and (2.19) the derivatives on the right hand side of (2.24) are

$$\frac{\partial^2}{\partial t^2}E(\omega_s) = -\omega_s^2\frac{1}{2}A_s e^{i(-\omega_s t + k_s z)}, \tag{2.27a}$$
$$\frac{\partial^2}{\partial t^2}P(\omega_s) = -\omega_s^2\left(\frac{1}{2}\epsilon_0\chi^{(1)}A_s e^{i(-\omega_s t + k_s z)} + \epsilon_0 d_{\text{eff}}A_p A_i^* e^{i(-\omega_s t + [k_p - k_i]z)}\right). \tag{2.27b}$$

Putting all these derivatives together in (2.24) we obtain

$$in_p\frac{\partial A_s}{\partial z}e^{ik_s z} = -\frac{\omega_s}{c}d_{\text{eff}}A_p A_i^* e^{i[k_p - k_i]z}, \tag{2.28}$$

where we used $\mu_0\epsilon_0 = 1/c^2$ as well as $1 + \chi^{(1)} = n^2$ and $k = \omega n/c$. For further simplification we introduce the *phase mismatch vector*

$$\Delta k = k_p - k_s - k_i. \tag{2.29}$$

So we obtain

$$\frac{\partial A_s}{\partial z} = i\frac{\omega_s}{n_s c}d_{\text{eff}}A_p A_i^* e^{i\Delta k z}. \tag{2.30}$$

This is an ordinary differential equation which can be integrated over:

$$A_s = i\frac{\omega_s}{n_s c}d_{\text{eff}}A_p A_i^*\int_0^L e^{i\Delta k z}dz. \tag{2.31}$$

Evaluating the integral yields

$$\begin{aligned}\int_0^L e^{i\Delta k z}dz &= \frac{1}{\Delta k}\frac{e^{i\Delta k L} - 1}{i}\\ &= \frac{1}{\Delta k}e^{i\Delta k L/2}\frac{e^{i\Delta k L/2} - e^{-i\Delta k L/2}}{i}\\ &= \frac{2}{\Delta k}e^{i\Delta k L/2}\sin\left(\frac{\Delta k L}{2}\right).\end{aligned} \tag{2.32}$$

Therefore

$$A_s = i\frac{2\omega_s}{\Delta k n_s c}d_{\text{eff}}A_p A_i^* e^{i\Delta k L/2}\sin\left(\frac{\Delta k L}{2}\right). \tag{2.33}$$

This expression can be simplified when we rearrange it as follows:

$$A_s = i\frac{\omega_s}{n_s c}L d_{\text{eff}}A_p A_i^* e^{i\Delta k L/2}\frac{\sin(\Delta k L/2)}{\Delta k L/2} \tag{2.34}$$

and express it in terms of the sinc function*, yielding the final expression:

*$\text{sinc}(x) = \sin(x)/x$ and $\text{sinc}(0) = 1$.

$$\boxed{A_s = i\frac{\omega_s}{n_s c} L d_{\text{eff}} A_p A_i^* e^{i\Delta k L/2} \operatorname{sinc}\left(\frac{\Delta k L}{2}\right).} \tag{2.35}$$

As we seek for high DFG efficiency we are interested in the intensity of the generated signal and idler fields. Using the relation

$$I = \frac{n}{2\mu_0 c}|A|^2 \tag{2.36}$$

we obtain the intensity of the signal field:

$$\begin{aligned} I_s &= \frac{n}{2\mu_0 c}\left(\frac{\omega_s}{n_s c} L d_{\text{eff}} |A_p||A_i|\right)^2 \operatorname{sinc}^2\left(\frac{\Delta k L}{2}\right) \\ &= \frac{\omega_s^2}{2\mu_0 n_s c^3} L^2 d_{\text{eff}}^2 |A_p|^2 |A_i|^2 \operatorname{sinc}^2\left(\frac{\Delta k L}{2}\right). \end{aligned} \tag{2.37}$$

To express the amplitudes in term of intensity, $|A|^2 = 2\mu_0 c I/n$, offers a little more insight:

$$I_s = \frac{\omega_s^2}{2\mu_0 n_s c^3} L^2 d_{\text{eff}}^2 \frac{4\mu_0^2 c^2 I_p I_i}{n_p n_i} \operatorname{sinc}^2\left(\frac{\Delta k L}{2}\right), \tag{2.38}$$

which can be simplified to

$$\boxed{I_s = \frac{2\mu_0 \omega_s^2}{n_p n_s n_i c} L^2 d_{\text{eff}}^2 I_p I_i \operatorname{sinc}^2\left(\frac{\Delta k L}{2}\right).} \tag{2.39}$$

Little surprising, the intensity of the produced radiation depends linearly on the intensities of the two input fields, pump and idler. The more significant observation however is the intensity's dependence on the wavevector mismatch $\Delta k$ which will be discussed at the end of this chapter.

### 2.2.2 Spontaneous Parametric Down-Conversion

In contrast to the above derivation of DFG, the process of SPDC cannot be described purely classically, since it doesn't proceed through mixing of two input fields but rather by spontaneous decay of only one input field. However, using a semi-classical approach we can recycle the description of DFG for our purposes. In order to do so we assume the presence of the a second auxiliary input field, additionally to the pump field. We denote this second input as idler radiation, whose origin are vacuum fluctuations and therefore purely quantum-mechanical. In order to describe the idler field quantum-mechanically we need to replace the classical description of the electric field by the quantum-mechanical field operator $\mathbf{E}(\mathbf{r}, t)$, given by [19]*

$$\begin{aligned} \mathbf{E} &= i\int_0^\infty \sqrt{\frac{\hbar\omega}{2\epsilon_0 n V_Q}} \left(a_{(\mathbf{k},\alpha)} e^{i(-\omega_\mathbf{k} t + \mathbf{kr})} - a_{(\mathbf{k},\alpha)}^\dagger e^{-i(-\omega_\mathbf{k} t + \mathbf{kr})}\right) d\omega \\ &= i\int_0^\infty \mathcal{E}\left(a_{(\mathbf{k},\alpha)} e^{i(-\omega_\mathbf{k} t + \mathbf{kr})} - a_{(\mathbf{k},\alpha)}^\dagger e^{-i(-\omega_\mathbf{k} t + \mathbf{kr})}\right) d\omega, \end{aligned} \tag{2.40}$$

where $\mathcal{E} = (\hbar\omega/(2\epsilon_0 n V_Q))^{1/2}$, $V_Q$ is the quantised volume and $a_{(\mathbf{k},\alpha)}^\dagger$ and $a_{(\mathbf{k},\alpha)}$ are the well known ladder operators which create and annihilate a photon with momentum $\mathbf{k}$ and polarisation $\alpha$ respectively. Also note

*For the sake of concise notation, and in order to avoid confusion with unit vectors (e.g. $\hat{\mathbf{k}}$), we abstain from a distinguished notation for quantum-mechanical operators. In this section as well as in the following ones the electric field $\mathbf{E}$ as well as the ladder operators $a^\dagger$ and $a$ and the Hamiltonian $\mathbf{H}$ are—if not denoted specifically as classical—all understood as operators and not as scalar or vector objects.

that the refractive index $n$ and the wavevector $\mathbf{k}$ are of course functions of the frequency $\omega$. For a monochromatic plane wave the integration over $\omega$ can be omitted:

$$\mathbf{E}(\omega) = i\mathcal{E}\left(a_{(\mathbf{k},\alpha)}e^{i(-\omega_\mathbf{k}t+\mathbf{kr})} - a^\dagger_{(\mathbf{k},\alpha)}e^{-i(-\omega_\mathbf{k}t+\mathbf{kr})}\right), \tag{2.41}$$

Comparison of the above electric field operator with the classical expression for the electric field

$$\mathbf{E}(\omega) = \frac{1}{2}\left(\mathbf{A}e^{i(-\omega t+\mathbf{kr})} + \mathbf{A}^* e^{-i(-\omega t+\mathbf{kr})}\right) \tag{2.42}$$

shows that the idler amplitude $\mathbf{A}_i^*$ can be quantised as follows:

$$\begin{aligned}\mathbf{A}_i^* \longrightarrow& -2i\mathcal{E}_i a^\dagger_{(\mathbf{k},\alpha)_i}|0\rangle \\ =& -2i\mathcal{E}_i\,|(\mathbf{k},\alpha)_i\rangle\,,\end{aligned} \tag{2.43}$$

where $|0\rangle$ describes the vacuum state and $|(\mathbf{k},\alpha)_i\rangle$ a single photon (idler) state with wavevector $\mathbf{k}$ and polarisation $\alpha$. In case of propagation along the $z$ axis the amplitude simplifies to

$$\begin{aligned}A_i^* \longrightarrow& -2i\mathcal{E}_i a^\dagger_{(k^z,\alpha)_i}|0\rangle \\ =& -2i\mathcal{E}_i\,|(k^z,\alpha)_i\rangle\,.\end{aligned} \tag{2.44}$$

We obtain the intensity of the idler vacuum fluctuation by Equation (2.36)*:

$$\begin{aligned}I_{i,\mathrm{vac}} &= \frac{n_i}{2\mu_0 c}|-2i\mathcal{E}|^2\,\langle(k^z,\alpha)_i|(k^z,\alpha)_i\rangle \\ &= \frac{2n_i}{\mu_0 c}\mathcal{E}^2,\end{aligned} \tag{2.45}$$

or if we write out the factor $\mathcal{E}_i$

$$\begin{aligned}I_{i,\mathrm{vac}} &= \frac{2n_i}{\mu_0 c}\frac{\hbar\omega_i}{2\epsilon_0 n_i V_Q} \\ &= \frac{\hbar\omega_i c}{V_Q},\end{aligned} \tag{2.46}$$

where we used again $1/(\mu_0\epsilon_0) = c^2$. Inserting the input intensity of idler radiation into (2.39) we obtain the semi-classically (SC) derived intensity of signal radiation generated by parametric down-conversion:

$$\begin{aligned}I_{s,\mathrm{SC}} &= \frac{2\mu_0\omega_s^2}{n_p n_s n_i c}L^2 d_{\mathrm{eff}}^2 I_p I_{i,\mathrm{vac}}\,\mathrm{sinc}^2\left(\frac{\Delta kL}{2}\right) \\ &= \frac{2\mu_0\omega_s^2}{n_p n_s n_i c}L^2 d_{\mathrm{eff}}^2 I_p \frac{\hbar\omega_i c}{V_Q}\,\mathrm{sinc}^2\left(\frac{\Delta kL}{2}\right),\end{aligned} \tag{2.47}$$

which leads to the final expression

$$\boxed{I_{s,\mathrm{SC}} = \frac{2\mu_0\hbar\omega_s^2\omega_i}{n_p n_s n_i V_Q}L^2 d_{\mathrm{eff}}^2 I_p\,\mathrm{sinc}^2\left(\frac{\Delta kL}{2}\right).} \tag{2.48}$$

In the following section we will compare this result with a fully quantum-mechanical derivation of the signal amplitude.

*Note that $I_{i,\mathrm{vac}}$ only describes the intensity of the vacuum fluctuations that we approximate as input to stimulate PDC and should therefore not be confused with the idler *output* intensity $I_i$ that we observe with our detectors.

## 2.3 Quantum-Mechanical Description

As seen in the previous section, the quantum-mechanical electric field operator is described by*

$$\begin{aligned}\mathbf{E} &= i\int_0^\infty \sqrt{\frac{\hbar\omega}{2\epsilon_0 n V_Q}}\left(a_{(\mathbf{k},\alpha)}e^{i(-\omega_\mathbf{k}t+\mathbf{kr})} - a^\dagger_{(\mathbf{k},\alpha)}e^{-i(-\omega_\mathbf{k}t+\mathbf{kr})}\right)\,d\omega \\ &= i\int_0^\infty \mathcal{E}\left(a_{(\mathbf{k},\alpha)}e^{i(-\omega_\mathbf{k}t+\mathbf{kr})} - a^\dagger_{(\mathbf{k},\alpha)}e^{-i(-\omega_\mathbf{k}t+\mathbf{kr})}\right)\,d\omega. \end{aligned} \tag{2.49}$$

In order to simplify notation we rewrite this expression in terms of a positive and negative frequency part:

$$\mathbf{E} = \mathbf{E}^+ + \mathbf{E}^-, \tag{2.50}$$

where

$$\mathbf{E}^+ = i\int_0^\infty \mathcal{E}a_{(\mathbf{k},\alpha)}e^{i(-\omega_\mathbf{k}t+\mathbf{kr})}\,d\omega, \tag{2.51a}$$

$$\mathbf{E}^- = -i\int_0^\infty \mathcal{E}a^\dagger_{(\mathbf{k},\alpha)}e^{-i(-\omega_\mathbf{k}t+\mathbf{kr})}\,d\omega. \tag{2.51b}$$

The Hamiltonian for SPDC, a second order non-linear process, where a pump photon gets annihilated whereas a signal and an idler photon get created, is described by

$$\mathbf{H} = \epsilon_0\chi^{(2)}\int_V \mathbf{E}_p^+\mathbf{E}_s^-\mathbf{E}_i^-\,d^3\mathbf{r} + \text{H.c.} \tag{2.52}$$

We consider now a pump source with certain spectral *pump envelope amplitude*, in most cases approximated by a Gaussian frequency spectrum

$$\mu(\omega_p) = \exp\left(\frac{-(\omega_p-\omega_{p,0})^2}{2(\Delta\omega_p)^2}\right), \tag{2.53}$$

where $\omega_{p,0}$ is the centre frequency and $\Delta\omega_p$ is the width of the spectrum. The presence of a certain spectral width of the pump source allows for infinitely many frequency combinations, only restricted by energy conservation $\omega_p = \omega_s + \omega_i$ and weighted by the pump amplitude (2.53). The pump field, typically a high power laser beam, can be assumed strong enough to be treated classically. So we replace the quantum-mechanical operator $\mathbf{E}_p^+$ by the *classical field*

$$\mathbf{E}_p^+ = A_p\int_0^\infty \mu(\omega_p)e^{i(-\omega_p t+\mathbf{k}_p\mathbf{r})}\,d\omega_p. \tag{2.54}$$

Insertion of $\mathbf{E}_p^+$, $\mathbf{E}_s^-$ and $\mathbf{E}_i^-$ in the Hamiltonian (2.52) then yields

$$\begin{aligned}\mathbf{H} = \epsilon_0\chi^{(2)}A_p\int_V\int_0^\infty\int_0^\infty\int_0^\infty &\mathcal{E}_s\mathcal{E}_i\mu(\omega_p) \\ &\times e^{i(-\omega_p t+\mathbf{k}_p\mathbf{r})}e^{-i(-\omega_i t+\mathbf{k}_i\mathbf{r})}e^{-i(-\omega_s t+\mathbf{k}_s\mathbf{r})}a_s^\dagger a_i^\dagger\,d\omega_p\,d\omega_s\,d\omega_i\,d^3\mathbf{r} + \text{H.c.},\end{aligned} \tag{2.55}$$

where $a_s^\dagger = a^\dagger_{(\mathbf{k},\alpha)_s}$ and analogous for $a_i^\dagger$. We assume a sufficiently narrow spectrum of the pump field, such that the coefficients $\mathcal{E}_s$ and $\mathcal{E}_i$ only vary slowly in the range of $\mu(\omega_p)$ and can therefore in good approximation be taken out of the integral. This and the definitions of $\Delta\mathbf{k} = \mathbf{k}_p - \mathbf{k}_s - \mathbf{k}_i$ and $\Delta\omega = \omega_p - \omega_s - \omega_i$ simplify the expression to

*For the following derivations cf. [20], p. 40 ff.

$$\begin{aligned}\mathbf{H} &= \epsilon_0\chi^{(2)}A_p\mathcal{E}_s\mathcal{E}_i\int_V\int_0^\infty\int_0^\infty\int_0^\infty \mu(\omega_p)e^{-i\Delta\omega t}e^{i\Delta\mathbf{kr}}a_s^\dagger a_i^\dagger\, d\omega_p\, d\omega_s\, d\omega_i\, d^3\mathbf{r} + \text{H.c.}\\ &= \mathcal{C}\int_V\int_0^\infty\int_0^\infty\int_0^\infty \mu(\omega_p)e^{-i\Delta\omega t}e^{i\Delta\mathbf{kr}}a_s^\dagger a_i^\dagger\, d\omega_p\, d\omega_s\, d\omega_i\, d^3\mathbf{r} + \text{H.c.},\end{aligned} \tag{2.56}$$

with $\mathcal{C} = \epsilon_0\chi^{(2)}A_p\mathcal{E}_s\mathcal{E}_i$. Having the proper Hamiltonian we can obtain the amplitude for SPDC by

$$|\Psi\rangle = e^{-i/\hbar\int_{-\infty}^{\infty}\mathbf{H}\,dt}\,|0\rangle\,, \tag{2.57}$$

which is in first order expansion

$$\begin{aligned}|\Psi\rangle &= \left(1 - \frac{i}{\hbar}\int_{-\infty}^{\infty}\mathbf{H}\,dt\right)|0\rangle\\ &= |0\rangle - \frac{i}{\hbar}\mathcal{C}\int_{-\infty}^{\infty}\int_V\int_0^\infty\int_0^\infty\int_0^\infty \mu(\omega_p)e^{-i\Delta\omega t}e^{i\Delta\mathbf{kr}}a_s^\dagger a_i^\dagger\, d\omega_p\, d\omega_s\, d\omega_i\, d^3\mathbf{r}\, dt,\end{aligned} \tag{2.58}$$

Note that the hermitian conjugate term of the Hamiltonian vanished by action of annihilation operators on the vacuum: $a\,|0\rangle = 0$. The time integral over $\exp(-i\Delta\omega t)$ yields a delta function:

$$\int_{-\infty}^{\infty} e^{-i\Delta\omega t}\,dt = \delta(\Delta\omega), \tag{2.59}$$

implying—little surprising—conservation of energy:

$$\omega_p = \omega_s + \omega_i, \tag{2.60}$$

which makes the integration over $d\omega_p$ a trivial task. So the amplitude reads

$$\begin{aligned}|\Psi\rangle &= |0\rangle - \frac{i}{\hbar}\mathcal{C}\int_V\int_0^\infty\int_0^\infty \mu(\omega_s+\omega_i)e^{i\Delta\mathbf{kr}}a_s^\dagger a_i^\dagger\, d\omega_s\, d\omega_i\, d^3\mathbf{r}\,|0\rangle\\ &= |0\rangle - \frac{i}{\hbar}\mathcal{C}\int_V\int_0^\infty\int_0^\infty \mu(\omega_s+\omega_i)e^{i\mathbf{k}_p\mathbf{r}}e^{-i\mathbf{k}_s\mathbf{r}}e^{-i\mathbf{k}_i\mathbf{r}}a_s^\dagger a_i^\dagger\, d\omega_s\, d\omega_i\, d^3\mathbf{r}\,|0\rangle\,,\end{aligned} \tag{2.61}$$

with the restriction $\mathbf{k}_p = \mathbf{k}(\omega_p) = \mathbf{k}(\omega_s+\omega_i)$. For the sake of simplicity we regard a collinear approximation where all waves are propagating in $z$-direction and the transverse wavevector mismatch disappears ($\Delta k^x = \Delta k^y = 0$), yielding the amplitude

$$|\Psi\rangle = |0\rangle - \frac{i}{\hbar}\mathcal{C}\int_0^L\int_0^\infty\int_0^\infty \mu(\omega_s+\omega_i)e^{i\Delta kz}a_s^\dagger a_i^\dagger\, d\omega_s\, d\omega_i\, dz\,|0\rangle\,, \tag{2.62}$$

where $L$ is again the crystal length. The result of the space integral is well known from the previous section:

$$\begin{aligned}\int_0^L e^{i\Delta kz}dz &= \frac{2}{\Delta k}e^{i\Delta kL/2}\sin\left(\frac{\Delta kL}{2}\right)\\ &= Le^{i\Delta kL/2}\,\mathrm{sinc}\left(\frac{\Delta kL}{2}\right).\end{aligned} \tag{2.63}$$

By insertion back into the amplitude we obtain

$$|\Psi\rangle = |0\rangle - \frac{i}{\hbar}\mathcal{C}L\int_0^\infty\int_0^\infty \mu(\omega_s+\omega_i)e^{i\Delta kL/2}\,\mathrm{sinc}\left(\frac{\Delta kL}{2}\right)a_s^\dagger a_i^\dagger\, d\omega_s\, d\omega_i\,|0\rangle\,, \tag{2.64}$$

or if we unwrap the factor $\mathcal{C}$ again

$$\boxed{|\Psi\rangle = |0\rangle - \frac{i}{\hbar}\epsilon_0\chi^{(2)}A_p\mathcal{E}_s\mathcal{E}_i L\int_0^\infty\int_0^\infty \mu(\omega_s+\omega_i)e^{i\Delta kL/2}\,\mathrm{sinc}\left(\frac{\Delta kL}{2}\right)a_s^\dagger a_i^\dagger\,d\omega_s\,d\omega_i\,|0\rangle\,.} \tag{2.65}$$

In order to compare the above result with our semi-classical derivation where we considered only monochromatic in- and output, we omit the integration over frequency and neglect the vacuum part:

$$|\Psi\rangle = 4\frac{i}{\hbar}d_{\mathrm{eff}}\chi^{(2)}A_p\sqrt{\frac{\hbar^2\omega_s\omega_i}{4\epsilon_0^2 n_s n_i V_Q^2}}Le^{i\Delta kL/2}\,\mathrm{sinc}\left(\frac{\Delta kL}{2}\right)a_s^\dagger a_i^\dagger\,|0\rangle\,, \tag{2.66}$$

where we used $\chi^{(2)} = 4d_{\mathrm{eff}}$ and $\mathcal{E} = (\hbar\omega/(2\epsilon_0 n V_Q))^{1/2}$. The quantum-mechanical (QM) intensity of the output (say signal) radiation is given by the scalar product of the wavefunction with itself:

$$I_{s,\mathrm{QM}} = \langle\Psi|\Psi\rangle = \frac{\hbar\omega_s\omega_i}{n_s n_i V_Q^2}L^2 d_{\mathrm{eff}}^2|A_p|^2\,\mathrm{sinc}^2\left(\frac{\Delta kL}{2}\right). \tag{2.67}$$

Using $|A|^2 = (2\mu_0 c/n)I$ we obtain

$$\boxed{I_{s,\mathrm{QM}} = \frac{2\mu_0\hbar\omega_s\omega_i c}{n_p n_s n_i V_Q^2}L^2 d_{\mathrm{eff}}^2 I_p\,\mathrm{sinc}^2\left(\frac{\Delta kL}{2}\right).} \tag{2.68}$$

Back in Section 2.2 we found the semi-classically derived result for signal intensity $I_{s,\mathrm{SC}}$ to be

$$I_{s,\mathrm{SC}} = \frac{2\mu_0\hbar\omega_s^2\omega_i}{n_p n_s n_i V_Q}L^2 d_{\mathrm{eff}}^2 I_p\,\mathrm{sinc}^2\left(\frac{\Delta kL}{2}\right). \tag{2.69}$$

Comparison with our quantum-mechanical result (2.68) yields

$$I_{s,\mathrm{SC}} = \frac{\omega_s V_Q}{c}I_{s,\mathrm{QM}}. \tag{2.70}$$

We rearrange the distinguishing factor to arrive at

$$\frac{\omega_s V_Q}{c} = \frac{2\pi\nu_s V_Q}{c} = \frac{2\pi V_Q}{\lambda_s} = \frac{V_Q k_s}{n_s}. \tag{2.71}$$

The quantised wavevector in a one-dimensional case is, by restrictions of field quantisation,

$$k = \frac{2\pi m}{V_Q}, \tag{2.72}$$

where $m$ is a positive integer. Assuming $m = 1$ and inserting $k$ in (2.71) we obtain

$$\frac{V_Q k_s}{n_s} = \frac{2\pi}{n_s}. \tag{2.73}$$

We see that the factor (2.73) which distinguishes our semi-classical and quantum result is a dimension-less number with the order of magnitude $\sim 1$. We can therefore safely claim that the both results coincide in very good approximation:

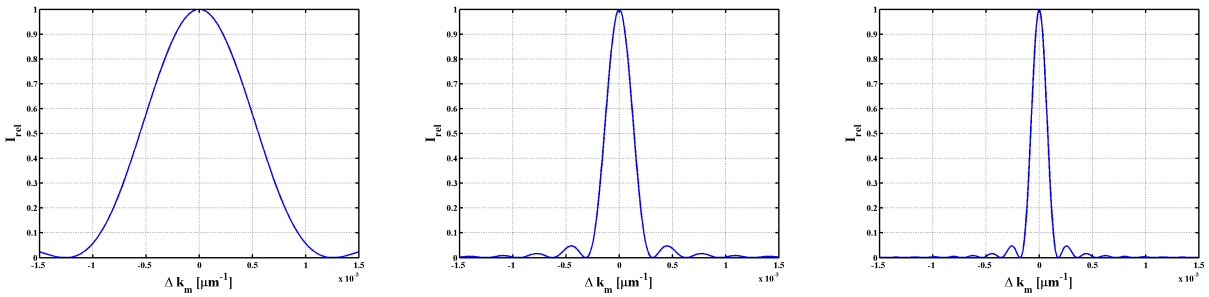


(a) $L = 5\,\mathrm{mm}$ (b) $L = 20\,\mathrm{mm}$ (c) $L = 35\,\mathrm{mm}$

Figure 2.3: Illustration of how the crystal length $L$ influences the phase-matching tolerance. The plots depict SPDC-intensity with respect to phase mismatch for crystals of (a) 5 mm, (b) 20 mm and (c) 35 mm length.

$$I_{s,\mathrm{SC}} \approx I_{s,\mathrm{QM}}. \tag{2.74}$$

The most crucial feature of the expression for the output intensity (2.68) is its dependence on the wavevector mismatch $\Delta k$. Since $\mathrm{sinc}(x) \leq 1$ and $\mathrm{sinc}(0) = 1$, maximum intensity can be achieved if $\Delta k = 0$ or equivalently

$$k_p = k_s + k_i. \tag{2.75}$$

This not only true in the collinear case that we are investigating, but for any three wave process with arbitrary propagation direction of the respective waves. So in the most general form maximal SPDC- (and also DFG-) efficiency can be achieved if and only if $\Delta\mathbf{k} = 0$, that is

$$\mathbf{k}_p = \mathbf{k}_s + \mathbf{k}_i. \tag{2.76}$$

This can also be understood in terms of the coherence length $L_c$ which is defined as the length along which there is a positive energy transfer from the input to the output fields: The function $\sin^2(\Delta kz/2)$ (and hence the output intensity) will grow together with propagation length $z$ until the argument of the sine arrives at $\pi/2$. So there is a positive energy transfer from input to output as long as $\Delta kz$ is smaller than $\pi$. Thus the coherence length is

$$L_c = \frac{\pi}{\Delta k}. \tag{2.77}$$

So a monotonous growth of the output intensity can be achieved if $L_c$ becomes infinite, i.e. when $\Delta k$ approaches zero. Techniques to eliminate $\Delta\mathbf{k}$ in order to maximise efficiency can be summarised by the term *phase-matching* and will be discussed in the next chapter. Note also that the intensity is proportional to $L^2$ which may incite to use very long crystals. The downside however is that due to the factor $\Delta kL$ in the sinc-function a long crystal makes the phase-matching tolerance smaller: the larger the length $L$ the quicker will the function $\mathrm{sinc}^2(\Delta\mathbf{k}L/2)$ decrease when $\Delta k$ deviates from zero (Figure 2.3).

## 2.4 Summary

As derived in two different fashions the output intensity of SPDC (as well as of any other three-wave mixing process) is proportional to $L^2\,\mathrm{sinc}^2(\Delta\mathbf{k}L/2)$. Therefore, for a given crystal length $L$, the intensity is maximal when the phase-matching condition is met:

$$\Delta\mathbf{k} = \mathbf{k}_p - \mathbf{k}_s - \mathbf{k}_i = 0.$$

Under this condition the coherence length of the process will approach infinity thus allowing for continuous energy transfer from pump to daughter fields, i.e. a monotonous growth of output intensity throughout the interaction length. A longer crystal length $L$ will increase the output intensity quadratically but will cause a more drastic loss when $\Delta\mathbf{k}$ deviates from zero.

# Chapter 3

# Phase-Matching

As seen in the previous chapter, maximal intensity is achieved when the phase mismatch is zero. This chapter introduces and compares the two main techniques to arrive at this condition: *birefringent phase-matching* (BPM), which makes use of the angle-dependent extraordinary index, and *quasi-phase-matching* (QPM) in which crystals with layers of periodically changing non-linearity $d_{\text{eff}}$ are used in order to reset the phase mismatch in multiples of the coherence length.

## 3.1 Fundamentals

Whereas for any three wave process energy conservation implies automatically

$$\omega_p = \omega_s + \omega_i \quad \text{and} \tag{3.1a}$$

$$\frac{1}{\lambda_p} = \frac{1}{\lambda_s} + \frac{1}{\lambda_i}, \tag{3.1b}$$

the phase-matching condition (2.76) can not be trivially achieved. The reason is that in a medium the wavevector doesn't exclusively depend on the wavelength but additionally on the refractive index:

$$\mathbf{k} = \frac{2\pi n}{\lambda}\hat{\mathbf{k}}, \tag{3.2}$$

where for dispersive media the refractive index itself is a function of the wavelength and—in case of extraordinary beams—of the propagation direction:

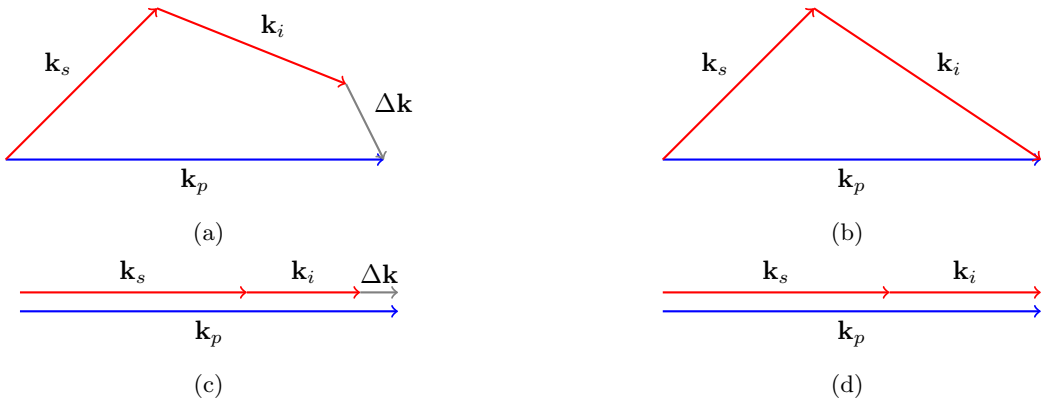


Figure 3.1: Schematic of (a,b) non-collinear and (c,d) collinear three-wave mixing. The figures on the left depict a wavevector mismatch whereas in the figures on the right side the mismatch $\Delta\mathbf{k}$ is zero, representing a phase-matched process.

$$n_o = n_o(\lambda, T), \tag{3.3a}$$
$$n_e = n_e(\lambda, \theta, T). \tag{3.3b}$$

Figure 3.1 graphically compares down-conversions where phase-matching is achieved and not achieved. In order to eliminate $\Delta\mathbf{k}$ it is sometimes possible to cut and then place the non-linear crystal such that the pump beam impinges the crystal in the exact angle $\theta$ which allows for the relation $\mathbf{k}_p - \mathbf{k}_s - \mathbf{k}_i = 0$. This technique is referred to as birefringent phase-matching. In the case of collinear three-wave mixing the phase mismatch can be compensated for by an additional term in the equation: $k_p - k_s - k_i - 2\pi m/\Lambda = 0$, where $m$ is an odd integer and $\Lambda$ is a periodicity constant in multiples of which the crystal's effective non-linearity switches its sign. This technique using periodically poled crystals is called quasi-phase-matching.

## 3.2 Birefringent Phase-Matching

The wavevector mismatch can be written as

$$\Delta\mathbf{k} = 2\pi \left( \frac{n_p}{\lambda_p}\hat{\mathbf{k}}_p - \frac{n_s}{\lambda_s}\hat{\mathbf{k}}_s - \frac{n_i}{\lambda_i}\hat{\mathbf{k}}_i \right). \tag{3.4}$$

Even if the three beams propagate in different directions, we can set the coordinate system such that they all propagate within one single plane. Therefore it's sufficient to describe the involved wavevectors as two-dimensional objects. Say, all waves propagate in the $xz$-plane then the wavevectors can be written as

$$\mathbf{k} = \begin{pmatrix} k^x \\ k^z \end{pmatrix}, \tag{3.5}$$

and same goes for the phase mismatch:

$$\Delta\mathbf{k} = \begin{pmatrix} \Delta k^x \\ \Delta k^z \end{pmatrix}. \tag{3.6}$$

For small pump beam divergence we can assume $k_s^x \approx -k_i^x$, so only the longitudinal component contributes to the phase mismatch vector:*

$$\Delta\mathbf{k} \approx \Delta k^z. \tag{3.7}$$

Assuming the pump beam to propagate in $z$-direction, i.e. $\mathbf{k}_p = k_p = k_p^z$ we can express the phase mismatch as

$$\Delta k^z = k_p - k_s^z - k_i^z = k_p - \sqrt{\mathbf{k}_s^2 - (k_s^x)^2} - \sqrt{\mathbf{k}_i^2 - (k_s^x)^2}. \tag{3.8}$$

When $\phi_s$ is the scattering angle of the signal with respect to the pump beam, then this can be reexpressed using

$$\mathbf{k}_s^2 - (k_s^x)^2 = \frac{n_s^2}{\lambda_s^2} - \frac{n_s^2}{\lambda_s^2}\sin^2\phi_s = \frac{n_s^2}{\lambda_s^2}(1 - \sin^2\phi_s) = \frac{n_s^2}{\lambda_s^2}\cos^2\phi_s \tag{3.9a}$$

and

$$\mathbf{k}_i^2 - (k_s^x)^2 = \frac{n_i^2}{\lambda_i^2} - \frac{n_s^2}{\lambda_s^2}\sin^2\phi_s = \frac{n_i^2}{\lambda_i^2}\left(1 - \frac{\lambda_i^2 n_s^2}{\lambda_s^2 n_i^2}\sin^2\phi_s\right). \tag{3.9b}$$

*For the following derivations cf. [5].

Reinserting these expressions as well as $k_p = 2\pi n_p/\lambda_p$ yields

$$\Delta k^z = 2\pi \left( \frac{n_p}{\lambda_p} - \frac{n_s}{\lambda_s} \cos\phi_s - \frac{n_i}{\lambda_i} \sqrt{1 - \frac{\lambda_i^2 n_s^2}{\lambda_s^2 n_i^2} \sin^2\phi_s} \right), \tag{3.10}$$

where each refractive index depends on the respective wavelength and—in case of extraordinary polarisation—on the angle of the beam with respect to the optic axis:

$$\frac{1}{n_e^2} = \frac{\cos^2\theta}{n_o^2} + \frac{\sin^2\theta}{n_{\text{opt}}^2}. \tag{3.11}$$

For collinear SPDC $\theta$ is just the pump beam's angle: $\theta_p = \theta_s = \theta_i$. For non-collinear SPDC the scattering angle has to be taken into account: $\theta_{s/i} = \theta_p + \phi_{s/i}$. In the collinear case, where the scattering angles $\phi_s = \phi_i = 0$, Equation (3.10) simplifies to

$$\Delta k^z = 2\pi \left( \frac{n_p}{\lambda_p} - \frac{n_s}{\lambda_s} - \frac{n_i}{\lambda_i} \right). \tag{3.12}$$

However in both—collinear and non-collinear—cases Equation (3.10) is highly angle-dependent (as long as there is extraordinary polarisation involved). So in order to achieve BPM we have to express the phase mismatch as a function of the angle, $\Delta k^z(\theta)$, evaluate numerically where this function has its root (see Figure 3.3 for an example) and finally cut the crystal accordingly such that the pump beam impinges at the desired angle.

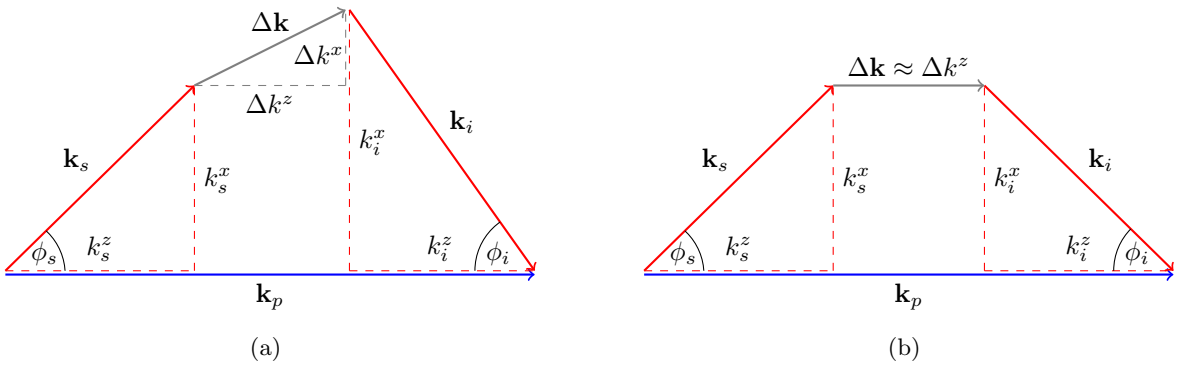


Figure 3.2: Geometry of birefringent scattering. In our derivations we simplify the (a) general case to (b) an approximation where only the longitudinal component of the wavevector mismatch contributes.

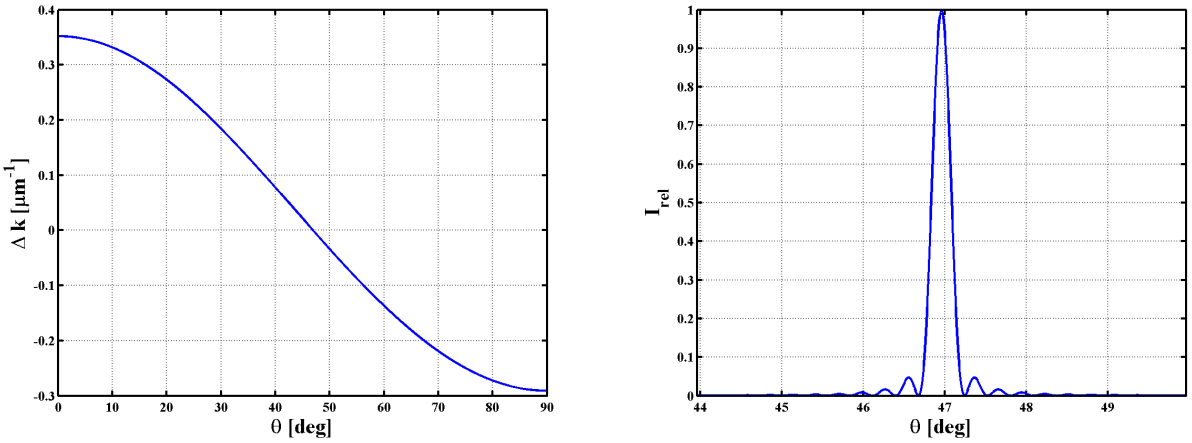


(a) (b)

Figure 3.3: Example for numerical determination of the phase-matching angle $\theta$: type I down-conversion ($e \longrightarrow o + o$) from 780 nm to 1064 nm and 2922 nm in lithium niobate. Figure (a) shows the wavevector mismatch as a function of $\theta$; Figure (b) shows the $\mathrm{sinc}^2$-shaped intensity of the signal radiation with respect to $\theta$. Both figures indicate that for this specific setup phase-matching is achieved at $\theta \approx 47°$.

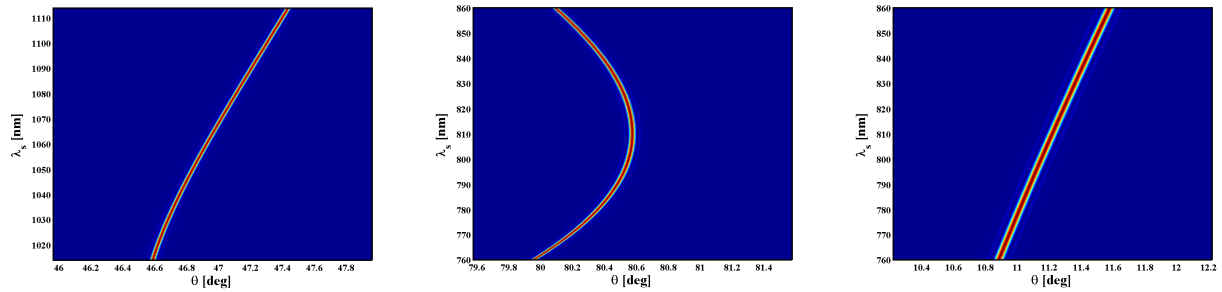


(a) $e \longrightarrow o + o$, LN, 780 nm $\longrightarrow$ 1064 nm + 2922 nm

(b) $e \longrightarrow o + o$, KTP, 405 nm $\longrightarrow$ 2 × 1064 nm

(c) $e \longrightarrow o + e$, BBO, 405 nm $\longrightarrow$ 2 × 1064 nm

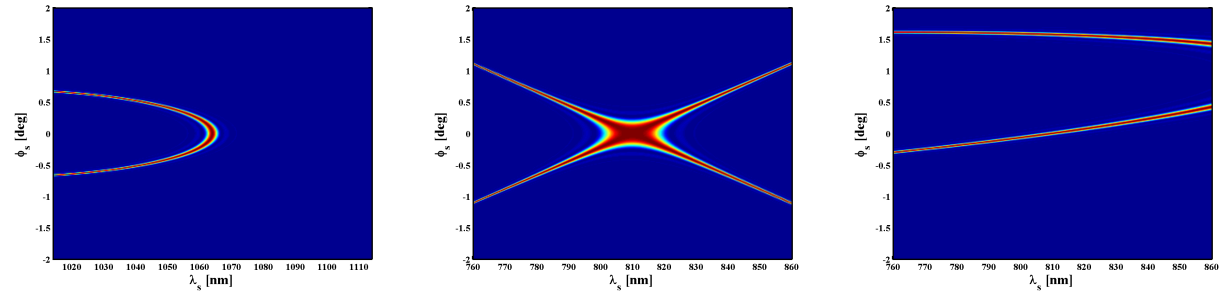


(d) $e \longrightarrow o + o$, LN, 780 nm $\longrightarrow$ 1064 nm + 2922 nm

(e) $e \longrightarrow o + o$, KTP, 405 nm $\longrightarrow$ 2 × 1064 nm

(f) $e \longrightarrow o + e$, BBO, 405 nm $\longrightarrow$ 2 × 1064 nm

Figure 3.4: Three examples for birefringent phase-matching: The left column describes type I down-conversion from 780 nm to 1064 nm and 2922 nm in LN; the middle column describes type I down-conversion from 405 nm to two times 810 nm in KTP; the right column describes type II down-conversion from 405 nm to two times 810 nm in BBO. Figures (a,b,c) show the intensity versus phase-match angle and signal wavelength; Figures (d,e,f) show the intensity with respect to wavelength and scattering angle $\phi$.

## 3.3 Quasi-Phase-Matching

While for certain processes birefringent phase-matching cannot be achieved within the range of the tuning angle $\theta = [0, \pi/2]$, quasi-phase-matching offers a more flexible approach. The idea is to reset the group velocity mismatch of primary and secondary fields by periodically reversing the non-linearity within the crystal, i.e. changing the sign of $d_{\text{eff}}$. This can be achieved by electric field poling of ferroelectric crystals. In this technique electrical contacts are applied in a periodic pattern on the crystal surface. When sufficiently high voltage is applied the domains under the contacts flip their poling permanently whereas the rest of the crystal remains unchanged. The most common materials used for quasi-phase-matching are periodically poled *lithium niobate* (ppLN) and *potassium titanyl phosphate* (ppKTP). Some properties of these crystals can be found in Appendix A.

To understand the idea of quasi-phase-matching (QPM) we have a look at Equation (2.33) which shows that the signal amplitude of difference frequency generation after a certain interaction length $z$ is proportional to the product of the effective non-linearity and the sine of $\Delta kz/2$:

$$A_s \propto d_{\text{eff}} \sin\left(\frac{\Delta kz}{2}\right). \tag{3.13}$$

In order to achieve maximum output intensity we want the signal amplitude to grow monotonously over the whole length of the crystal. In other words, we want the derivative of $A_s$ with respect to the length $z$ to be positive for all values of $z$:

$$\frac{\partial A_s}{\partial z} \propto d_{\text{eff}} \cos\left(\frac{\Delta kz}{2}\right) \overset{!}{>} 0. \tag{3.14}$$

As soon as $z$ exceeds the coherence length $L_c = \pi/\Delta k$ the cosine becomes negative and so does the derivative $\partial_z A_s$. The cosine will not become positive again before the propagation length $z$ reaches $3L_c$. So in order for the amplitude to keep growing, the sign of $d_{\text{eff}}$ is switched periodically at odd multiples of $L_c$.

To describe the requirements for QPM more quantitatively we go back to the differential equation which describes the amplitude of the signal amplitude of DFG, which is—analogous to (2.30)—*

$$\frac{\partial A_s}{\partial z} = i\frac{\omega_s}{n_s c} d_{\text{eff}}(z) A_p A_i^* e^{i\Delta kz}. \tag{3.15}$$

The major difference to our derivation in Section 2.2 is that the effective non-linearity is now a function of space and has to be included in the integral:

$$A_s = i\frac{\omega_s}{n_s c} A_p A_i^* \int_0^L d_{\text{eff}}(z) e^{i\Delta kz} dz. \tag{3.16}$$

The function $d(z)$ is of rectangular shape with periodicity constant $\Lambda$, and it can be represented by the Fourier series:

$$d_{\text{eff}}(z) = |d_{\text{eff}}| \sum_{m=-\infty}^{\infty} \frac{2}{\pi m} \sin\left(\frac{m\pi}{2}\right) e^{-i(2\pi m/\Lambda)z}. \tag{3.17}$$

The definitions of

$$k_m = \frac{2\pi}{\Lambda} m \tag{3.18}$$

and

$$C_m = \frac{2}{\pi m} \sin\left(\frac{m\pi}{2}\right) \tag{3.19}$$

*For the following derivations cf. [25], p. 120 ff.

simplify the expression to:

$$d_{\text{eff}}(z) = |d_{\text{eff}}| \sum_m C_m e^{-ik_m z}. \tag{3.20}$$

Inserting this function in (3.16) yields

$$A_s = i\frac{\omega_s}{n_s c}|d_{\text{eff}}|A_p A_i^* \sum_m C_m \int_0^L e^{i(\Delta k - k_m)z} dz, \tag{3.21}$$

where everything which is not explicitly $z$-dependent was taken out of the integral. For the sake of a compact notation we introduce another definition:

$$\Delta\tilde{k}_m = \Delta k - k_m. \tag{3.22}$$

The solution to the integral in

$$A_s = i\frac{\omega_s}{n_s c}|d_{\text{eff}}|A_p A_i^* \sum_m C_m \int_0^L e^{i\Delta\tilde{k}_m z} dz, \tag{3.23}$$

is well known from Section 2.2. Analogously to (2.35) we obtain

$$A_s = i\frac{\omega_s}{n_s c} L|d_{\text{eff}}|A_p A_i^* \sum_m C_m e^{i\Delta\tilde{k}_m L/2} \operatorname{sinc}\left(\frac{\Delta\tilde{k}_m L}{2}\right). \tag{3.24}$$

As before, the intensity is proportional to the amplitude squared:

$$I_s \propto |A|^2 \propto L^2 \operatorname{sinc}^2\left(\frac{\Delta\tilde{k}_m L}{2}\right). \tag{3.25}$$

Again, maximum conversion efficiency can be achieved when the sinc function gets equal to one, i.e. when $\Delta\tilde{k}_m = 0$. So in our phase-matching ambitions we will strive for

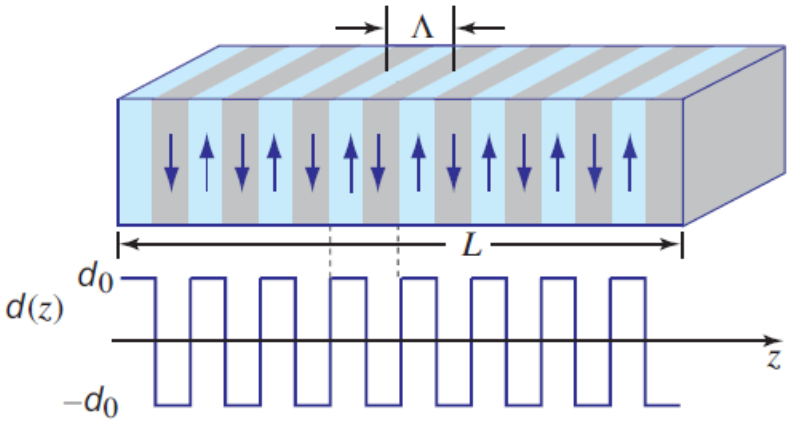


Figure 3.5: Schematic of a periodically poled crystal. The sign of the effective non-linearity is changed in multiples of $\Lambda$ in order to reset the phase mismatch periodically. Figure from [26].

$$\Delta\tilde{k}_m = \Delta k - k_m = \Delta k - \frac{2\pi}{\Lambda}m = 0. \tag{3.26}$$

Remembering the definition $\Delta k = k_p - k_s - k_i$, the quasi-phase-matching condition becomes

$$\Delta\tilde{k}_m = 2\pi\left(\frac{n_p}{\lambda_p} - \frac{n_s}{\lambda_s} - \frac{n_i}{\lambda_i} - \frac{m}{\Lambda}\right) = 0. \tag{3.27}$$

In contrast to birefringent phase-matching, where the impinging angle of the pump with respect to the crystal's optic axis is tuned, quasi-phase-matching works by tuning of the crystal's periodicity $\Lambda$. A rearrangement of (3.26) yields

$$\Lambda = \frac{2\pi}{\Delta k}m. \tag{3.28}$$

Since the Sellmeier equations and—due to thermal expansion—also the periodicity constant carry a temperature dependence, the entire phase-matching process is highly temperature-dependent. This can be used to compensate for small deviations from the optimal crystal periodicity by adjusting the temperature accordingly. This method is referred to as *temperature-tuning*. Examples for the temperature-dependence of the phase mismatch, the output intensity and frequencies are illustrated in Figures 3.7 and 3.8.

The non-linearity (3.17) is written in its most general form. However, regarding only cases in which the QPM condition (3.28) is fulfilled, we can actually omit the summation over $m$, since for a certain $\Lambda$ and $\Delta k$ there is only one $m$ to fulfil this equation. The non-linearity then simplifies to

$$d_{\text{eff}}(z) = |d_{\text{eff}}|\frac{2}{\pi m}\sin\left(\frac{m\pi}{2}\right)e^{-i(2\pi m/\Lambda)z}, \tag{3.29}$$

and accordingly do the respective amplitudes for signal and idler. Equation (3.28) shows that the periodicity has to shrink when the wavevector mismatch grows. Today's techniques allow for a poling periodicity down to roughly 5 µm. If a large $\Delta k$ requires a periodicity which is too small to be manufactured properly, then phase-matching can still be achieved by raising the order $m$ and thus increasing the required $\Lambda$ by the same factor. Any QPM order higher than one, however, will by Equation (3.29) decrease the effective non-linearity and therefore the resulting intensity. Also note that the function $\sin(m\pi/2)$ in (3.29) only allows for odd integers $m$.

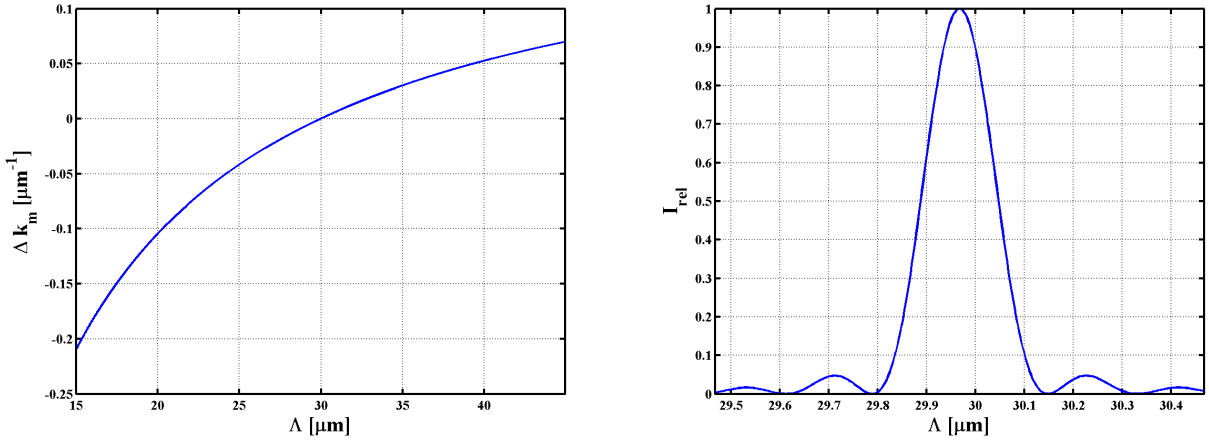


(a) (b)

Figure 3.6: Example for numerical determination of the crystal periodicity $\Lambda$: type 0 down-conversion ($e \longrightarrow e + e$) from 1064 nm to 1550 nm and 3393.4 nm in lithium niobate. Figure (a) shows the wavevector mismatch as a function of $\Lambda$; Figure (b) shows the $\mathrm{sinc}^2$-shaped output intensity with respect to $\Lambda$. Both figures indicate that for this specific setup phase-matching is achieved at $\Lambda \approx 30\,\mu\mathrm{m}$.

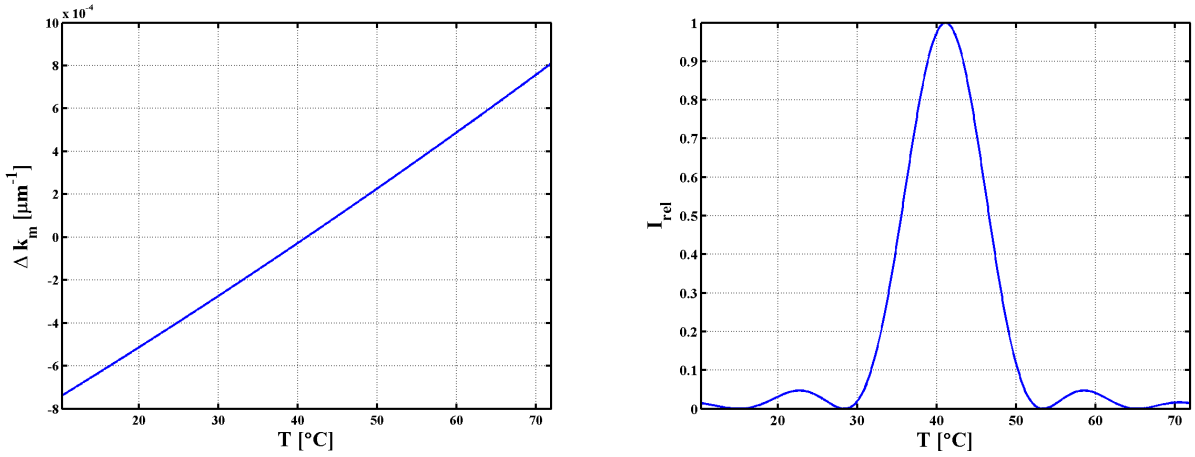


(a) (b)

Figure 3.7: Illustration of temperature-tuning: This example discusses the same down-conversion process as in Figure 3.6. The periodicity was set to 30 µm. Figure (a) shows the wavevector mismatch as a function of $T$; Figure (b) shows the output intensity with respect to $T$. Both figures indicate that for this specific setup phase-matching is achieved at $T \approx 41\,^{\circ}\mathrm{C}$.

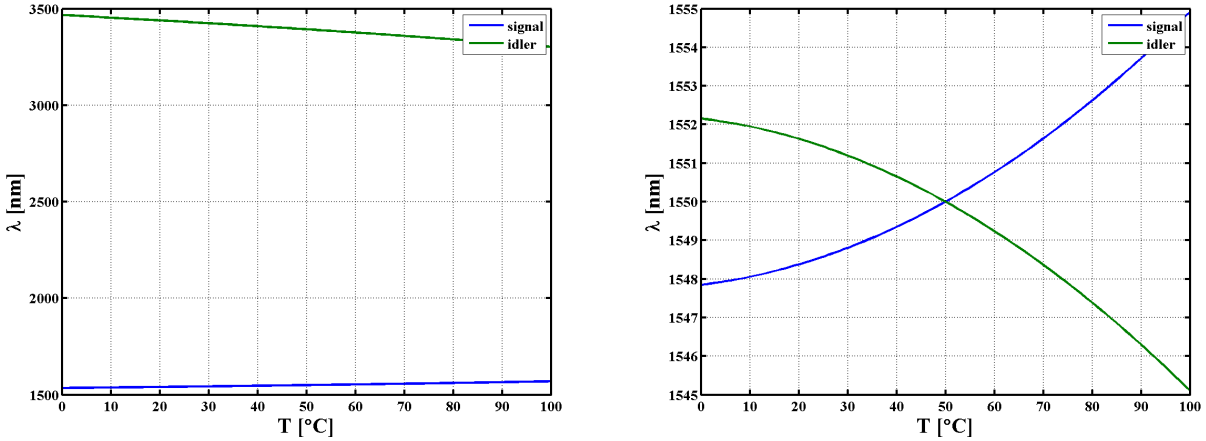


(a) (b)

Figure 3.8: Examples for the temperature dependence of the output wavelengths $\lambda_s$ and $\lambda_i$. For a fixed pump wavelength and crystal periodicity the setup allows for phase-matching of only specific output wavelengths. Figure (a) describes type 0 down-conversion 1064 nm $\longrightarrow$ 1550 nm + 3393.4 nm in LN; Figure (b) describes type II SPDC 775 nm $\longrightarrow$ 1550 nm + 1550 nm in KTP.

## 3.4 Summary

In order to achieve birefringent phase-matching the angle of the pump beam with respect to the crystal's optic axis is tuned. The phase-matching condition is met where the function $\Delta\mathbf{k}(\theta)$ has its zero-point. The disadvantage of BPM is clearly the limited range of angle-tuning, since there is often no $\theta$ between 0 and 90° which allows for phase-matching. At the quasi-phase-matching technique we choose the crystal's periodicity $\Lambda$ such that the condition

$$\Delta\tilde{k}_m = \Delta k - \frac{2\pi}{\Lambda} m = 0$$

is fulfilled. The technique of QPM is insofar more flexible than BPM as for any collinear three-wave mixing there exists a $\Lambda$ which allows for the above relation to be met. Both functions, $\Delta\mathbf{k}(\theta)$ and $\Delta\tilde{k}_m(\Lambda)$ are evaluated numerically using the respective temperature-dependent Sellmeier equations and—in case of BPM—the angle-dependant expression for extraordinary indices.

# Chapter 4

# Entanglement, Factorability and Purity

In order to observe quantum interference, crucial to any kind of quantum-based experiment or application, the photons arriving at the beamsplitter need to be indistinguishable and pure. Quantitatively this can be pointed out by the expression for the visibility of Hong-Ou-Mandel interference [13] which reads [21]

$$V = \frac{\mathcal{P}_1 + \mathcal{P}_2 - \|\rho_1 - \rho_2\|^2}{2}, \tag{4.1}$$

where $\mathcal{P}$ is the purity and $\rho$ the density operator of the two respective single photon states. Obviously the visibility equals one only if the two incident states are pure ($\mathcal{P}_1 = \mathcal{P}_2 = 1$) and indistinguishable ($\rho_1 = \rho_2$). Spontaneous parametric down-conversion is a popular source of single photon states and the fact that the photons are generated in pairs makes it a convenient tool for *single photon heralding*, a process where detection of one photon predicts the arrival of another one: Say two photons, a signal and an idler, are produced by SPDC. The photons are brought into different spatial modes, e.g. by birefringent scattering or, in case of collinear SPDC, by a polarising beamsplitter. The photons propagating along one of the two paths are collected by a detector, which, whenever triggered, heralds the presence of another photon in the other spatial mode. If the initial bipartite state $|\Psi\rangle$ is entangled in frequency space and the idler photon is detected (by a detector which cannot resolve its frequency), the heralded signal photon is projected into a mixed state (as derived below within this chapter). The only way to avoid the nuisance of a mixed single photon state is to make the bipartite state separable—either by use of narrow bandpass filters or by engineering $|\Psi\rangle$ such that it is *a priori* separable in frequency space.

In this chapter we briefly introduce the concepts of state purity and mixedness and derive in which way quantum entanglement of a bipartite state affects the purity of the respective single photon states. Then we show how the state purity of the signal and idler single states, i.e. the degree of separability of the SPDC wavefunction $|\Psi\rangle$, can be evaluated numerically. We demonstrate how intrinsically pure quantum states can be achieved in the lab and conclude with a brief discussion how the relation of pump pulse duration and crystal length influences the visibility of Hong-Ou-Mandel interference in the experiment.

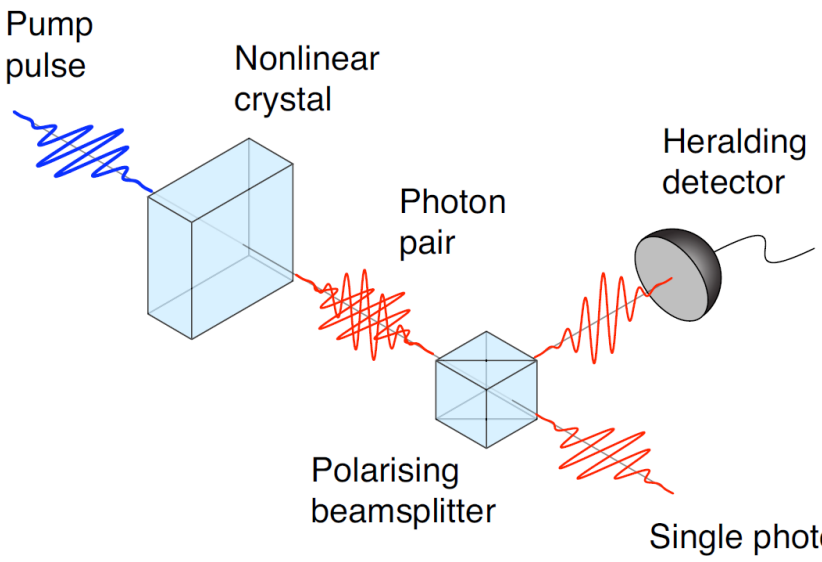


Figure 4.1: Schematic of photon heralding. A polarising beamsplitter separates a photon pair whereupon one photon triggers the detector and therefore predicts the presence of a photon in the other spacial mode. Figure from [20].

## 4.1 Pure and Mixed States

In quantum mechanics a pure state is defined as a state which can be described by a single ket-vector, e.g. $|\Psi\rangle$. This state can also be expressed by the density operator

$$\rho = |\Psi\rangle \langle\Psi| . \tag{4.2}$$

A mixed state is an ensemble of pure states $|\Psi_j\rangle$, each weighted by a probability $p_j$:

$$\rho = \sum_j p_j |\Psi_j\rangle \langle\Psi_j| , \tag{4.3}$$

where $\sum_j p_j = 1$. To determine the degree of a state's purity $\mathcal{P}$ we take the trace of the square of the density operator:

$$\mathcal{P} = \mathrm{Tr}(\rho^2) = \sum_j p_j^2 . \tag{4.4}$$

Clearly $\mathcal{P}$ is only equal to one if there is only one non-vanishing probability coefficient $p_j = 1$, thus allowing the state to be represented like in Equation (4.2). On the contrary, if there are many terms in (4.4) each $p_j$ will approach zero and so will the purity $\mathcal{P}$.

Any pure state which is a composite of two subsystems $A$ and $B$ can be written as

$$|\Psi\rangle = \sum_j \sum_k c_{j,k} |\tilde{\alpha}_j\rangle_A \otimes |\tilde{\beta}_k\rangle_B . \tag{4.5}$$

It is however possible to express a composite bipartite system in terms of a shared complete set of orthonormal basis states:

$$|\Psi\rangle = \sum_j \sqrt{\lambda_j} |\alpha_j\rangle_A \otimes |\beta_j\rangle_B , \tag{4.6}$$

which is known as the *Schmidt decomposition* of the state $|\Psi\rangle$. The vectors $|\alpha_j\rangle_A$ and $|\beta_j\rangle_B$ are the so-called *Schmidt modes* of the respective subsystems, and $\lambda_j$ are the *Schmidt coefficients* which add up to one: $\sum_j \lambda_j = 1$. The pairs $|\alpha_j\rangle_A \otimes |\beta_j\rangle_B$ form a complete set of basis states of the total system. The Schmidt decomposition provides an intuitive measurement of entanglement within a pure state: If the state is entangled, then there is more than just one term present in (4.6). The number of Schmidt modes with non-vanishing coefficients $\lambda_j$ is sometimes used to describe the degree of entanglement of a state. A more illuminative measure is however provided by the *Schmidt number* $K$, defined as [8]

$$K = \frac{1}{\sum_j \lambda_j^2}, \tag{4.7}$$

which not only takes the number of coefficients $\lambda_j$ into account but also their magnitude.

The density operator of the state (4.6) is

$$\begin{aligned}\rho &= \sum_j \sum_k \sqrt{\lambda_j \lambda_k}\, |\alpha_j\rangle \otimes |\beta_j\rangle \langle\alpha_k| \otimes \langle\beta_k| \\ &= \sum_j \sum_k \sqrt{\lambda_j \lambda_k}\, |\alpha_j\rangle \langle\alpha_k| \otimes |\beta_j\rangle \langle\beta_k|\end{aligned} \tag{4.8}$$

The density operator of one of the subsystems can be obtained by tracing out the respective other one, e.g.:

$$\begin{aligned}\rho_A &= \sum_l \langle\beta_l| \left( \sum_j \sum_k \sqrt{\lambda_j \lambda_k}\, |\alpha_j\rangle \langle\alpha_k| \otimes |\beta_j\rangle \langle\beta_k| \right) |\beta_l\rangle \\ &= \sum_l \sum_j \sum_k \sqrt{\lambda_j \lambda_k}\, |\alpha_j\rangle \langle\alpha_k| \otimes \langle\beta_l|\beta_j\rangle \langle\beta_k|\beta_l\rangle \\ &= \sum_l \sum_j \sum_k \sqrt{\lambda_j \lambda_k}\, |\alpha_j\rangle \langle\alpha_k| \otimes \delta^{lj} \delta^{kl} \\ &= \sum_j \lambda_j\, |\alpha_j\rangle \langle\alpha_j|\,,\end{aligned} \tag{4.9}$$

where we used the orthonormality of the basis states $|\beta_j\rangle$. So in other words, the quantum state of a subsystem is given by the partial trace of the total state $\rho = |\Psi\rangle \langle\Psi|$ over the respective other subsystem:

$$\rho_A = \mathrm{Tr}_B\, \rho, \tag{4.10a}$$

$$\rho_B = \mathrm{Tr}_A\, \rho. \tag{4.10b}$$

Equation (4.9) shows that the trace over a subsystem's squared density operator is just the sum of the squares of the Schmidt coefficients $\lambda_j$:

$$\mathrm{Tr}(\rho_A^2) = \mathrm{Tr}(\rho_B^2) = \sum_j \lambda_j^2. \tag{4.11}$$

Comparing the above expression with (4.7) yields

$$K = \frac{1}{\mathrm{Tr}(\rho_A^2)} = \frac{1}{\mathrm{Tr}(\rho_B^2)}, \tag{4.12}$$

or equivalently

$$\mathcal{P}_A = \mathcal{P}_B = \frac{1}{K} = \sum_j \lambda_j^2. \tag{4.13}$$

As we can see, the purity of the single photon states is, little surprising, proportional to the inverse degree of entanglement of the total state. A bipartite state $|\Psi\rangle$ can be factorised if and only if there is only one non-vanishing pair of Schmidt modes:

$$|\Psi\rangle = |\alpha\rangle \otimes |\beta\rangle \tag{4.14}$$

Since in the above case there is only one Schmidt coefficient $\lambda = 1$, the Schmidt number itself becomes $K = 1$ yielding maximum purity $\mathcal{P}_A = \mathcal{P}_B = 1$. An equivalent result can be obtained by another observation of (4.9): Tracing over one subsystem projects the other subsystem into a mixed state (even of course if the total initial state $\rho = |\Psi\rangle\langle\Psi|$ was pure). Experimentally this is the case when a frequency-correlated photon pair is used for heralding. The detection of one photon traces the other subsystem out, projecting it into a mixed state. The only case in which $\rho_A$ in (4.9) can be pure, is when there is only one non-vanishing Schmidt coefficient, hence when the total state was separable in the first place.

## 4.2 Factorability of the SPDC Amplitude

Back in Section 2.3 we found the amplitude for SPDC to be

$$\begin{aligned}|\tilde{\Psi}\rangle &= |0\rangle - \frac{i}{\hbar}\epsilon_0\chi^{(2)}A_p\mathcal{E}_s\mathcal{E}_i L\int_0^\infty\int_0^\infty \mu(\omega_s+\omega_i)e^{i\Delta kL/2}\,\mathrm{sinc}\left(\frac{\Delta kL}{2}\right)a_s^\dagger a_i^\dagger\, d\omega_s\, d\omega_i\,|0\rangle \\ &= |0\rangle + \mathcal{N}\int_0^\infty\int_0^\infty \mu(\omega_s+\omega_i)\psi(\omega_s,\omega_i)a_s^\dagger a_i^\dagger\, d\omega_s\, d\omega_i\,|0\rangle\,,\end{aligned} \tag{4.15}$$

where $\mathcal{N}$ is a normalisation constant that contains all the prefactors and $\psi(\omega_s,\omega_i)$ is the *phase-matching amplitude*

$$\psi(\omega_s,\omega_i) = e^{i\Delta kL/2}\,\mathrm{sinc}\left(\frac{\Delta kL}{2}\right). \tag{4.16}$$

Since we are only interested in pair coincidences where the detection of one photon heralds the presence of its twin, we can just as well ignore the vacuum part of the SPDC amplitude. Moreover, the amplitude can be rewritten in terms of the *joint spectral amplitude* (JSA), defined as

$$f(\omega_s,\omega_i) = \mu(\omega_s+\omega_i)\psi(\omega_s,\omega_i), \tag{4.17}$$

yielding the final expression

$$\boxed{|\Psi\rangle = \mathcal{N}\int_0^\infty\int_0^\infty f(\omega_s,\omega_i)a_s^\dagger a_i^\dagger\, d\omega_s\, d\omega_i\,|0\rangle\,.} \tag{4.18}$$

This clearly represents a pure state. This doesn't mean of course that the single photon states of signal and idler are pure themselves. As seen in the previous section, the purity of the single photon states can be obtained by tracing over the square of the respective density operator:

$$\mathcal{P}_s = \mathrm{Tr}(\rho_s^2) = \sum_j \lambda_j^2, \tag{4.19a}$$

$$\mathcal{P}_i = \mathrm{Tr}(\rho_i^2) = \sum_j \lambda_j^2, \tag{4.19b}$$

where $\lambda_j$ are the mutual Schmidt coefficients and, according to above,

$$\rho_s = \mathrm{Tr}_i\, \rho, \tag{4.20a}$$
$$\rho_i = \mathrm{Tr}_s\, \rho. \tag{4.20b}$$

As mentioned above, pure single photon states require a bipartite state $|\Psi\rangle$ which is separable in frequency space. In this case the joint spectral amplitude could be factorised

$$f(\omega_s, \omega_i) = f_s(\omega_s) f_i(\omega_i), \tag{4.21}$$

so Equation (4.18) can be written as

$$|\Psi\rangle = \mathcal{N} \int_0^\infty f_s(\omega_s) a_s^\dagger \, d\omega_s \int_0^\infty f_i(\omega_i) a_i^\dagger \, d\omega_i \, |0\rangle \,. \tag{4.22}$$

Thus, in order to obtain high purity in the single photon states, we are interested in making $f(\omega_s, \omega_i)$ as factorable as possible. However, the correlations of $\omega_s$ and $\omega_i$ in the joint spectral amplitude $f(\omega_s, \omega_i)$ *do* indicate a frequency entanglement of signal and idler photons. In order to investigate the entanglement of the SPDC-amplitude $|\Psi\rangle$—a pure bipartite state—we would like to express it in terms of a Schmidt decomposition:

$$|\Psi\rangle = \sum_j \sqrt{\lambda_j} \, |s_j\rangle \otimes |i_j\rangle \,, \tag{4.23}$$

with Schmidt modes $|s_j\rangle$ and $|i_j\rangle$, representing the respective subsystems, signal and idler. When a state or an amplitude cannot be Schmidt-decomposed analytically (as it is the case for the JSA $f(\omega_s, \omega_i)$), we can still perform a Schmidt decomposition with numerical means using the *singular value decomposition* (SVD) [8, 21, 28, 6]. Therefore we first split the relevant range of signal and idler frequencies into discrete values $\omega_{s,m}$ and $\omega_{i,n}$. Then we express the state as a sum over all possible combinations of signal and idler eigenfunctions, $|\tilde{s}_m\rangle$ and $|\tilde{i}_n\rangle$, weighted by their respective joint amplitude $f(\omega_{s,m}, \omega_{i,n})$ each of which is calculated numerically:

$$|\Psi\rangle = \sum_m \sum_n f(\omega_{s,m}, \omega_{i,n}) \, |\tilde{s}_m\rangle \otimes |\tilde{i}_n\rangle \,. \tag{4.24}$$

The amplitudes $f(\omega_{s,m}, \omega_{i,n})$ can be understood as components of an $M \times N$-matrix $\mathcal{F}$, of which each row (column) represents a particular discretised signal (idler) frequency:

$$f(\omega_{s,m}, \omega_{i,n}) = \langle \tilde{s}_m | \mathcal{F} | \tilde{i}_n \rangle = \langle \tilde{i}_n | \mathcal{F}^\dagger | \tilde{s}_m \rangle \,. \tag{4.25}$$

$\mathcal{F}\mathcal{F}^\dagger$ is the partial trace of the total state over the idler subsystem, which is in turn just the definition of the reduced density operator of the signal subsystem:

$$\mathcal{F}\mathcal{F}^\dagger = \sum_n \langle i_n | \rho | i_n \rangle = \rho_s. \tag{4.26a}$$

Analogously $\mathcal{F}^\dagger\mathcal{F}$ represents just the opposite:

$$\mathcal{F}^\dagger\mathcal{F} = \sum_m \langle s_m | \rho | s_m \rangle = \rho_i. \tag{4.26b}$$

We now express the respective amplitudes $f(\omega_{s,m}, \omega_{i,n})$ in (4.24) as components of $\mathcal{F}$ and obtain

$$|\Psi\rangle = \sum_m \sum_n \mathcal{F}^{mn} \, |\tilde{s}_m\rangle \otimes |\tilde{i}_n\rangle \,. \tag{4.27}$$

The SVD allows us to decompose any matrix into two unitary matrices $U$ and $V^\dagger$ and a diagonal matrix $D$, such that

$$\mathcal{F} = UDV^\dagger, \tag{4.28}$$

where the columns of $U$ represent the eigenvectors of $\mathcal{F}\mathcal{F}^\dagger = \rho_s$ and the columns of $V$ (or rows of $V^\dagger$) are the eigenvectors of $\mathcal{F}^\dagger\mathcal{F} = \rho_i$. The entries in $D$ are real, positive, appear in descending order on the diagonal and represent the eigenvalues of the eigenvectors described by the columns of $U$ and $V$:

$$\mathcal{F}\mathcal{F}^\dagger U^{mj} = d_j U^{mj}, \tag{4.29a}$$

$$\mathcal{F}^\dagger\mathcal{F} V^{nj} = d_j V^{nj} = d_j \left(V^\dagger\right)^{jn}, \tag{4.29b}$$

where $d_j = D^{jj}$ are just the coefficients of the diagonal matrix. It is important to note that the $j$th column of $U$ and the $j$th row of $V^\dagger$ are associated with the same eigenvalue $d_j$, i.e. the columns of $U$ and $V$ have a shared spectrum. We now replace $\mathcal{F}$ by its SVD representation, so (4.27) becomes

$$\begin{aligned}
|\Psi\rangle &= \sum_m \sum_n \left(UDV^\dagger\right)^{mn} |\tilde{s}_m\rangle \otimes |\tilde{i}_n\rangle \\
&= \sum_j \sum_m \sum_n U^{mj} D^{jj} \left(V^\dagger\right)^{jn} |\tilde{s}_m\rangle \otimes |\tilde{i}_n\rangle \\
&= \sum_j d_j \left(\sum_m U^{mj} |\tilde{s}_m\rangle\right) \otimes \left(\sum_n \left(V^\dagger\right)^{jn} |\tilde{i}_n\rangle\right).
\end{aligned} \tag{4.30}$$

So we expressed the state $|\Psi\rangle$ in terms of a complete set of basis states, each weighted by a coefficient $d_j$. As long as the squares of the coefficients sum up to one, this is just the unique expression for the Schmidt decomposition of $|\Psi\rangle$. So after $D$ has been normalised such that $\sqrt{\mathrm{Tr}(D^2)} = 1$ we can identify its entries with the Schmidt coefficients: $d_j = \sqrt{\lambda_j}$. Furthermore we define

$$|s_j\rangle = \sum_m U^{mj} |\tilde{s}_m\rangle, \tag{4.31a}$$

$$|i_j\rangle = \sum_n \left(V^\dagger\right)^{jn} |\tilde{i}_n\rangle, \tag{4.31b}$$

yielding the desired expression (4.23). The purity of $\rho_s$ and $\rho_i$ can then be easily obtained by Equation (4.19).

In the experiment we are only able to measure intensities rather than amplitudes. In our case the intensity is proportional to the square of the joint spectral amplitude:

$$F(\omega_s, \omega_i) = |f(\omega_s, \omega_i)|^2 = |\mu(\omega_s + \omega_i)\psi(\omega_s, \omega_i)|^2, \tag{4.32}$$

where we denote $F(\omega_s, \omega_i)$ as the *joint spectral intensity* (JSI). Similar to above we can split the frequencies up into discrete values $\omega_{s,m}$ and $\omega_{i,n}$ and construct a matrix $\mathbb{F}$ whose components represent the respective intensities $F(\omega_{s,m}, \omega_{i,n})$ for a certain pair of signal and idler frequency. A singular value decomposition delivers the Schmidt coefficients $\lambda_j = d_j^2$ which are squared and then summed over in order to obtain the purity $\mathcal{P}$.

The above discussion shows that for the sake of optimal purity of the single photon states we would like to make the joint spectral intensity separable. This requires an engineering of the JSI such that $K \approx 1$, or equivalently, that signal and idler frequency are as uncorrelated as possible. The correlation of the frequencies become beautifully apparent in the shape of the JSI when plotted against signal and idler frequency. High correlation of $\omega_s$ and $\omega_i$ (and therefore low purity) corresponds to an asymmetric shape, whereas low correlation (and therefore high purity) corresponds to a symmetric—i.e. circular—shape of the JSI (see Figure 4.2).

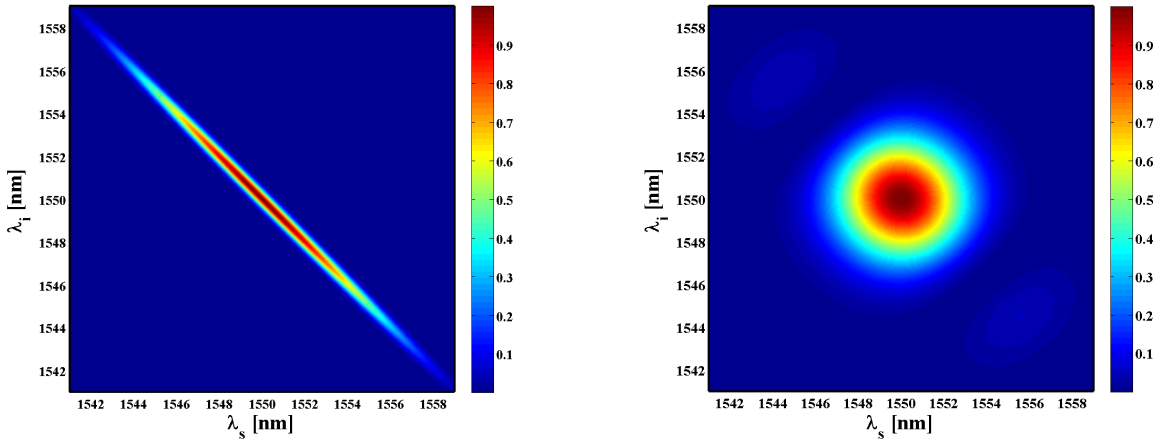


(a) (b)

Figure 4.2: Graphical representation of the JSI in two examples. Figure (a) shows a case where signal and idler wavelengths are highly (anti-) correlated, resulting in a purity $\mathcal{P} \sim 0$; Figure (b) illustrates a frequency-uncorrelated down-conversion, represented by a circular JSI with $\mathcal{P} \sim 1$.

In experiment it is common to use bandpass filters in order to get rid of frequency-correlated photon pairs such that only uncorrelated ones reach the detectors. Trivially spoken, this is equivalent to cutting a circular shape out of the JSI, discarding photons in frequency ranges which are beyond the circle. Although easy to implement this method demands a high price to pay, which is of course the drastic loss of intensity due to the frequency filters. Another approach is to make the initial state $|\Psi\rangle$ separable such that no filtering is required in order to reshape the JSI. This—an *intrinsically pure* SPDC—can be achieved by firstly choosing the right crystal settings for a desired wavelength configuration (crystal type, poling period, angle adjustment, etc.) and secondly by mutual matching of the spectral width of the pump source $\Delta\lambda_p$ and the crystal's length $L$.

### 4.2.1 Tailoring of the Joint Spectral Intensity

As seen in the previous section, the JSI is the product of the pump intensity $|\mu(\omega_s+\omega_i)|^2$ and the phase-matching intensity $|\psi(\omega_s,\omega_i)|^2$. So in order to engineer a state of high spectral purity it is necessary to investigate those two components closer. The pump spectrum depends primarily on the centre frequency $\omega_{p,0}$ and the spectral width $\Delta\omega_p$ or $\Delta\lambda_p$. For pulsed laser sources the spectral width $\Delta\lambda_p$ is intrinsically connected to the pulse duration $\tau$. The mutual relationship of both can be approximated with

$$\tau = \sqrt{\frac{\log 2}{2}}\frac{\lambda_0^2}{\pi c \Delta\lambda}, \tag{4.33a}$$

$$\Delta\lambda = \sqrt{\frac{\log 2}{2}}\frac{\lambda_0^2}{\pi c \tau}, \tag{4.33b}$$

where $\lambda_0$ is the centre wavelength, $c$ is the speed of light and $\Delta\lambda$ is understood as the Gaussian width of the pump spectrum (not to be confused the full width at half maximum which is $2\sqrt{2\log 2}\Delta\lambda$). The influence of spectral width/pulse duration on the spectral shape of $\mu$ is illustrated in Figure 4.3. Note that—apart from energy conservation, $\omega_p = \omega_s + \omega_i$—there is no further physics involved in the amplitude $\mu(\omega_s + \omega_i)$, i.e. it can be treated independently of the type of phase-matching and down-conversion. On the contrary, the phase-matching amplitude $\psi(\omega_s,\omega_i)$ contains the parameters $L$ and $\Delta k$ which is itself determined by a number of further parameters: $\Delta k = \Delta k(n_{p/s/i}, \lambda_{p/s/i}, \theta_{p/s/i}, T, \Lambda, d_{\text{eff}})$. So $\psi$ does depend strongly on the specific setup. The crystal length $L$ has a direct impact on the spectral width of the output radiation (Figure 4.4) whereas the rest of the setup, such as wavelength configuration, down-conversion type and the choice of the crystal, determine—graphically spoken—the orientation of the phase-matching intensity $|\psi|^2$ (Figure 4.5).

The final shape of the JSI can be understood as the intersection of $|\mu|^2$ and $|\psi|^2$ (Figure 4.6). A circular shape of the JSI can be achieved when $|\mu|^2$ and $|\psi|^2$ are angled orthogonally to each other, as illustrated in

Figure 4.7. Note however that this is only possible in a very limited amount of configurations. Since the spectral shape of $\mu$ can only be influenced in its width but not in its orientation, the shape of the JSI depends primarily on $|\psi|^2$, which in the very most cases is *not* oriented orthogonally to $|\mu|^2$. Once a setup is found which allows for roughly orthogonal pump and phase-matching intensities, a circular shape of the JSI can be achieved by mutual matching of crystal length and spectral pump width (Figures 4.8 and 4.9).

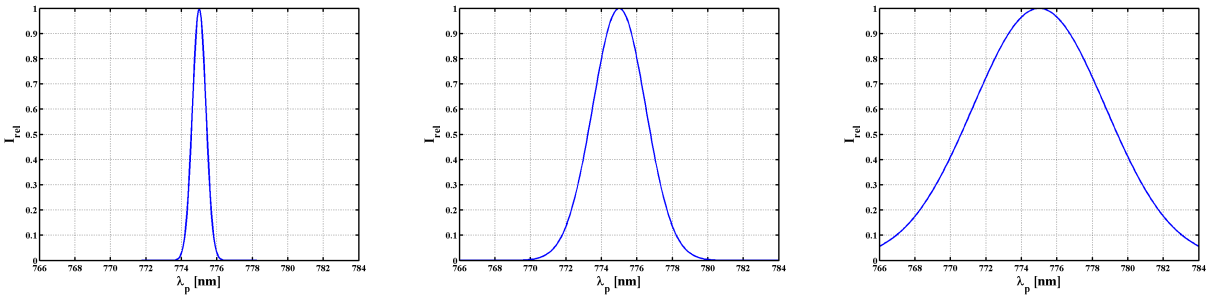


(a) $\Delta\lambda_p = 0.38\,\mathrm{nm}/\tau = 1\,\mathrm{ps}$ (b) $\Delta\lambda_p = 1.5\,\mathrm{nm}/\tau = 250\,\mathrm{fs}$ (c) $\Delta\lambda_p = 3.75\,\mathrm{nm}/\tau = 100\,\mathrm{fs}$

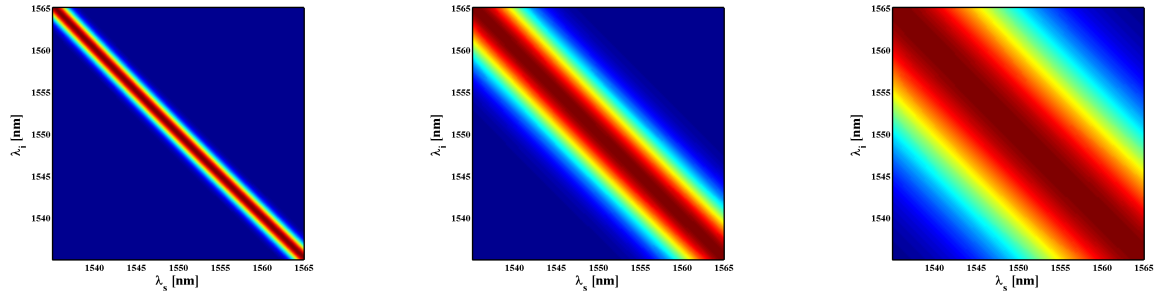


(d) $\Delta\lambda_p = 0.38\,\mathrm{nm}/\tau = 1\,\mathrm{ps}$ (e) $\Delta\lambda_p = 1.5\,\mathrm{nm}/\tau = 250\,\mathrm{fs}$ (f) $\Delta\lambda_p = 3.75\,\mathrm{nm}/\tau = 100\,\mathrm{fs}$

Figure 4.3: Plots of the pump envelope amplitude $\mu(\omega_p)$ (first row) and intensity $|\mu(\omega_s + \omega_i)|^2$ (second row) for a 775 nm laser. Note that the lower plots are generated only by energy conservation, $1/\lambda_p = 1/\lambda_s + 1/\lambda_i$, and are independent of crystal properties, refractive indices, periodic poling, phase-matching etc.

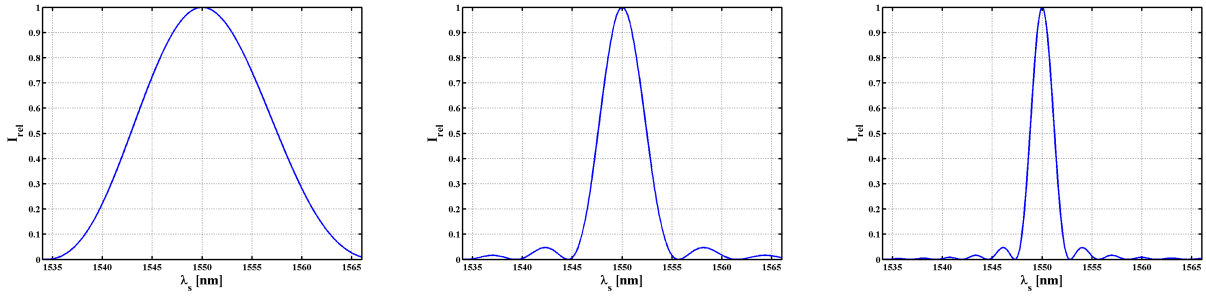


(a) $L = 5\,\mathrm{mm}$ (b) $L = 15\,\mathrm{mm}$ (c) $L = 30\,\mathrm{mm}$

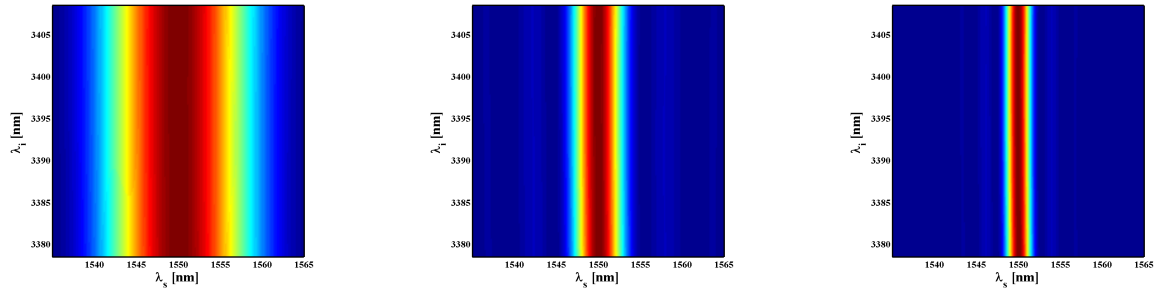


(d) $L = 5\,\mathrm{mm}$ (e) $L = 15\,\mathrm{mm}$ (f) $L = 30\,\mathrm{mm}$

Figure 4.4: Illustration of how the crystal length influences the bandwidth of the output. The plots depict the output intensity $|\psi(\omega_s, \omega_i)|^2$ vs. signal wavelength $\lambda_s$ at fixed idler wavelength $\lambda_i$ (first row) and vs. both varying $\lambda_s$ and $\lambda_i$ (second row). The plots correspond to a crystal length of (a,d) 5 mm, (b,e) 15 mm and (c,f) 30 mm. Note that the actual shape of the phase-match intensity plot, i.e. the orientation with respect to the axes, varies strongly with the specific SPDC process and crystal type (here: type 0: $1064\,\mathrm{nm} \longrightarrow 1550\,\mathrm{nm} + 3393.4\,\mathrm{nm}$ in lithium niobate).

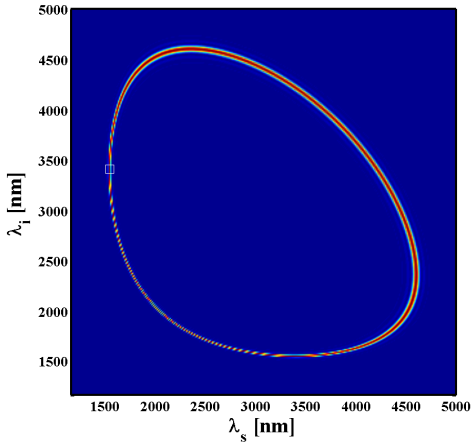


(a) $e \longrightarrow e + e$, LN,
$\Lambda = 30\,\mu\text{m}$

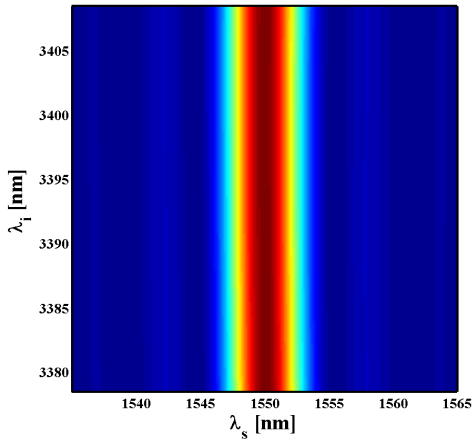


(b) $e \longrightarrow e + e$, LN,
$\Lambda = 30\,\mu\text{m}$

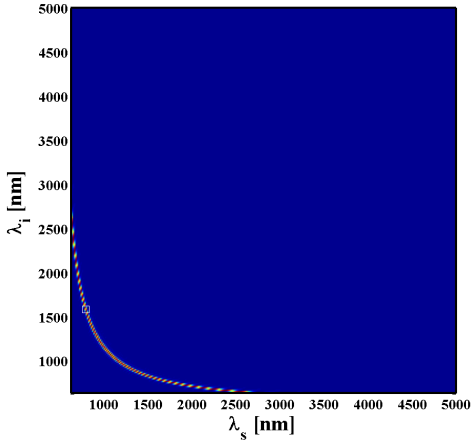


(c) $o \longrightarrow e + e$, KTP,
$\Lambda = 3.8\,\mu\text{m}$

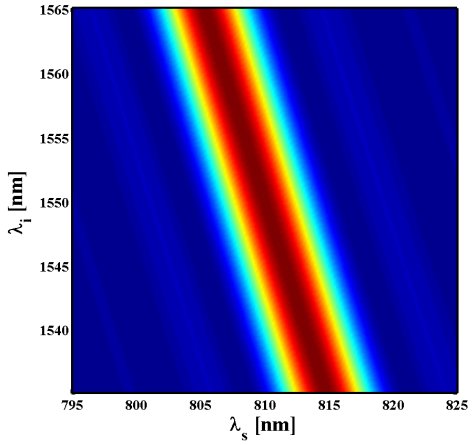


(d) $o \longrightarrow e + e$, KTP,
$\Lambda = 3.8\,\mu\text{m}$

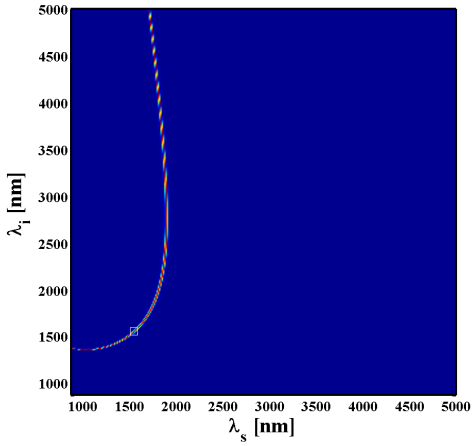


(e) $e \longrightarrow o + e$, KTP,
$\Lambda = 46.1\,\mu\text{m}$

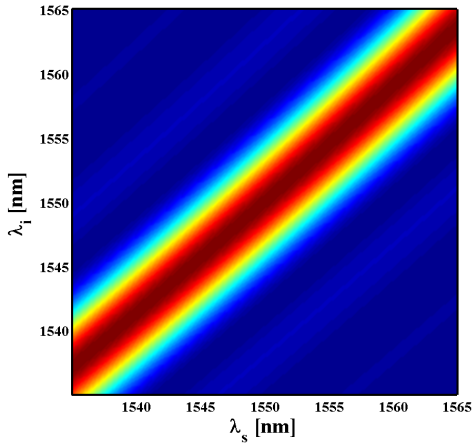


(f) $e \longrightarrow o + e$, KTP,
$\Lambda = 46.1\,\mu\text{m}$

Figure 4.5: Three examples of the phase-matching intensity $|\psi(\omega_s, \omega_i)|^2$. The plots correspond to type 0 SPDC from 1064 nm to 1550 nm and 3393.4 nm in LN (first row), type I from 532 nm to 810 nm and 1550 nm in KTP (second row) and type II from 775 nm to two times 1550 nm in KTP (third row). The figures within one row are equivalent to each other, the only difference being range of plotted $\lambda_s$ and $\lambda_i$. The wavelength regions plotted on the right are marked by a white square in the respective plot on the left side.

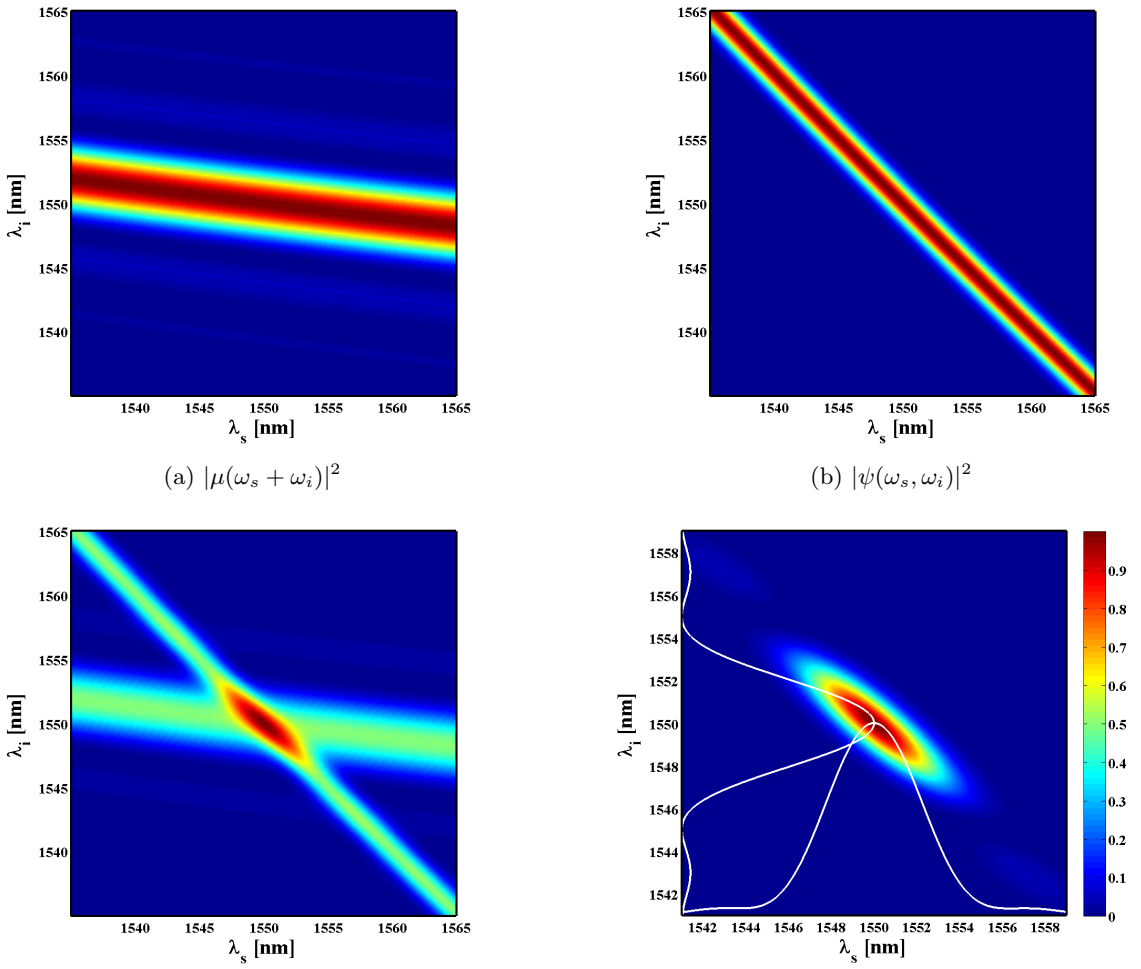


(a) $|\mu(\omega_s + \omega_i)|^2$

(b) $|\psi(\omega_s, \omega_i)|^2$

(c) $|\mu|^2 + |\psi|^2$

(d) $F = |\mu\psi|^2$

Figure 4.6: Graphical illustration of the composition of the joint spectral intensity $F(\omega_s, \omega_i)$. The plots describe a type II down-conversion from 775 nm to two times 1550 nm in LN. Figure (a) shows the pump intensity $|\mu(\omega_s+\omega_i)|^2$; Figure (b) shows the phase-matching intensity $|\psi(\omega_s, \omega_i)|^2$; Figure (c) depicts how the intersection of both shapes the JSI; and Figure (d) shows the JSI, $F = |\mu\psi|^2$, with spectral shape of signal and idler output.

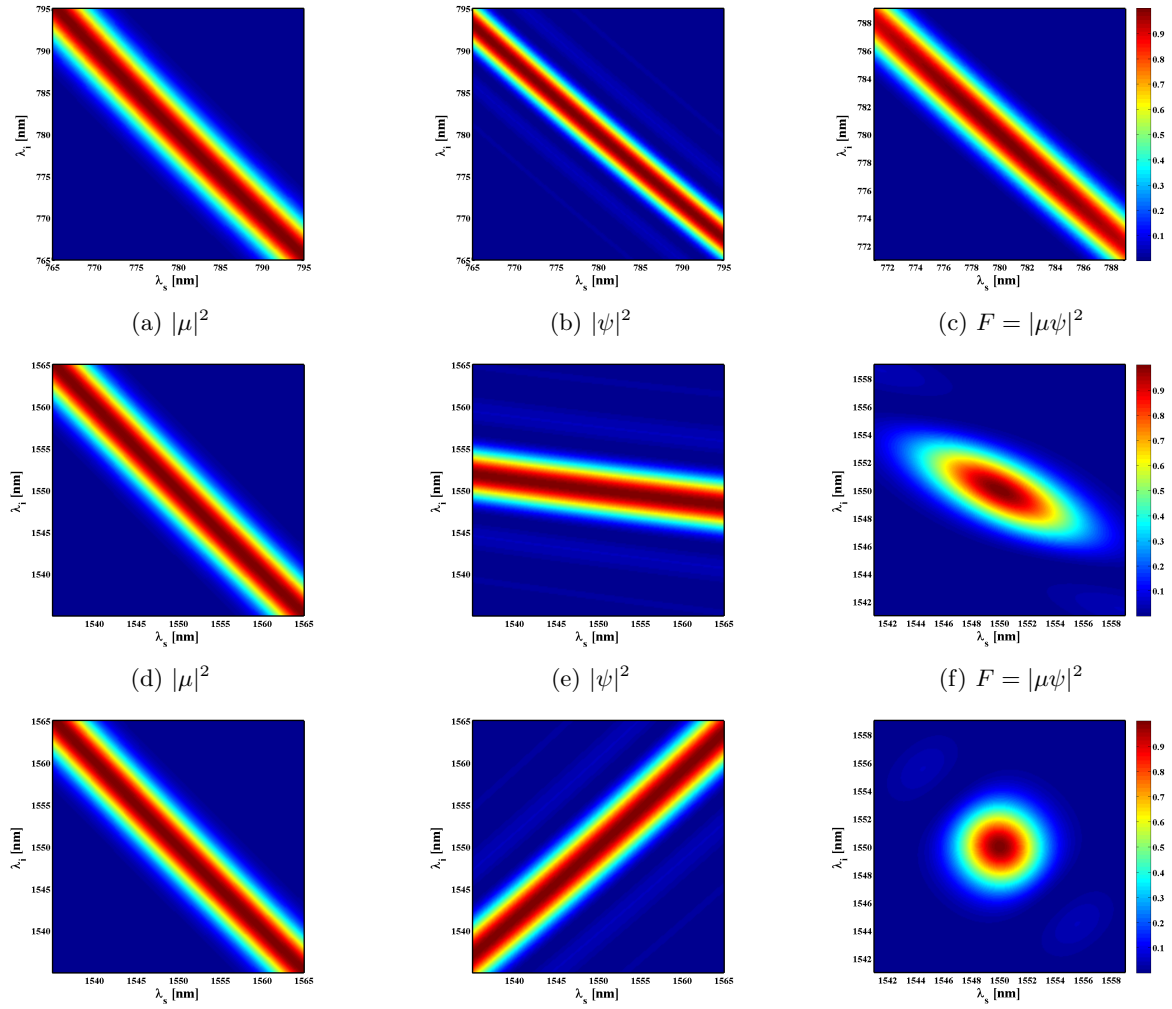


(a) $|\mu|^2$ (b) $|\psi|^2$ (c) $F = |\mu\psi|^2$

(d) $|\mu|^2$ (e) $|\psi|^2$ (f) $F = |\mu\psi|^2$

(g) $|\mu|^2$ (h) $|\psi|^2$ (i) $F = |\mu\psi|^2$

Figure 4.7: Illustration of how the graphical orientation of $|\mu|^2$ and $|\psi|^2$ towards each other determines the shape of the joint spectral intensity. The first row illustrates a type II down-conversion from 390 nm to two times 780 nm in LN. We see that if $|\psi|^2$ and $|\mu|^2$ do not intersect in a finite spectral region but basically overlap, then the output fields are highly correlated. The lower two rows show the composition of the JSI for type II SPDC from 775 nm to two times 1550 nm in LN (second row) and KTP (third row). The plots emphasise that in order to achieve a circular shape of the JSI, the graphical representations of $|\psi|^2$ and $|\mu|^2$ should be oriented orthogonally to each other, which is the case in the third row.

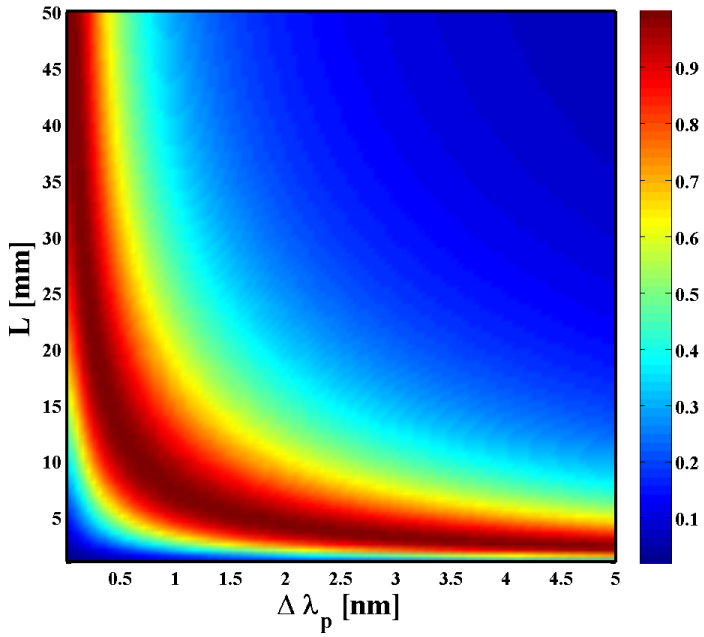


Figure 4.8: Spectral purity $\mathcal{P}$ versus spectral pump width $\Delta\lambda_p$ and crystal length $L$ for a specific SPDC process (here: type II, 775 nm $\longrightarrow 2 \times 1550$ nm in KTP). Along the dark red region of $\mathcal{P} \sim 1$ the output varies only in the spectral width of signal and idler as illustrated in Figure 4.9.

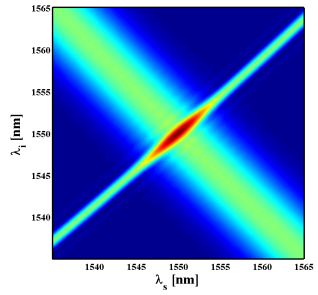


(a) $\Delta\lambda_p = 1.5\,\text{nm}/\tau = 0.25\,\text{ps}$, $L = 30\,\text{mm}$

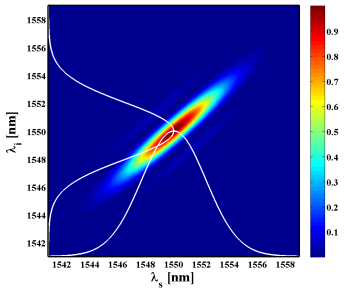


(b) $\Delta\lambda_{s/i} = 2.35/2.10\,\text{nm}$

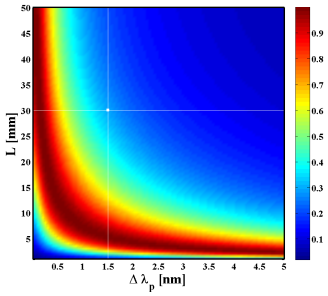


(c) $\mathcal{P} = 0.298$

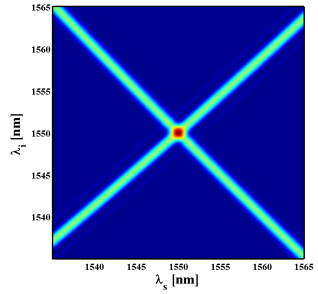


(d) $\Delta\lambda_p = 0.24\,\text{nm}/\tau = 1.563\,\text{ps}$, $L = 30\,\text{mm}$

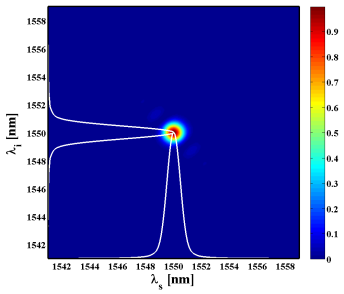


(e) $\Delta\lambda_{s/i} = 0.51/0.46\,\text{nm}$

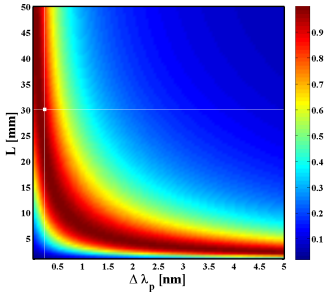


(f) $\mathcal{P} = 0.991$

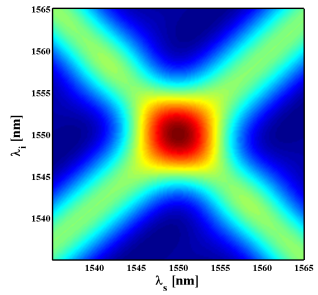


(g) $\Delta\lambda_p = 1.5\,\text{nm}/\tau = 250\,\text{ps}$, $L = 4.6\,\text{mm}$

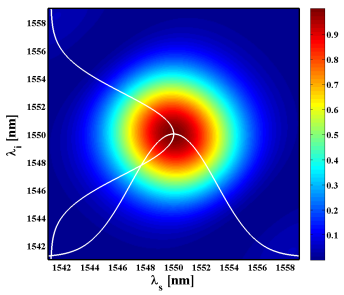


(h) $\Delta\lambda_{s/i} = 3.07/2.91\,\text{nm}$

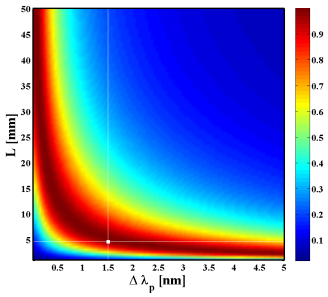


(i) $\mathcal{P} = 0.996$

Figure 4.9: Engineering high purity states. The process is a type II SPDC from 775 nm to two times 1550 nm in KTP. In the first row the spectral width of the pump light $\Delta\lambda_p$ and the crystal length $L$ do not match which leads to (b) an oval shape of the JSI and therefore (c) low spectral purity $\mathcal{P}$ of the single photon states; this can be corrected by either by narrowing the spectral pump width (second row) or by using a shorter crystal (third row).

## 4.3 Implications on HOM Visibility

Consider the experimental setup illustrated in Figure 4.10, designed to measure Hong-Ou-Mandel (HOM) interference. Two photon pairs are generated by type II SPDC using laser pulses which—by a 50/50 beamsplitter—were separated into two in order to simultaneously impinge two identical non-linear crystals. Polarising beamsplitters separate the respective pairs such that the detection of the idler photon heralds the arrival of a signal photon. When identical signal photons, $s_A$ and $s_B$, arrive simultaneously at the beamsplitter ($BS_2$) one of them will always be reflected whereas the other one will be transmitted. In other words, they will never be both reflected or both transmitted, hence the two detectors $Det._0$ and $Det._1$ will not be triggered simultaneously. This is referred to as the Hong-Ou-Mandel effect.

The visibility of HOM interference depends on the temporal and spectral indistinguishability of the arriving quanta. As pointed out elaborately earlier in this chapter the pulse duration of the pump laser and the length of the crystal play a decisive role in the setup. Just as a narrow pump spectrum corresponds to a long pulse duration, the narrow phase-matching amplitude of a long crystal corresponds to a longer temporal spread. Short pulses (broad spectrum) travelling through comparatively long crystals (narrow spectrum, broad temporal amplitude) will generate temporally coherent photon pairs, but their spectral correlation will make them distinguishable (Figure 4.11 (a)). Contrariwise, long pulses in comparatively short crystals will generate photon pairs with high spectral coherence but with low temporal concurrence (Figure 4.11 (b)). This scenario is brought to an extreme when a continuous-wave (CW) laser is used as a pump source for down-conversion. In this case the photon pairs generated within the crystals are each produced at random times and carry therefore no temporal correlation at all. Both scenarios mentioned above result in poor HOM visibility. When pulse duration and crystal length are matched such that the envelope amplitudes of pump and output fields overlap in the time *and* frequency picture (Figure 4.12), then the photons carry no more information about their origin and will interfere at the beamsplitter.

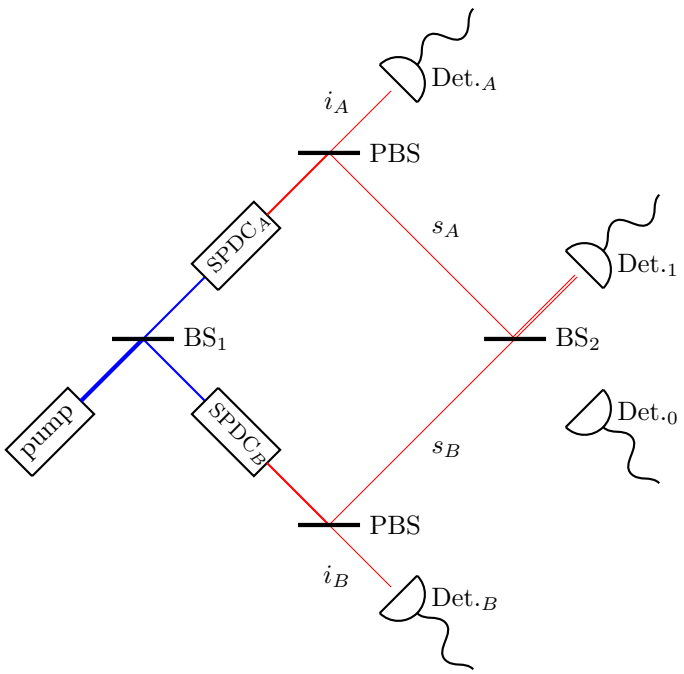


Figure 4.10: Setup of the Hong-Ou-Mandel interference experiment. The pulses of the pump laser are split in half ($BS_1$) and travel simultaneously through two non-linear crystals, generating photon pairs due to type II spontaneous parametric down-conversion ($SPDC_{A/B}$). Polarising beamsplitters (PBS) separate the photons within one pair with respect to polarisation. The idler photons trigger the heralding detectors ($Det._{A/B}$), announcing the arrival of a signal photon at the beamsplitter ($BS_2$). When indistinguishable photons arrive simultaneously at the BS they will exit together and no coincidence counts will be recorded by the detectors ($Det._{0/1}$).

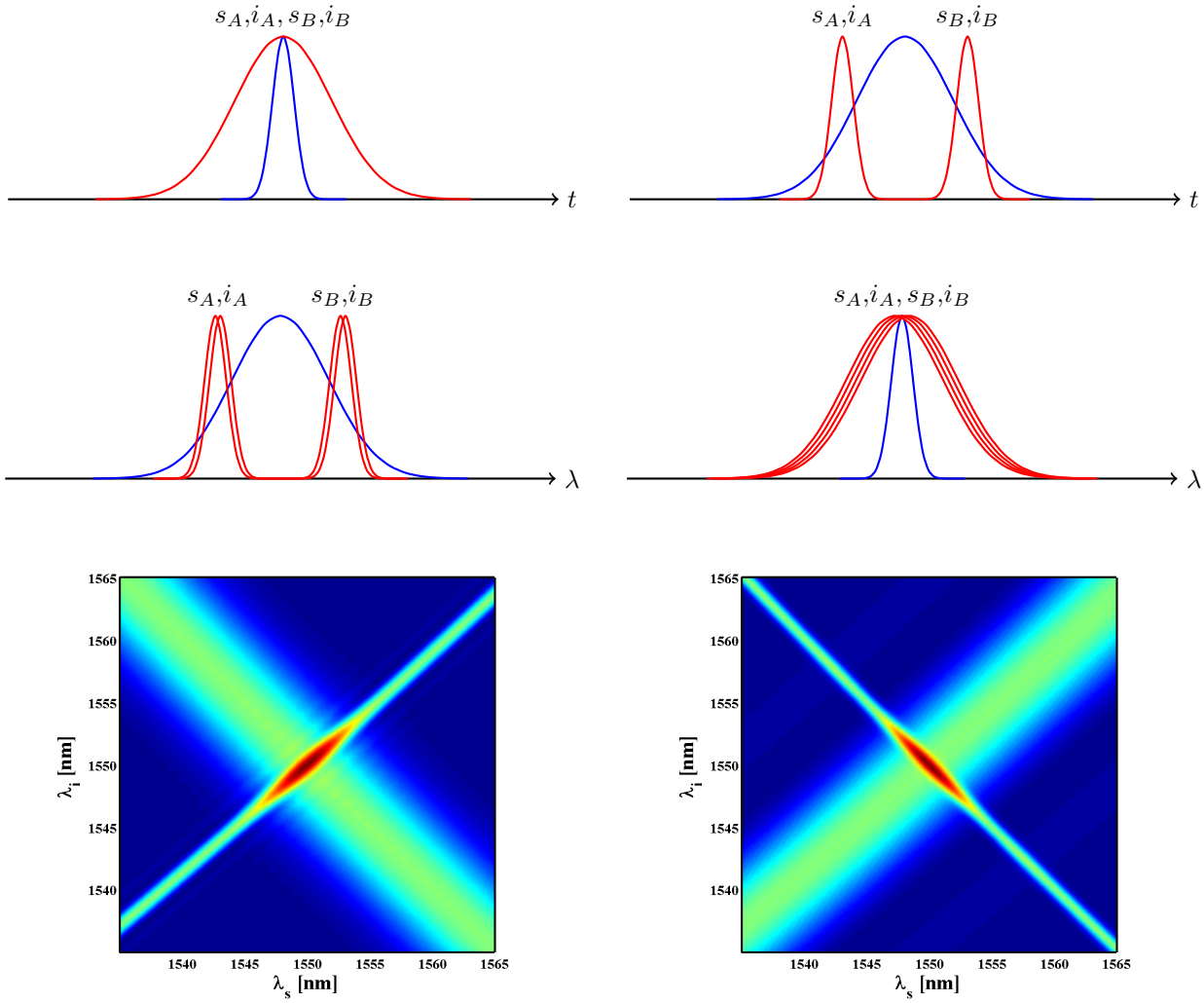


(a) (b)

Figure 4.11: Two examples for unmatched pulse duration and crystal length. In Figure (a) a short pulse (blue) with broad frequency spectrum travels through a crystal which—due to its extensive length—generates narrow output spectra (red). In this case the temporal envelope amplitude of the generated pairs overlaps with the one of the pump laser, thus allowing for temporal coherence and simultaneous arrival at the beamsplitter. However, the frequency correlation within the photon pairs makes them distinguishable, therefore undermining HOM visibility. Figure (b) depicts the opposite case where a laser with long pulse duration impinges a short crystal. In this case the output fields will be spectrally coherent but will in turn be temporally distinguishable.

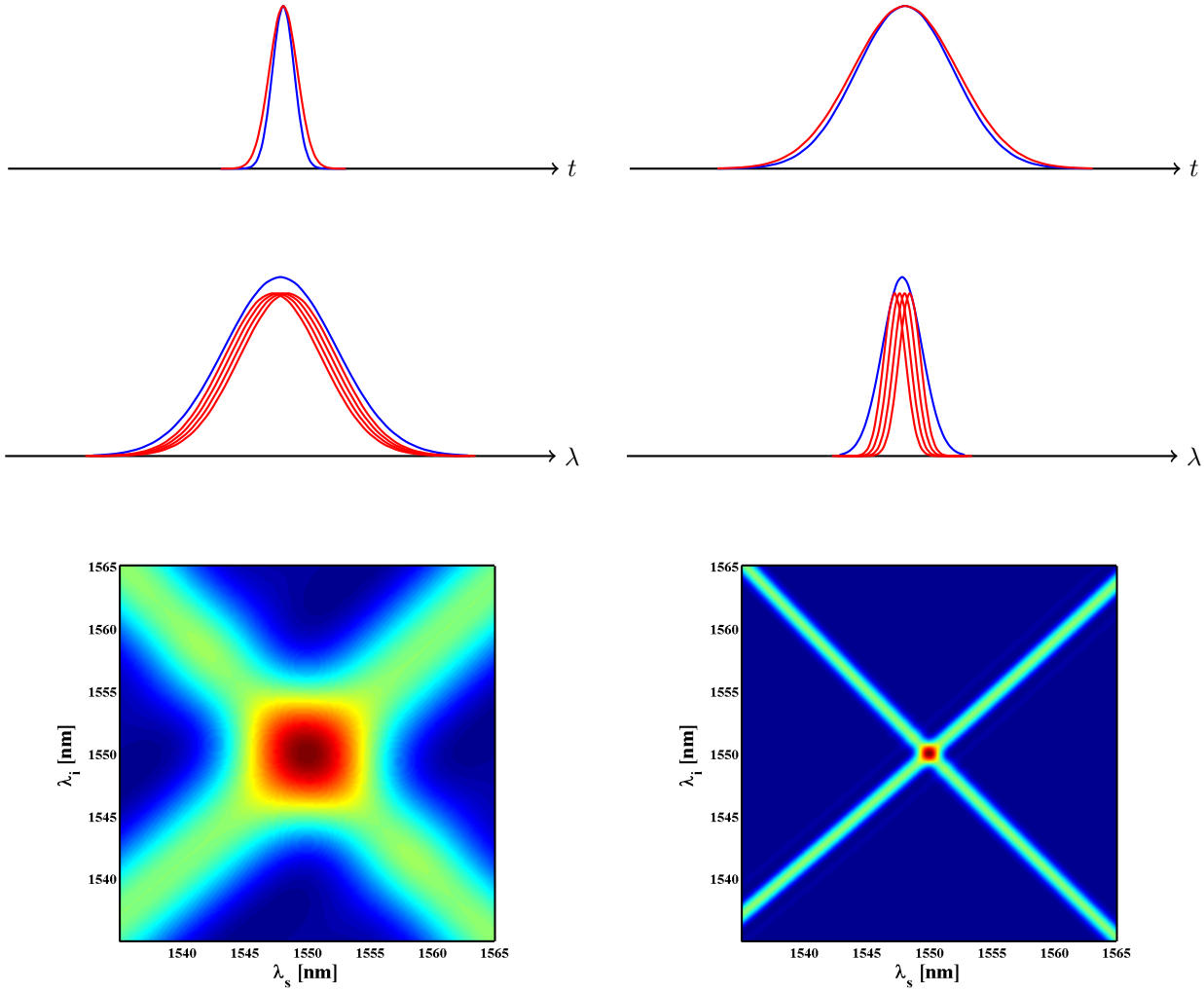


(a) (b)

Figure 4.12: Two examples of matched pulse duration and crystal length. When the temporal *and* spectral envelope amplitudes of pump and output radiation overlap, then the photons arriving at the beamsplitter will be indistinguishable and simultaneous, thus allowing for high HOM visibility.

## 4.4 Summary

The signal and idler single photon states can be considered spectrally pure when the joint spectral amplitude $f(\omega_s, \omega_i) = \mu(\omega_s + \omega_i)\psi(\omega_s, \omega_i)$ of the SPDC process is separable in terms of signal and idler frequency, i.e. when

$$f(\omega_s, \omega_i) = f_s(\omega_s) f_i(\omega_i).$$

The degree of separability can be evaluated by examination of the Schmidt components of the bipartite state $|\Psi\rangle$. The Schmidt components can be found by a singular value decomposition of a matrix $\mathcal{F}$ whose elements are the joint spectral amplitudes for discretised signal and idler frequencies: $\mathcal{F}^{mn} = f(\omega_{s,m}, \omega_{i,n})$. We find that in order to engineer a separable joint spectral intensity $F = |\mu\psi|^2$ the pump intensity $|\mu|^2$ and the phase-match intensity $|\psi|^2$ have to be oriented orthogonally to each other, which is only the case for a very limited amount of SPDC processes, thus submitting the approach of engineering intrinsically pure states to a natural restriction. The choice of non-linear crystal may influence strongly the way $|\mu|^2$ and $|\psi|^2$ intersect and should therefore be taken into account. If $|\mu|^2$ and $|\psi|^2$ can be oriented orthogonally then a purity $\mathcal{P} \sim 1$ can be achieved by appropriate choice of crystal length and pulse duration of the pump laser.

# Chapter 5

# Numerical Results

We use our self-written program *QPMoptics* (source code in Appendix B) in order to investigate the phase-matching conditions, output spectra and state purity of a variety of different SPDC setups. First we examine the phase-matching conditions of frequency-degenerate SPDC with 390 and 780 nm pump in all kinds of polarisation configurations and both kinds of periodically poled crystals, ppKTP and ppLN. Afterwards we focus on frequency-degenerate type II SPDC with signal and idler in the telecom band, where we compare the performance of the two crystals as well different crystal lengths and pulse durations. Finally we investigate both crystals for further setups that offer promising opportunities for generation of intrinsically pure quantum states.

## 5.1 Frequency-degenerate SPDC with 390 nm and 780 nm Pump

In this section we consider quasi phase-matching for the down-conversion processes

- $390\,\mathrm{nm} \longrightarrow 780\,\mathrm{nm} + 780\,\mathrm{nm}$,
- $780\,\mathrm{nm} \longrightarrow 1560\,\mathrm{nm} + 1560\,\mathrm{nm}$,

each in all kind of polarisation configurations and in both kinds of periodically poled crystals, KTP and LN. We find that for most of these processes the joint spectral intensity is highly correlated due to the overlap of pump envelope intensity $|\mu(\omega_s + \omega_i|^2$ and phase-match intensity $|\psi(\omega_s, \omega_i|^2$, an example of which is depicted in the first row of Figure 4.7. In these cases the high spectral correlation of signal and idler has to be conquered by according bandpass filters in both channels. There are however processes which *do* allow for high spectral purity without filters, for example a type II down-conversion with signal and idler in the telecom regime. This process will be discussed in more detail in the next section. Table 5.1 shows the collected poling periodicities $\Lambda$ required for QPM for all types of frequency-degenerated down-conversion with 390 and 780 nm pump in both crystals at 50 °C. Figures 5.1 and 5.2 depict the phase-matching envelope intensities $|\mu(\omega_s, \omega_i)|^2$ for three kinds of SPDC in both crystals.

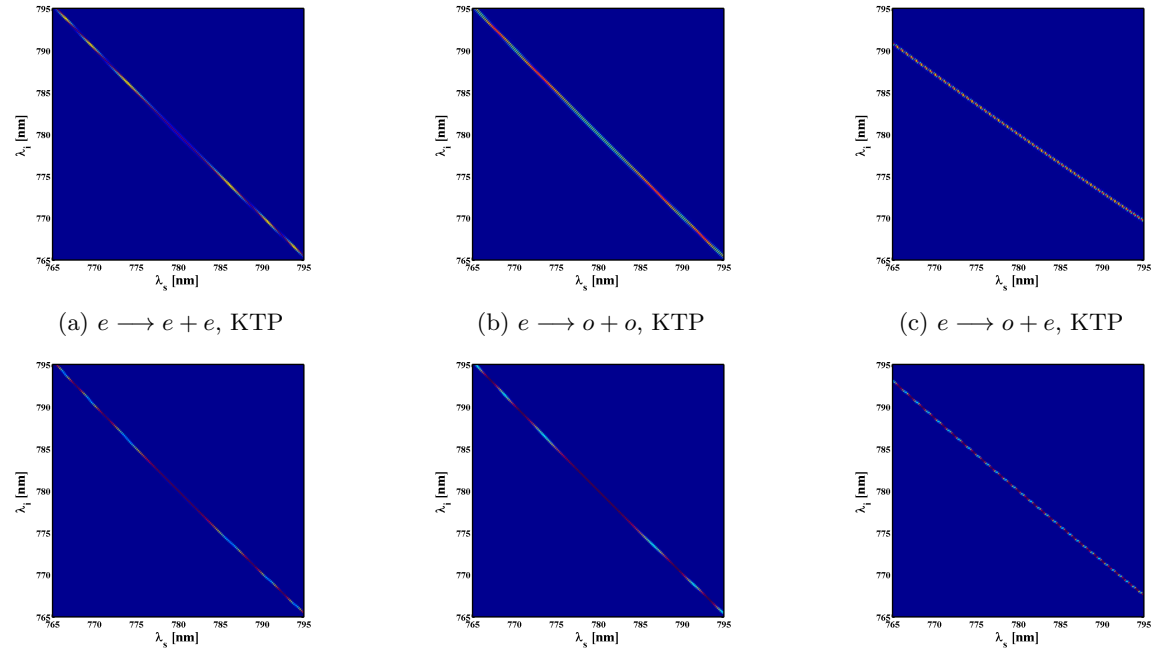


(a) $e \longrightarrow e + e$, KTP (b) $e \longrightarrow o + o$, KTP (c) $e \longrightarrow o + e$, KTP

(d) $e \longrightarrow e + e$, LN (e) $e \longrightarrow o + o$, LN (f) $e \longrightarrow o + e$, LN

Figure 5.1: Phase-matching envelope intensities for type 0, I and II SPDC from 390 nm to two times 780 nm in KTP (first row) and LN (second row). All plots correspond to a crystal length of 8 mm.

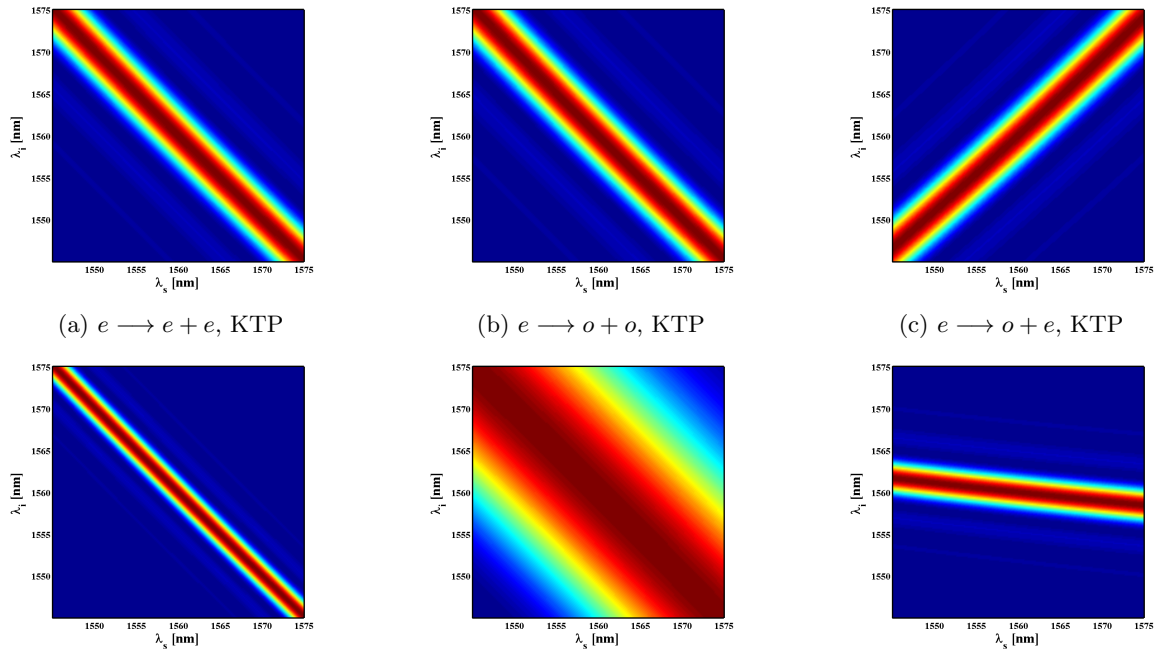


(a) $e \longrightarrow e + e$, KTP (b) $e \longrightarrow o + o$, KTP (c) $e \longrightarrow o + e$, KTP

(d) $e \longrightarrow e + e$, LN (e) $e \longrightarrow o + o$, LN (f) $e \longrightarrow o + e$, LN

Figure 5.2: Phase-matching envelope intensities for type 0, I and II SPDC from 780 nm to two times 1560 nm in KTP (first row) and LN (second row). All plots correspond to a crystal length of 8 mm. Here only in the case of (c) type II SPDC in KTP the orientation of $|\psi|^2$ allows for orthogonal intersection with the pump envelope intensity $|\mu|^2$. Also note the relatively broad output spectrum of (e) type I SPDC in LN.

| Crystal | SPDC Type | | Poling Periodicity $\Lambda$ [µm] | |
|---|---|---|---|---|
| | | | 390 nm $\longrightarrow 2 \times 780$ nm | 780 nm $\longrightarrow 2 \times 1560$ nm |
| KTP | 0 | $o \longrightarrow o + o$ | 2.94 | 25.00 |
| | | $e \longrightarrow e + e$ | 4.13 | 32.37 |
| | I | $o \longrightarrow e + e$ | 1.76 | 6.89 |
| | | $e \longrightarrow o + o$ | 73.98 | -13.46 |
| | II | $o \longrightarrow o + e$ | 2.20 | 10.80 |
| | | $e \longrightarrow o + e$ | 7.82 | -46.07 |
| LN | 0 | $o \longrightarrow o + o$ | 1.99 | 16.55 |
| | | $e \longrightarrow e + e$ | 2.34 | 19.16 |
| | I | $o \longrightarrow e + e$ | 1.41 | 6.52 |
| | | $e \longrightarrow o + o$ | 4.43 | -24.57 |
| | II | $o \longrightarrow o + e$ | 1.65 | 9.36 |
| | | $e \longrightarrow o + e$ | 3.06 | 174.07 |

Table 5.1: Numerical results for required poling periodicity in frequency-degenerate SPDC with 390 and 780 nm pump at $T = 50\,°\text{C}$. A minus sign in front of $\Lambda$ is supposed to indicate a negative phase mismatch $\Delta k$ for the specific process, in which case the QPM order $m$ has to go negative as well (Equation (3.28)). All values of $\Lambda$ in this table correspond to a QPM order of $m = \pm 1$. Note that for too small $\Lambda$ ($< 5\,\mu\text{m}$), which cannot be manufactured properly, $m$ may be raised to an odd integer, thus increasing $\Lambda$ by the same factor.

## 5.2 Frequency-degenerate Type II SPDC at Telecom Wavelength

For signal and idler at wavelengths in the regime of telecom networks, numerical calculations predict a good performance (i.e. high spectral purity) in the case of type II down-conversion: $e \longrightarrow o + e$. In this section we pick as an example the process from 780 nm to two times 1560 nm at a temperature of 50 °C. We present two different approaches for tailoring a factorable JSI:

- finding the appropriate pump spectrum for a given crystal length ($L = 20$ and 40 mm; see Table 5.2, Figures 5.4, 5.5 and 5.6),
- finding the appropriate crystal length for a given pump spectrum ($\tau = 0.2$ and 2 ps; see Table 5.3, Figures 5.7, 5.8 and 5.9).

All numerical results and graphical representations in this section show that for the sake of high purity output generation in the frequency-degenerate telecom regime, the crystal KTP ($\mathcal{P} \sim 1$) is clearly more favourable than LN ($\mathcal{P} \sim 0.8$). Figure 5.3 shows plots of the output's spectral purity with respect to $\Delta\lambda_p$ and $L$ in KTP and LN respectively.

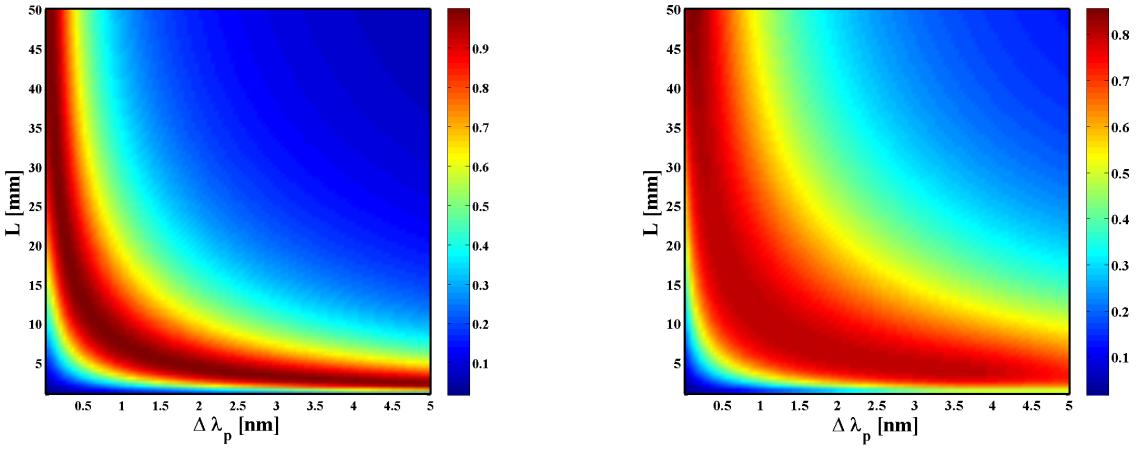


(a) KTP (b) LN

Figure 5.3: Purity $\mathcal{P}$ versus spectral pump width $\Delta\lambda_p$ and crystal length $L$ for frequency-degenerate type II SPDC with 780 nm pump in (a) KTP and (b) LN. The plots show that for KTP there exist many configurations for which $\mathcal{P} \sim 1$ whereas with LN a maximal purity of only $\mathcal{P} \sim 0.8$ can be achieved.

| Crystal | $L$ [mm] | $\Delta\lambda_p$ [nm] | $\tau$ [ps] | $\Delta\lambda_s$ [nm] | $\Delta\lambda_i$ [nm] | $\mathcal{P}$ |
|---|---|---|---|---|---|---|
| KTP | 20 | 0.35 | 1.086 | 0.72 | 0.72 | 0.992 |
| | 40 | 0.17 | 2.235 | 0.36 | 0.36 | 0.992 |
| LN | 20 | 0.51 | 0.745 | 1.79 | 0.61 | 0.801 |
| | 40 | 0.28 | 1.357 | 0.97 | 0.31 | 0.801 |

Table 5.2: Spectral pump width, pulse duration and output spectra for optimal purity assuming crystals with 20 and 40 mm length.

| Crystal | $\tau$ [ps] | $\Delta\lambda_p$ [nm] | $L$ [mm] | $\Delta\lambda_s$ [nm] | $\Delta\lambda_i$ [nm] | $\mathcal{P}$ |
|---|---|---|---|---|---|---|
| KTP | 0.2 | 1.9 | 3.6 | 3.94 | 3.78 | 0.998 |
| | 2 | 0.19 | 36.7 | 0.41 | 0.41 | 0.992 |
| LN | 0.2 | 1.9 | 5.3 | 6.47 | 2.07 | 0.834 |
| | 2 | 0.19 | 55.3 | 0.66 | 0.26 | 0.801 |

Table 5.3: Crystal length and output spectra for optimal purity assuming pump pulses of 200 fs and 2 ps duration.

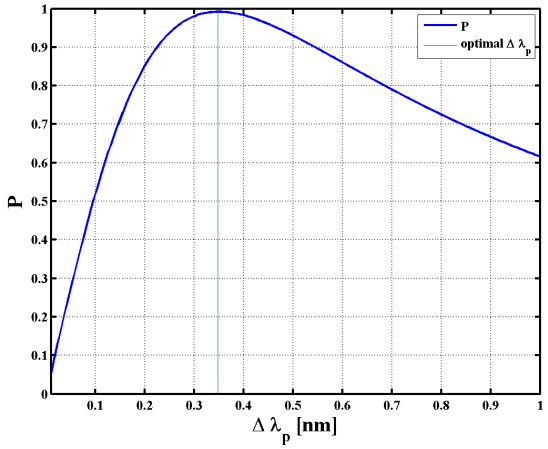


(a) KTP, $L = 20\,\mathrm{mm}$

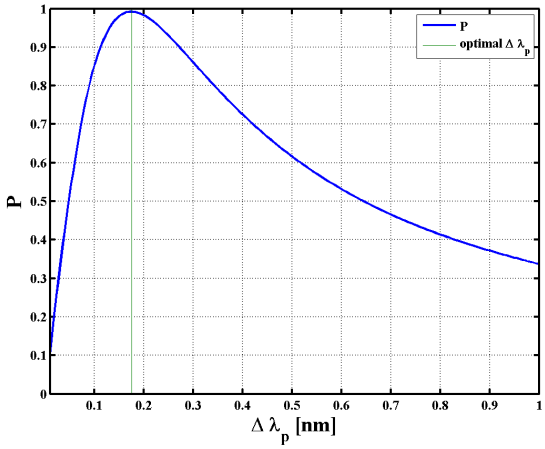


(b) KTP, $L = 40\,\mathrm{mm}$

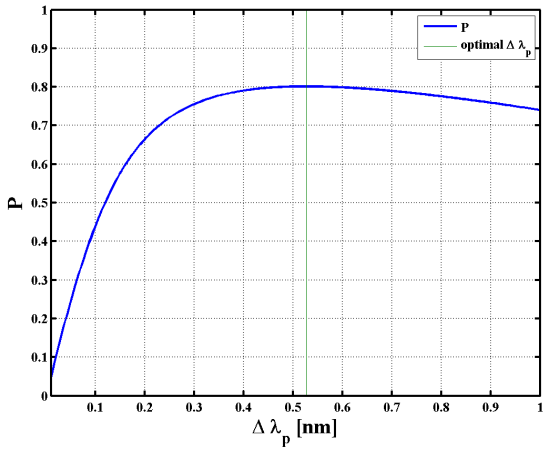


(c) LN, $L = 20\,\mathrm{mm}$

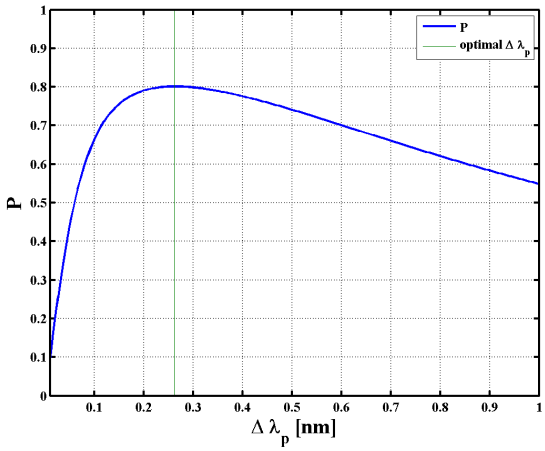


(d) LN, $L = 40\,\mathrm{mm}$

Figure 5.4: Purity $\mathcal{P}$ with respect to spectral pump width $\Delta\lambda_p$ for (a,b) KTP and (c,d) LN at (a,c) $L = 20\,\mathrm{mm}$ and (b,d) $L = 40\,\mathrm{mm}$.

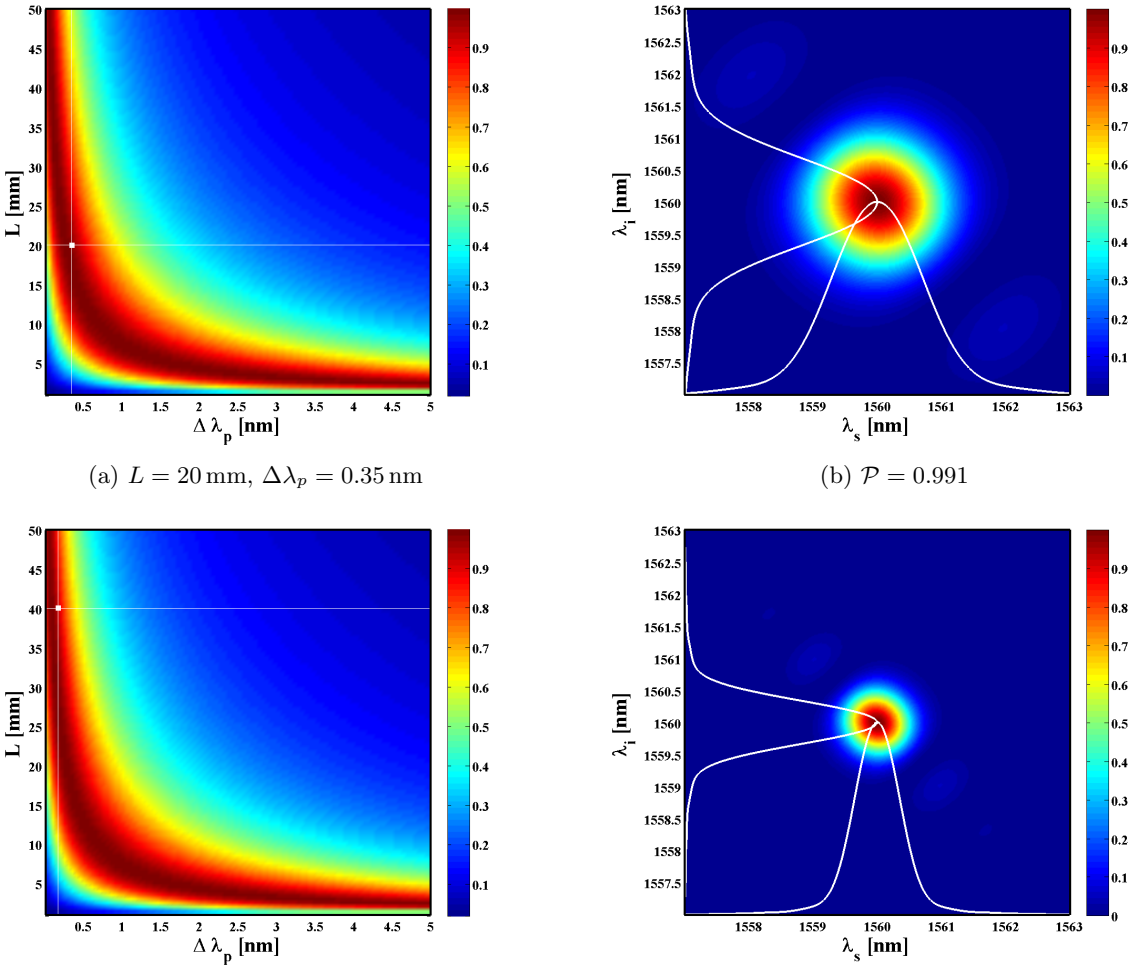


(a) $L = 20\,\mathrm{mm}$, $\Delta\lambda_p = 0.35\,\mathrm{nm}$

(b) $\mathcal{P} = 0.991$

(c) $L = 40\,\mathrm{mm}$, $\Delta\lambda_p = 0.17\,\mathrm{nm}$

(d) $\mathcal{P} = 0.992$

Figure 5.5: Joint spectral intensity and respective purity for (a,b) $L = 20\,\mathrm{mm}$ and (c,d) $L = 40\,\mathrm{mm}$ in KTP. The respective configuration of pump width and crystal length is marked by the intersection of the white lines in the purity plots (a,c).

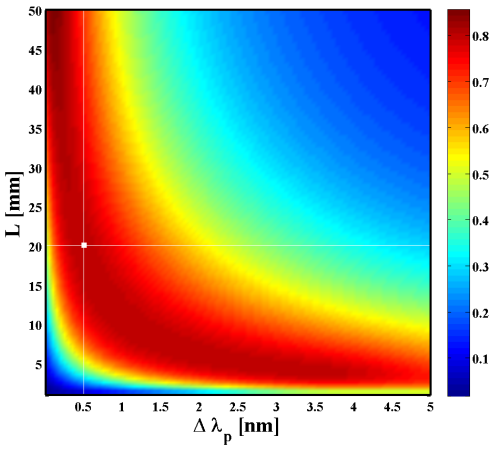


(a) $L = 20\,\mathrm{mm}$, $\Delta\lambda_p = 0.51\,\mathrm{nm}$

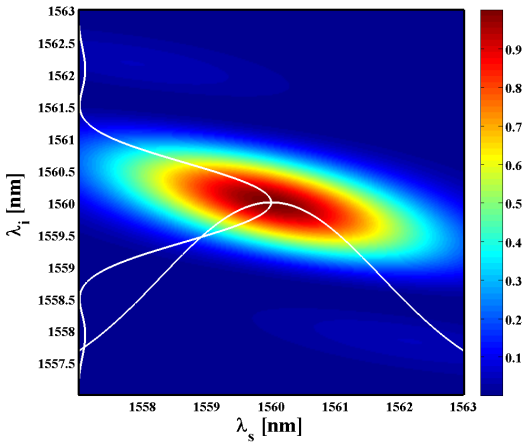


(b) $\mathcal{P} = 0.801$

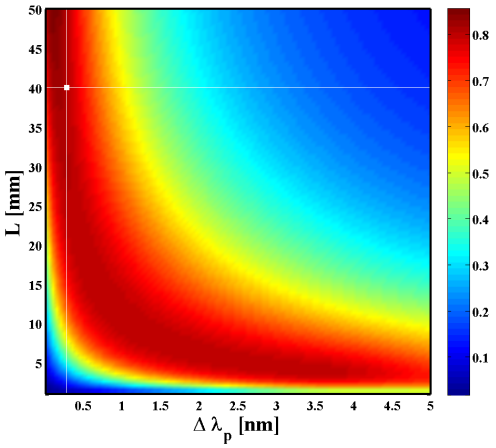


(c) $L = 40\,\mathrm{mm}$, $\Delta\lambda_p = 0.28\,\mathrm{nm}$

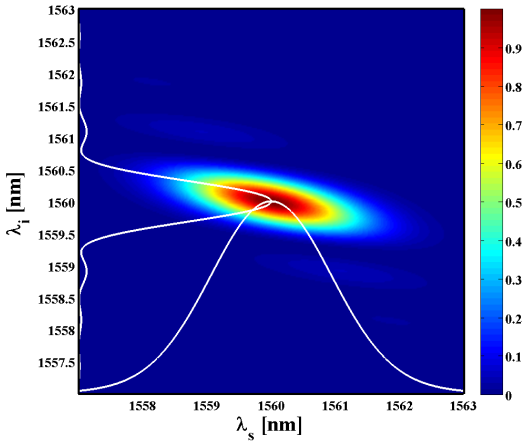


(d) $\mathcal{P} = 0.801$

Figure 5.6: Joint spectral intensity and respective purity for (a,b) $L = 20\,\mathrm{mm}$ and (c,d) $L = 40\,\mathrm{mm}$ in LN.

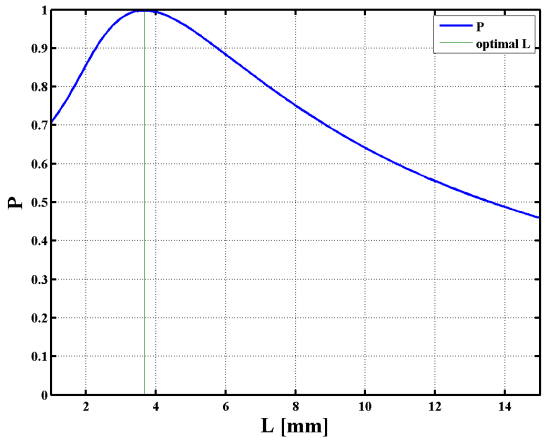


(a) KTP, $\tau = 0.2\,\mathrm{ps}$

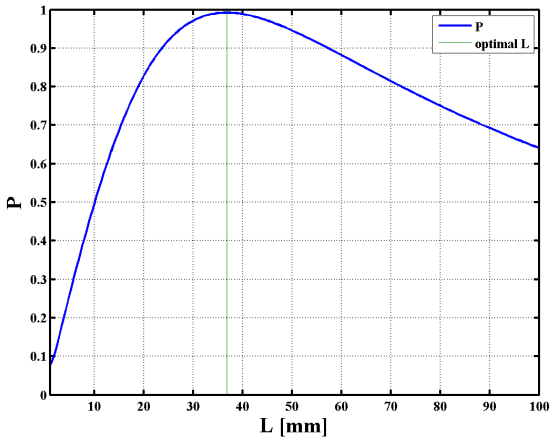


(b) KTP, $\tau = 2\,\mathrm{ps}$

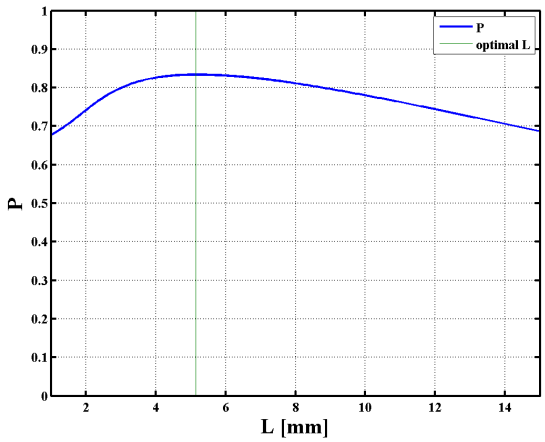


(c) LN, $\tau = 0.2\,\mathrm{ps}$

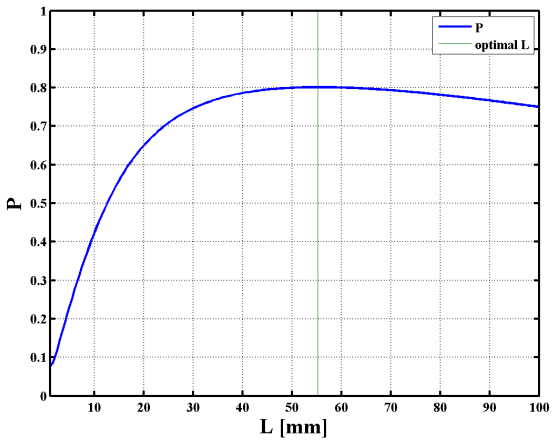


(d) LN, $\tau = 2\,\mathrm{ps}$

Figure 5.7: Purity $\mathcal{P}$ with respect to crystal length $L$ for (a,b) KTP and (c,d) LN at (a,c) $\tau = 0.2\,\mathrm{ps}$ and (b,d) $2\,\mathrm{ps}$.

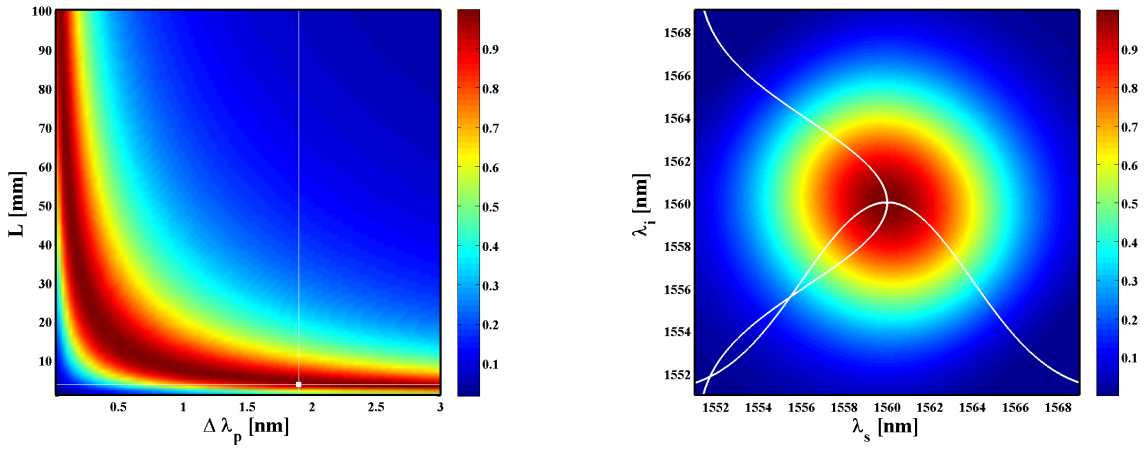


(a) $\tau = 0.2\,\mathrm{ps}$, $L = 3.6\,\mathrm{mm}$ (b) $\mathcal{P} = 0.997$

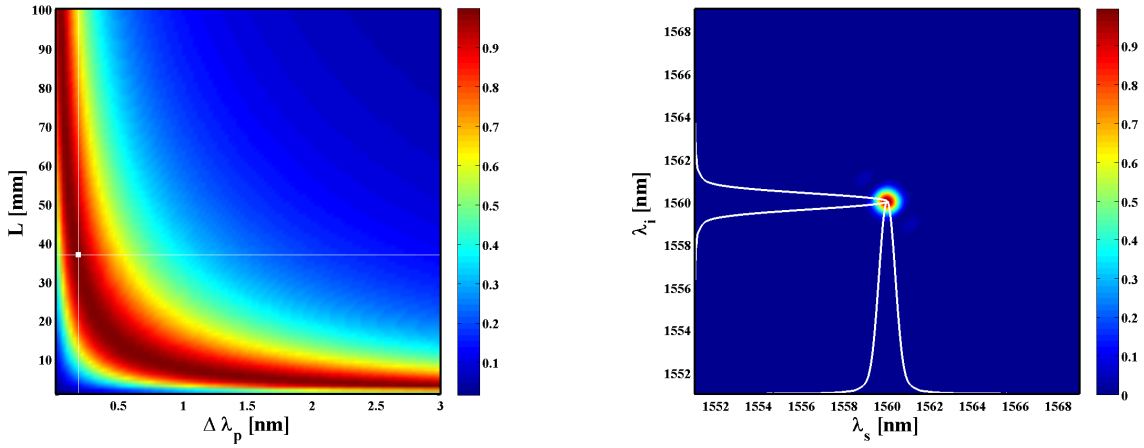


(c) $\tau = 2\,\mathrm{ps}$, $L = 36.7\,\mathrm{mm}$ (d) $\mathcal{P} = 0.992$

Figure 5.8: Joint spectral intensity and respective purity for (a,b) $\tau = 0.2\,\mathrm{ps}$ and (c,d) $\tau = 2\,\mathrm{ps}$ in KTP.

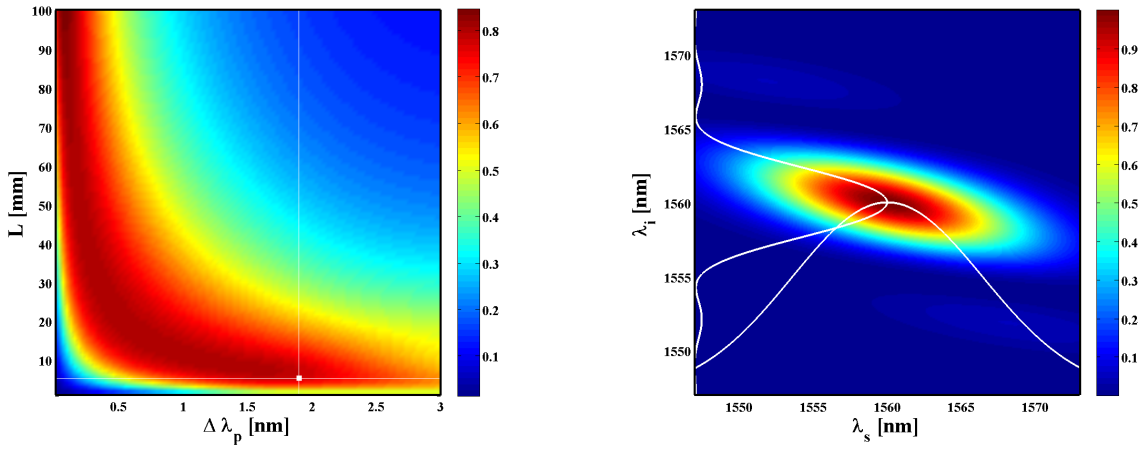


(a) $\tau = 0.2\,\mathrm{ps}$, $L = 5.3\,\mathrm{mm}$

(b) $\mathcal{P} = 0.834$

(c) $\tau = 2\,\mathrm{ps}$, $L = 55.3\,\mathrm{mm}$

(d) $\mathcal{P} = 0.801$

Figure 5.9: Joint spectral intensity and respective purity for (a,b) $\tau = 0.2\,\mathrm{ps}$ and (c,d) $\tau = 2\,\mathrm{ps}$ in LN.

## 5.3 Other Processes of High Spectral Purity

Numerical calculations offer some insight in how maximum spectral purity can be achieved for a given type of down-conversion and periodically poled crystal. By varying the pump wavelength as well as the crystal's periodicity, we are able find a pattern which allows us to predict for which wavelength configuration we can expect pure output states.

In this section we will demonstrate the procedure and present the results for the following cases:

- type II SPDC in lithium niobate,
- type II SPDC in potassium titanyl phosphate,
- type I SPDC in lithium niobate,
- type I SPDC in potassium titanyl phosphate.

### 5.3.1 Type II SPDC in LN

As seen in Section 5.2 lithium niobate is not the crystal of choice for frequency-degenerate SPDC in the telecom regime. There is however a variety of phase-matched down-conversion processes which do allow for spectrally pure output states. The plots in Figure 5.10 show the overlap of pump envelope intensity $|\mu|^2$ and QPM envelope intensity $|\psi|^2$ for a fixed pump wavelength $\lambda_p$ and varying crystal periodicity $\Lambda$. For a certain range of $\Lambda$ the two functions are oriented orthogonally to each other, thus offering the opportunity for an uncorrelated JSI. For a given pump wavelength the wavelengths of the pure output states depend on the periodicity which allows only for specific wavelength configurations due to the phase-matching condition; and it is possible to find such configurations for each pump wavelength between 650 and 1500 nm, as seen in Figure 5.11. (Pump wavelengths beyond this range can also achieve an uncorrelated JSI, but only with signal or idler wavelength above 5 µm and will therefore not be considered here.)

Investigation of Figure 5.11 shows that for a pump source of $\lambda_p = 1000\,\text{nm}$ we can achieve pure and frequency-degenerate output states with $\lambda_s = \lambda_i = 2000\,\text{nm}$. Moreover, Figure 5.11 (a) shows that in the case of $\lambda_p = 1064\,\text{nm}$ the signal wavelength asymptotically approaches 2200 nm as the periodicity $\Lambda$ goes to infinity. This indicates that for type II down-conversion from 1064 nm to 2200 nm and 2060.6 nm with spectrally pure output states no periodic poling at all is required. The JSI for these processes is depicted in Figure 5.12.

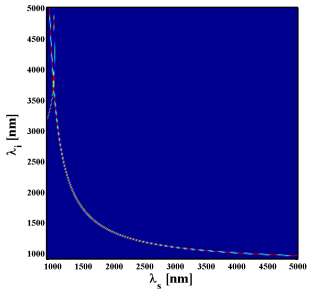


(a) $\Lambda = 35\,\mu\text{m}$,
$\lambda_{s/i} = 1017/3749.3\,\text{nm}$

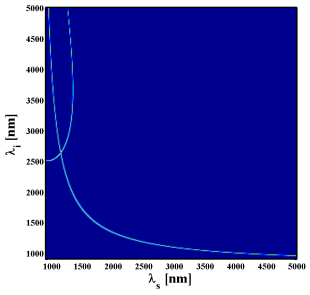


(b) $\Lambda = 55\,\mu\text{m}$,
$\lambda_{s/i} = 1154/2607.9\,\text{nm}$

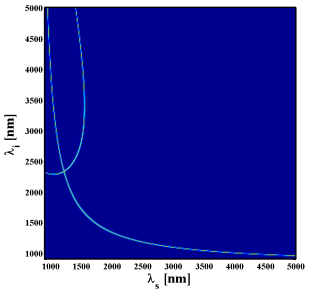


(c) $\Lambda = 75\,\mu\text{m}$,
$\lambda_{s/i} = 1223/2313\,\text{nm}$

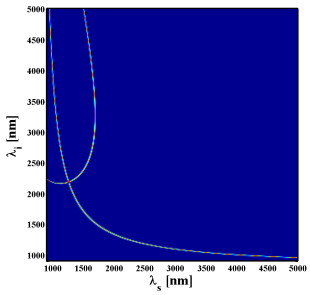


(d) $\Lambda = 95\,\mu\text{m}$,
$\lambda_{s/i} = 1265/2167.3\,\text{nm}$

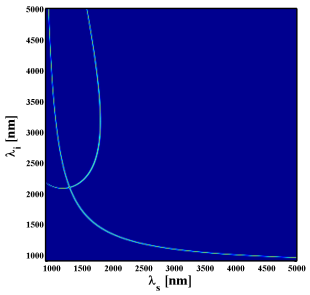


(e) $\Lambda = 115\,\mu\text{m}$,
$\lambda_{s/i} = 1290/2106.1\,\text{nm}$

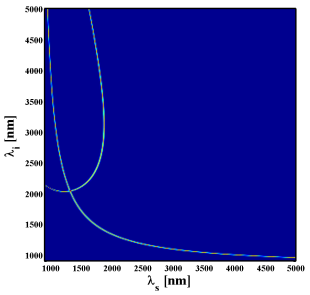


(f) $\Lambda = 135\,\mu\text{m}$,
$\lambda_{s/i} = 1318/2035.5\,\text{nm}$

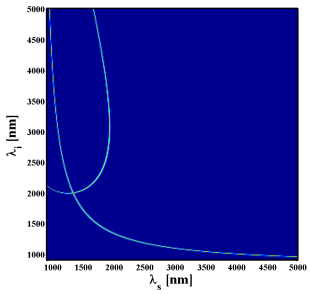


(g) $\Lambda = 155\,\mu\text{m}$,
$\lambda_{s/i} = 1331/2005.3\,\text{nm}$

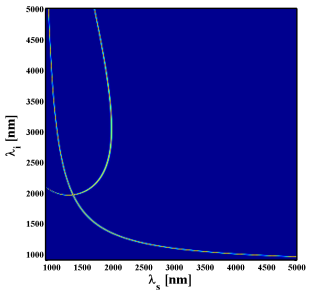


(h) $\Lambda = 175\,\mu\text{m}$,
$\lambda_{s/i} = 1351/1961.5\,\text{nm}$

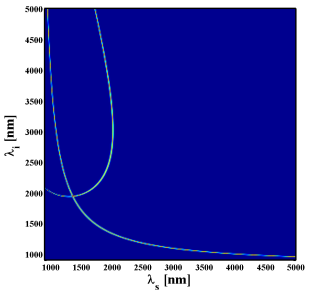


(i) $\Lambda = 195\,\mu\text{m}$,
$\lambda_{s/i} = 1358/1947\,\text{nm}$

Figure 5.10: Type II SPDC ($e \longrightarrow o + e$) in LN; plots of $|\mu|^2 + |\psi|^2$ for fixed $\lambda_p = 800\,\text{nm}$ and varying $\Lambda$. Figures (d,e,f) illustrate that for a given range of $\Lambda$ the two functions are oriented orthogonally, allowing for pure output states. For a given pump wavelength each $\Lambda$ determines uniquely the centre wavelength of signal and idler radiation due to the phase-matching condition.

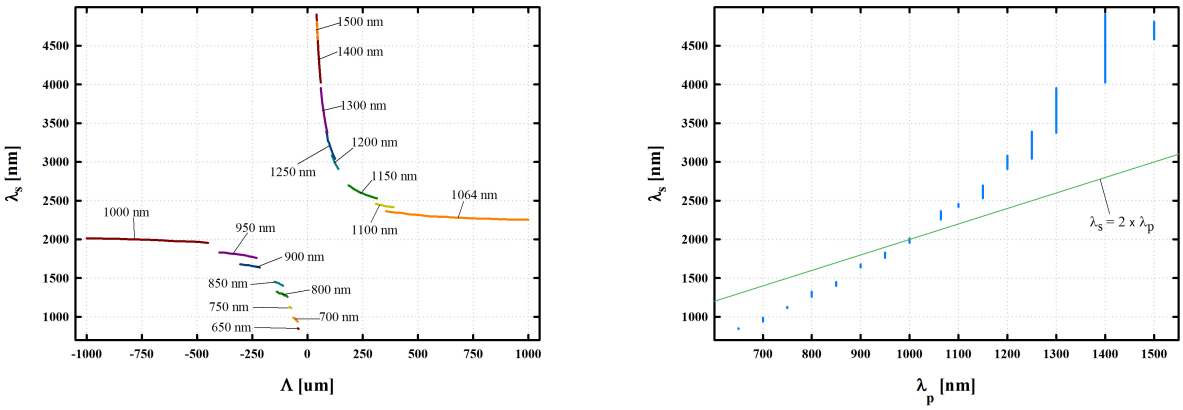


(a) (b)

Figure 5.11: Signal wavelength versus (a) crystal periodicity $\Lambda$ and (b) pump wavelength $\lambda_p$ for type II SPDC ($e \longrightarrow o + e$) in LN. Both plots exclusively display configurations which allow for an uncorrelated JSI (provided matched pump spectrum and crystal length). A negative periodicity in Figure (a) corresponds to QPM order $m = -1$. Each coloured line in Figure (a) corresponds to a certain $\lambda_p$ as denoted in the graph; we see that for pump wavelengths between 1000 and 1064 nm the periodicity approaches infinity, thus enabling spectrally pure output generation without periodic poling. The green line in Figure (b) represents frequency-degenerate SPDC; its intersection with the blue line at $\lambda_p = 1000\,\text{nm}$ illustrates that LN allows for pure output states at $1000\,\text{nm} \longrightarrow 2 \times 2000\,\text{nm}$.

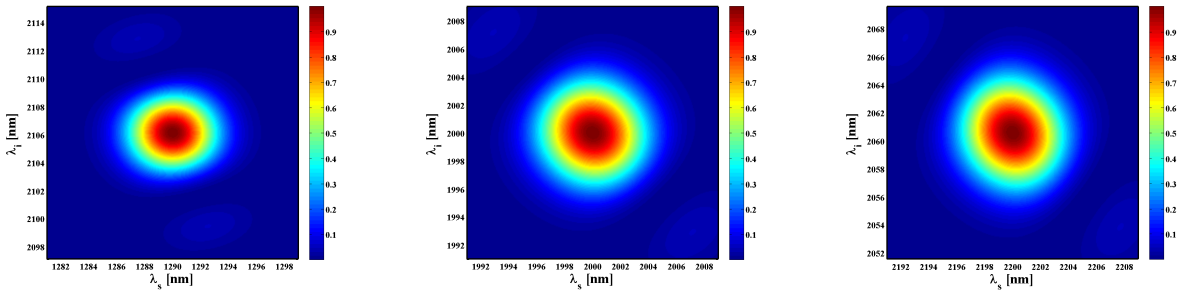


(a) $800\,\text{nm} \longrightarrow 1290\,\text{nm} + 2106.1\,\text{nm}$ (b) $1000\,\text{nm} \longrightarrow 2 \times 2000\,\text{nm}$ (c) $1064\,\text{nm} \longrightarrow 2200\,\text{nm} + 2060.6\,\text{nm}$

Figure 5.12: Three examples of pure output state generation by type II down-conversion in LN. Figure (a) corresponds to the example shown in Figure 5.10; Figure (b) shows a frequency-degenerate down-conversion; and Figure (c) shows a case where no periodic poling of the crystal is required ($\Lambda \geq 2l$).

### 5.3.2 Type II SPDC in KTP

Similarly to the previous subsection we scan $\lambda_p$ as well as $\Lambda$ watching out for orthogonal orientation of the envelope intensities $|\mu(\omega_s + \omega_i)|^2$ and $|\psi(\omega_s, \omega_i)|^2$. We find good opportunities for pure state generation using pump wavelengths between 500 and 1400 nm; for wavelengths beyond this range signal and/or idler wavelengths exceed 5 µm for which reason we neglect these cases. Figure 5.13 shows which configurations of $\lambda_p$, $\lambda_s$ and $\Lambda$ allow for an uncorrelated JSI. Three examples are depicted in Figure 5.14, among them a spectrally pure down-conversion which doesn't require periodic poling of the KTP crystal.

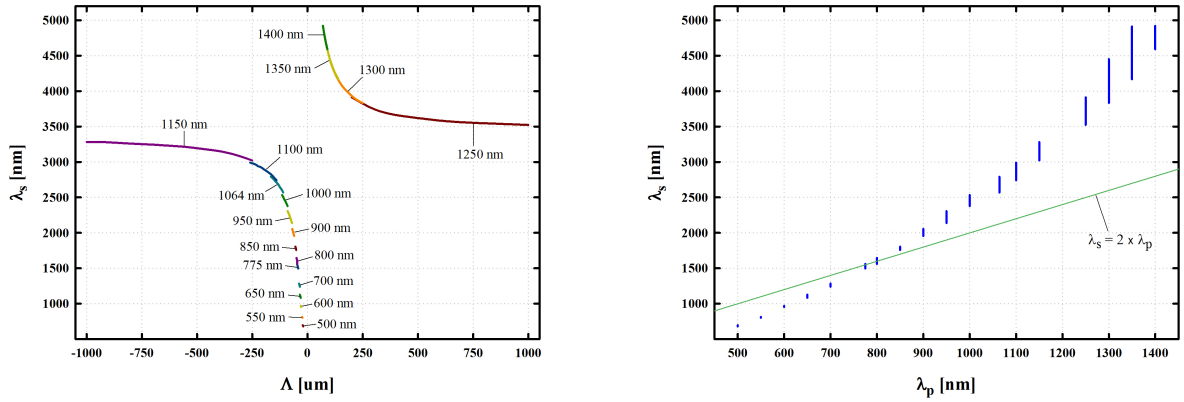


(a) (b)

Figure 5.13: Signal wavelength versus (a) crystal periodicity and (b) pump wavelength for type II SPDC ($e \longrightarrow o+e$) in KTP. Again, both plots only display configurations which allow for an uncorrelated JSI (provided matched pump spectrum and crystal length). For pump wavelengths between 1150 and 1250 nm the periodicity approaches infinity, thus enabling generation of spectrally pure output states without periodic poling. The intersection of the green line with the blue lines in Figure (b) illustrates that KTP allows for pure output states in the telecom regime.

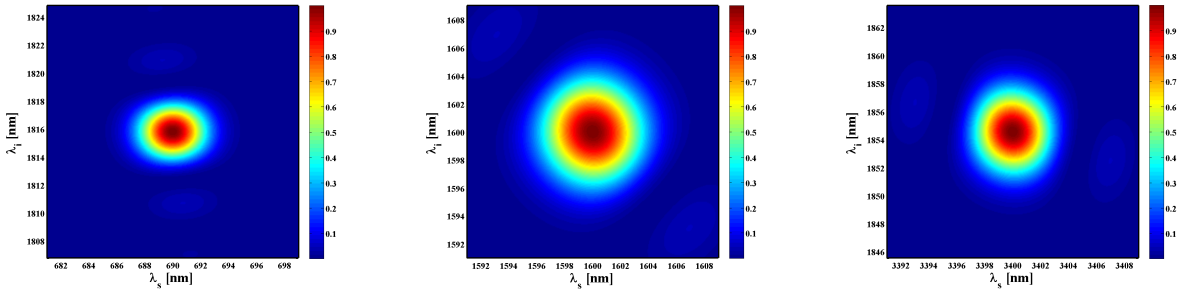


(a) 500 nm $\longrightarrow$ 690 nm + 1815.8 nm (b) 800 nm $\longrightarrow$ 2 × 1600 nm (c) 1200 nm $\longrightarrow$ 3400 nm + 1854.5 nm

Figure 5.14: Three examples of pure output state generation by type II down-conversion in KTP. Figure (b) shows a frequency-degenerate down-conversion; and Figure (c) shows a case where no periodic poling of the crystal is required ($\Lambda \geq 2l$).

### 5.3.3 Type I SPDC in LN

A similar procedure like in the previous subsections was carried out in order to find possible setups for generation of pure output states by type I down-conversion ($e \longrightarrow o + o$) in lithium niobate. Figure 5.15 shows the behaviour of the phase-match envelope intensity for a fixed pump and varying periodicity. We find that for pump wavelengths between 600 and 800 nm LN allows for intrinsically pure polarisation-degenerate SPDC. The configurations which allow for pure output states are illustrated in Figure 5.16, three of which are depicted as an example in Figure 5.17.

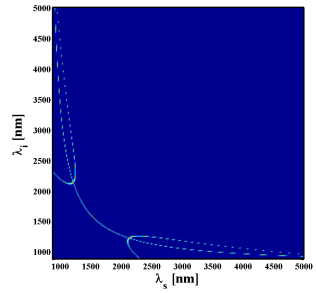


(a) $\Lambda = 23.55\,\mu\text{m}$,
$\lambda_{s/i} = 1223/2115.7\,\text{nm}$

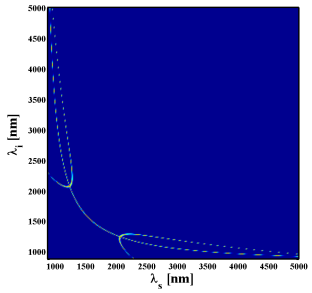


(b) $\Lambda = 23.70\,\mu\text{m}$,
$\lambda_{s/i} = 1237/2075.1\,\text{nm}$

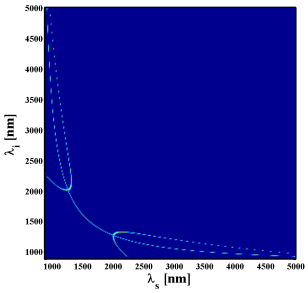


(c) $\Lambda = 23.85\,\mu\text{m}$,
$\lambda_{s/i} = 1260/2313.4\,\text{nm}$

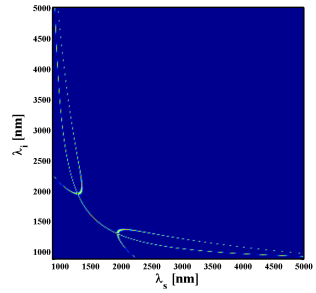


(d) $\Lambda = 24.00\,\mu\text{m}$,
$\lambda_{s/i} = 1289/1943.5\,\text{nm}$

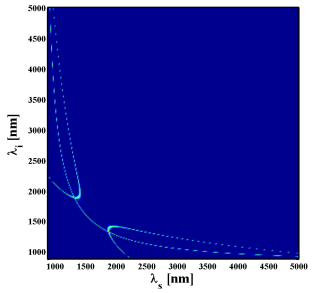


(e) $\Lambda = 24.15\,\mu\text{m}$,
$\lambda_{s/i} = 1318/1881.1\,\text{nm}$

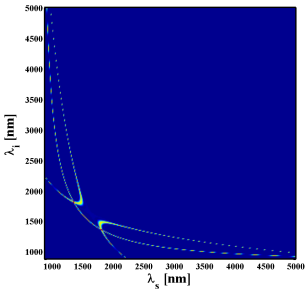


(f) $\Lambda = 24.30\,\mu\text{m}$,
$\lambda_{s/i} = 1357/1807\,\text{nm}$

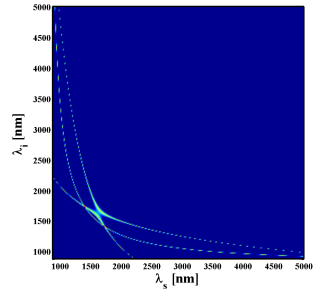


(g) $\Lambda = 24.45\,\mu\text{m}$,
$\lambda_{s/i} = 1403/1731.4\,\text{nm}$

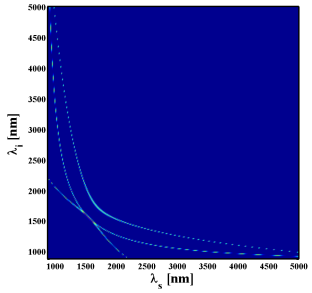


(h) $\Lambda = 24.60\,\mu\text{m}$,
$\lambda_{s/i} =$1450 nm to 1650 nm

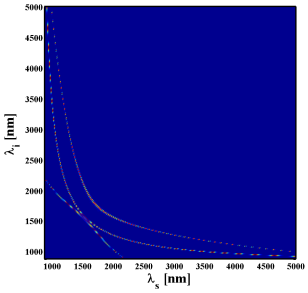


(i) $\Lambda = 24.75\,\mu\text{m}$,
no down-conversion

Figure 5.15: Type I SPDC ($e \longrightarrow o + o$) in LN; plots of $|\mu|^2 + |\psi|^2$ for fixed $\lambda_p = 775\,\text{nm}$ and varying $\Lambda$. In Figure (c) the two functions are oriented orthogonally. Similar conditions can be found for any other pump wavelengths between 600 and 800 nm. Note that due to polarisation-degeneracy in type I SPDC the plots are symmetric along the $\pi/4$-axis, which means that signal and idler are indistinguishable and their wavelengths can be interchanged.

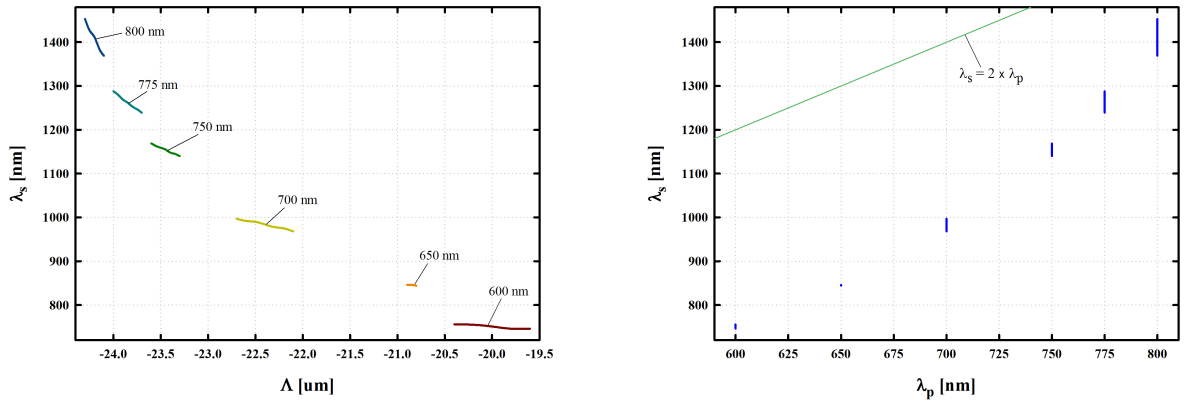


(a) (b)

Figure 5.16: Signal wavelength versus (a) crystal periodicity and (b) pump wavelength for intrinsically pure type I SPDC ($e \longrightarrow o + o$) in LN. Figure (b) illustrates that no pure frequency-degenerate down-conversion is supported in this setup since the blue plot lines do not intersect with the green line.

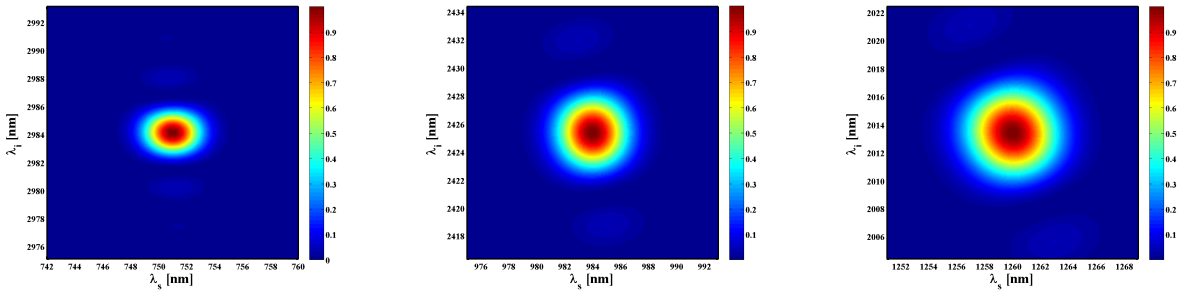


(a) 600 nm $\longrightarrow$ 751 nm + 2984.1 nm (b) 700 nm $\longrightarrow$ 984 nm + 2425.4 nm (c) 775 nm $\longrightarrow$ 1260 nm + 2013.4 nm

Figure 5.17: Three examples of pure output state generation by type I down-conversion in LN, picked according to Figure 5.16.

### 5.3.4 Type I SPDC in KTP

Numerical evaluation shows that KTP allows for intrinsically pure polarisation-degenerate SPDC for pump wavelengths between 475 and 600 nm. The configurations which allow for pure output states are illustrated in Figure 5.18, three of which are depicted as an example in Figure 5.19.

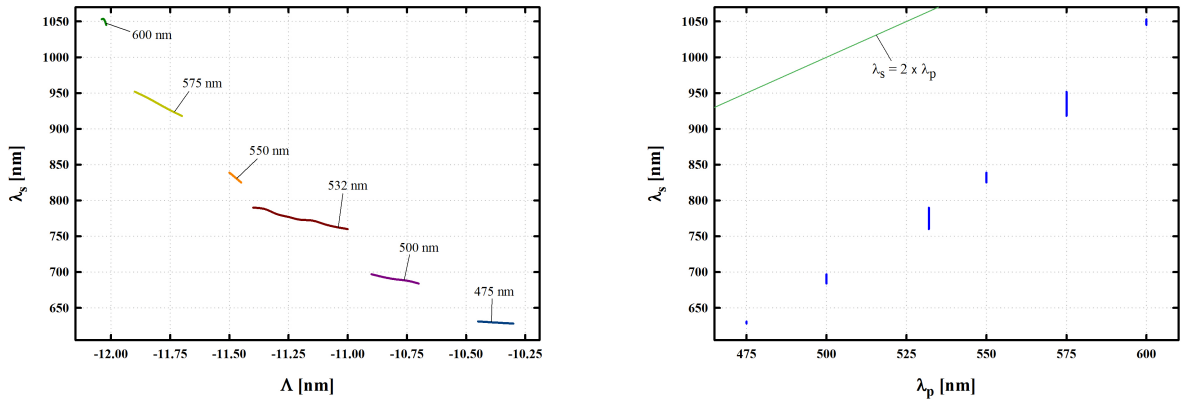


(a) (b)

Figure 5.18: Signal wavelength versus (a) crystal periodicity and (b) pump wavelength for intrinsically pure type I SPDC ($e \longrightarrow o+o$) in KTP. Figure (b) illustrates that no pure frequency-degenerate down-conversion is supported in this setup.

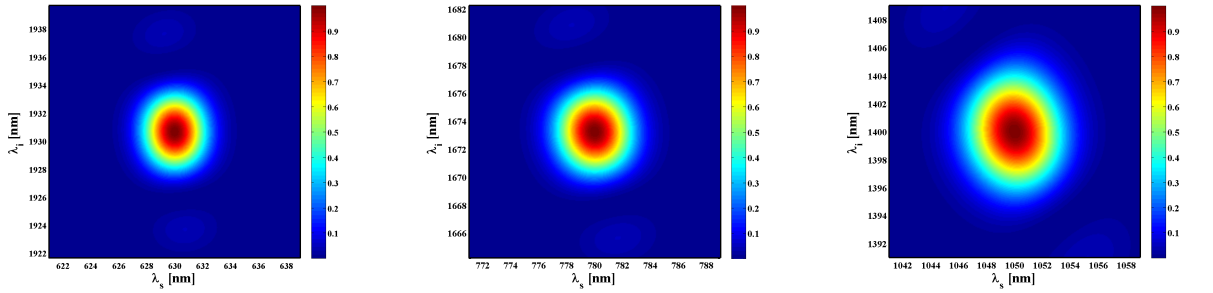


(a) 475 nm $\longrightarrow$ 630 nm + 1930.6 nm (b) 532 nm $\longrightarrow$ 780 nm + 1673.2 nm (c) 600 nm $\longrightarrow$ 1050 nm + 1400 nm

Figure 5.19: Three examples of pure output state generation by type I down-conversion in KTP, picked according to Figure 5.18.

## 5.4 Summary

As seen in this chapter, for frequency-degenerate SPDC in the telecom band periodically poled KTP is clearly superior to LN when it comes to state purity of signal and idler. We see however that lithium niobate offers high spectral purity for type II down-conversions 1000 nm $\longrightarrow$ 2 $\times$ 2000 nm. Furthermore we found that the type II down-conversions 1064 nm $\longrightarrow$ 2200 nm + 2060.6 nm in LN and 1200 nm $\longrightarrow$ 3400 nm + 1854.5 nm in KTP allow for phase-matching and spectral purity without periodic poling of the respective crystals. Moreover we discovered that both crystals do not support generation of intrinsically pure frequency- *and* polarisation-degenerate (type I) single photon states. However LN allows for intrinsic spectral purity at type I SPDC with one daughter field in the range of 750 to 1450 nm; KTP does the job with one daughter field in the range of 630 to 1050 nm.

# Conclusion

In this thesis we presented how periodically poled crystals pumped by pulsed laser sources can be used to achieve high spectral purity of SPDC-generated single photon states. Up to now bandpass filters had to be used for this purpose, bringing the disadvantage of decreasing the count rates drastically. The approach presented in this thesis aims for tailoring the setup such that the output states are intrinsically pure, therefore making bandpass filtering obsolete. The technique is based upon mutual matching of crystal length and pulse duration in order for signal and idler radiation to be spectrally uncorrelated. This is however only possible for a limited amount of setups; the JSI depends on the mutual relation of pump envelope intensity and phase-matching envelope intensity. The latter depends ultimately on the material's Sellmeier equations which provide the refractive index for a given polarisation and wavelength. As it turns out, each crystal allows for generation of intrinsically pure down-converted photons only in the case of very specific polarisation- and wavelength configurations.

We showed how the state purity of single photons that are generated by SPDC can be determined numerically by a singular value decomposition of the joint spectral intensity. Using this approach we investigated the suitability of two periodically poled crystals, lithium niobate (LN) and potassium titanyl phosphate (KTP), for various kinds of down-conversion processes. This systematic and extensive search for setups which allow for generation of intrinsically pure quantum states is—to our knowledge—unprecedented so far. This way we were able not only to confirm the choice of specific crystals in recent experiments but also to find many other promising setups that were previously unknown.

In particular we found that in the case of frequency-degenerate type II SPDC with signal and idler in the telecom band KTP is clearly superior to LN in terms of single photon state purity. It turns out however that—according to our calculations—LN offers high spectral purity in the type II process $1000\,\mathrm{nm} \longrightarrow 2 \times 2000\,\mathrm{nm}$. Moreover we found that LN and KTP each allow for specific type II down-conversions where phase matching and intrinsic spectral purity can be achieved even without periodic poling of the crystal. Besides, our evaluations revealed that both crystals offer many opportunities for pure state generation in the case of type I SPDC (although none of them is frequency-degenerate).

# Appendices

# Appendix A

# Material Properties

## A.1 Lithium Niobate, $LiNbO_3$

For lithium niobate (uniaxial: $n_x = n_y = n_o$, transparency range: 330 nm to 5500 nm) we used the following Sellmeier equations for ordinary [9] and extraordinary [17] index:

$$n_o^2 = 4.9048 + \frac{0.117\,75 + 2.2314 \times 10^{-8} F}{\lambda^2 - (2.1802 \times 10^{-2} - 2.9671 \times 10^{-8} F)^2} + 2.1429 \times 10^{-8} F - 2.7153 \times 10^{-2} \lambda^2, \tag{A.1a}$$

$$n_z^2 = 5.355\,83 + \frac{0.100\,473 + 3.862 \times 10^{-8} F}{\lambda^2 - (0.206\,92 - 8.9 \times 10^{-9} F)^2} + 4.629 \times 10^{-7} F + \frac{100 + 2.657 \times 10^{-5} F}{\lambda^2 - 128.806} - 1.5334 \times 10^{-2} \lambda^2. \tag{A.1b}$$

where $\lambda$ is the wavelength in micrometers and

$$F = (T - 24.5)(T + 570.5) \tag{A.2}$$

with temperature $T$ in °C.

The components of the non-linearity tensor are [25]

$$d^{22} = 2.1\,\mathrm{pm\,V^{-1}}, \tag{A.3a}$$

$$d^{31} = -4.35\,\mathrm{pm\,V^{-1}}, \tag{A.3b}$$

$$d^{33} = -27.2\,\mathrm{pm\,V^{-1}}. \tag{A.3c}$$

Clearly polarisation along the $z$-axis allows us to exploit the by far highest non-linearity $d^{33}$.

In our calculations the thermal expansion coefficients in $x$-direction were used to correct for temperature dependent fluctuations of crystal length $L$ and poling period $\Lambda$ [23]:

$$\alpha_{x,0} = 13.3 \times 10^{-6}, \tag{A.4a}$$

$$\alpha_{x,1} = 9.7 \times 10^{-9}, \tag{A.4b}$$

such that

$$L = L_0 \left(1 + \alpha_{x,0}(T - 25) + \alpha_{x,1}(T - 25)^2\right) \tag{A.5}$$

(and similar for $\Lambda$) with $T$ in °C.

## A.2 Potassium Titanyl Phosphate, $KTiOPO_4$

For potassium titanyl phosphate (biaxial, transparency range: 350 nm to 4000 nm) the Sellmeier equations for $n_y$ [18] and $n_z$ [11] are

$$n_y^2 = 2.099\,30 + \frac{0.922\,683\lambda^2}{\lambda^2 - 4.676\,95 \times 10^{-2}} - 1.384\,08 \times 10^{-2}\lambda^2, \tag{A.6a}$$

$$n_z^2 = 2.127\,25 + \frac{1.184\,31\lambda^2}{\lambda^2 - 5.148\,52 \times 10^{-2}} + \frac{0.6603\lambda^2}{\lambda^2 - 100.005\,07} - 9.689\,56 \times 10^{-3}\lambda^2, \tag{A.6b}$$

Since theses equations only depend on the wavelength and not on the temperature ($n = n(\lambda)$), the temperature dependence is taken into account by an additional term $\Delta n(\lambda, T)$ such that [10]

$$n(\lambda, T) = n(\lambda) + \Delta n(\lambda, T) \tag{A.7}$$

for each principle axis. The temperature dependent portion is defined by

$$\Delta n(\lambda, T) = n_1(\lambda)(T - 25) + n_2(\lambda)(T - 25)^2, \tag{A.8}$$

where the temperature is entered in °C and

$$n_{1,2}(\lambda) = \sum_{m=0}^{3} \frac{a_m}{\lambda^m}. \tag{A.9}$$

The components $a_m$ for respective axis are listed in Table A.1.

The non-linearity tensor has the components [25]

$$d^{31} = 1.95\,\mathrm{pm\,V^{-1}}, \tag{A.10a}$$

$$d^{32} = 3.9\,\mathrm{pm\,V^{-1}}, \tag{A.10b}$$

$$d^{33} = 15.3\,\mathrm{pm\,V^{-1}}. \tag{A.10c}$$

Similar to $LiNbO_3$ orientation of the fields along the $z$-axis gives access to the highest non-linearity term $d^{33}$. However in the case of ppKTP numerical QPM calculations often yield a required poling period $\Lambda$ lower than 5 µm, which can—with today's means—hardly be manufactured. So in order to avoid increasing the QPM order $m$ (and thus decreasing the output intensity) it sometimes turns out to be more advantageous to have the fields polarised along the $y$-axis, putting up with a lower effective non-linearity.

In our calculations we used the thermal expansion coefficients [10]

$$\alpha_{x,0} = 6.7 \times 10^{-6}, \tag{A.11a}$$

$$\alpha_{x,1} = 11.0 \times 10^{-9}. \tag{A.11b}$$

| | $z$-axis | | $y$-axis | |
|---|---|---|---|---|
| | $n_1$ [$10^{-6}$] | $n_2$ [$10^{-8}$] | $n_1$ [$10^{-6}$] | $n_2$ [$10^{-8}$] |
| $a_0$ | 9.9587 | -1.1882 | 6.2897 | -0.14445 |
| $a_1$ | 9.9228 | 10.459 | 6.3061 | 2.2244 |
| $a_2$ | -8.9603 | -9.8136 | -6.0269 | -3.5770 |
| $a_3$ | 4.1010 | 3.1481 | 2.6486 | 1.3470 |

Table A.1: Temperature coefficients for $z$ and $y$-axis in KTP [10].

# Appendix B

# Source Code

The program *QPMoptics* can be executed using *GNU Octave* and *Matlab*. Its purpose is to optimise the setup for production of photon pairs, given a set of input parameters that are entered by the user. The inputs include the spectral shape of the pump laser, the desired wavelengths of the daughter photons, the type of down-conversion, the type of non-linear crystal (KTP or LN), the crystal length, the temperature and the poling periodicity. For each set of input parameters *QPMoptics* delivers

- the crystal periodicity $\Lambda$ for a fixed temperature $T$ required for phase-matching,
- or $T$ for a fixed $\Lambda$, required for phase-matching,
- the QPM order $m$,
- a plot of the phase mismatch $\Delta k$ versus $\Lambda$,
- a plot of the output intensity $I$ versus $\Lambda$,
- a plot of $\Delta k$ versus $T$,
- a plot of $I$ versus $T$,
- a plot of phase-matched signal and idler wavelength versus temperature,
- plots of intensity versus signal (idler) wavelength at fixed pump and idler (signal),
- a plot of the pump envelope amplitude $\mu(\omega_p)$,
- a plot of the pump intensity $|\mu(\omega_s + \omega_i)|^2$,
- plots of the phase-matching intensity $|\psi(\omega_s, \omega_i)|^2$,
- plots of the joint spectral intensity $F(\omega_s, \omega_i)$,
- a plot of signal and idler spectra,
- spectral widths of signal and idler,
- Schmidt number $K$ and purity $\mathcal{P}$ of the JSI,
- optimal crystal length for highest purity at given pump width,
- optimal pump width for highest purity at given crystal length,
- a plot of $\mathcal{P}$ versus crystal length $L$,
- a plot of $\mathcal{P}$ versus pump width $\Delta\lambda_p$,
- a plot of $\mathcal{P}$ versus $L$ and $\Delta\lambda_p$.

The input parameters can be entered by a user interface within the program *QPMoptics*. Alternatively the program can read the input data from an external file, named *QPMinputs.m*. In order to calculate the output parameters and to draw the plot, *QPMoptics* accesses a number of external files and functions, all of which have to be saved in the same folder as *QPMoptics* itself:

- *QPMinputs.m* to read input parameters (optional),
- *fffQPM.m*: a function which calculates the phase mismatch $\Delta k$ for a given wavelength configuration, down-conversion type and crystal using the respective Sellmeier equations,
- *fffrootfinder.m*: a function which finds the zero point of $\Delta k(\Lambda)$, $\Delta k(T)$ and $\Delta k(\lambda_s)$ by use of the bisection method; it accesses *fffQPM.m* to evaluate the above functions,
- *fffpumpspectrum.m*: a function to calculate and plot the pump envelope amplitude and intensity. (The program *QPMoptics* by default assumes a Gaussian pump spectrum; it allows however for any spectral shape of the pump. In case of a non-Gaussian pump source it can be specified within the file *fffpumpspectrum.m* by the user.)

## B.1 QPMoptics

```
1  clear;
2  clc;
3
4
5  fprintf('\n:::::::::::::::::::: WELCOME TO QPMoptics! ::::::::::::::::::::\n\n\n')
6
7  % the program reads the input parameters from an external file. alternatively the input parameters can be
       entered into the program manually:
8  fprintf('do you want me to read the input data from file QPMinputs.m...\n...or do you want to enter the data
        one by one?\n\n(btw, calculating signal and idler spectra will take quite some time.\nyou can skip it
       by entering f for fast.)\n\nhit return key to load data file normally,\nf to load without computing the
        output spectra,\nor e to enter the inputs yourself: ');
9
10 readorenter=input('','s');
11
12 if (strcmp(readorenter,'e')==0)
13
14     % calling external file to read input data:
15     QPMinputs
16
17
18 % manual data input:
19 elseif (strcmp(readorenter,'e'))
20
21     % in case input parameters need to be re-entered after typo:
22     answer='c';
23
24     while (strcmp(answer,'c'))
25
26     clc
27
28     fprintf('\n________enter your input parameters_____________________\n\n')
29
30     %_____________QPM order (default)_____________________________________________________
31
32     m=1;
33
34     %_____________wavelengths_____________________________________________________________
35
36     lambdap_nm=input('enter pump wavelength in nm: ');
37     lambdas_nm=input('enter signal wavelength in nm: ');
38
39     % conversion from nm to microns:
40     lambdap=lambdap_nm./1000;
41     lambdas=lambdas_nm./1000;
42     lambdap0=lambdap;
43
44     % calculation of idler wavelength by energy conservation:
45     lambdai=1/(1/lambdap-1/lambdas);
46
47
48     %_____________down conversion type____________________________________________________
49
50     Type=input('enter down conversion type (0, I or II): ' , 's');
```

```
51
52      if (strcmp(Type,'0'))
53
54          polp='e';
55          pols=polp;
56          poli=polp;
57
58      elseif (strcmp(Type,'I'))
59
60          polp=input('enter pump polarisation (o or e): ' , 's');
61
62          if (strcmp(polp,'o'))
63
64              pols='e';
65
66          elseif (strcmp(polp,'e'))
67
68              pols='o';
69
70          end
71
72          poli=pols;
73
74      elseif (strcmp(Type,'II'));
75
76          polp=input('enter pump polarisation (o or e): ' , 's');
77          pols=input('enter signal polarisation (o or e): ' , 's');
78
79              if (strcmp(pols,'o'))
80
81                  poli='e';
82
83              elseif (strcmp(pols,'e'))
84
85                  poli='o';
86
87              end
88
89      end
90
91      pol=[polp,pols,poli];
92
93      %-------------pump width-----------------------------------------------------------
94
95      % choose to enter spectral width or pulse duration of pump source:
96      timeorwidth=input('hit t to enter the pulse duration or return to enter the spectral width: ', 's');
97
98          if (strcmp(timeorwidth,'t'))
99
100             tau=input('enter pulse duration in ps: ');
101
102             % calculation of spectral width by pulse duration:
103             Deltalambdap=sqrt(log(2)/2)*lambdap.^2./(pi*3e8*tau)*1e6;
104
105         else
106
107             Deltalambdap_nm=input('enter spectral width of pump light in nm: ');
108             Deltalambdap=Deltalambdap_nm./1000;
109
110             tau=sqrt(log(2)/2)*lambdap.^2./(pi*3e8*Deltalambdap)*1e6;
111
112         end
113
114     %-------------gaussian?------------------------------------------------------------
115
116     gaussian=input('is the spectrum of your pump source gaussian? (y or n): ', 's');
117
118     if (strcmp(gaussian,'n'))
119
120         fprintf('please go to file fffpumpspectrum.m and specify the pump spectrum.\n')
121
122     end
123
124     %-------------crystal--------------------------------------------------------------
125
126     crystal=input('please choose a crystal (KTP or LN): ', 's');
127
128     if (strcmp(crystal,'KTP'))
129
130         % optional choice of ordinary and extraordinary crystal axis (only for KTP):
131         KTPoptax=input('select optic axis of KTP (z or y): ' ,'s');
132
133     else
134
```

```
135         % no choice in case of LN:
136         KTPoptax='dummy';
137
138     end
139
140     L_mm=input('enter crystal length in mm?: ');
141
142     % conversion from mm to microns:
143     L=L_mm.*1000;
144
145     %_____________fixed and to-be-optimsied parameter_____________________________________
146
147     opt=input('what would you like to optimise (Lambda or T): ' , 's');
148         if (strcmp(opt,'Lambda'))
149             T=input('enter a temperature in celsius: ');
150             Lambda=0; % dummy
151         elseif (strcmp(opt,'T'))
152             Lambda=input('enter a poling periodicity constant in um: ');
153             T=0; % dummy
154         end
155
156     clc;
157     fprintf('\n')
158
159     %_____________input check_____________________________________________________________
160
161     fprintf('________please check you inputs_____________________________\n\n')
162
163     fprintf('pump, signal and idler wavelength:\nlambda_p = %6.1f nm\nlambda_s = %6.1f nm\nlambda_i = %6.1f
            nm\n\n', lambdap.*1000,lambdas.*1000,lambdai.*1000)
164
165     fprintf('downconversion:\ntype %s: %s --> %s + %s\n\n', Type,polp,pols,poli)
166
167     if (strcmp(gaussian,'y'))
168
169         fprintf('pump spectrum:\ngaussian\n\n')
170
171     elseif (strcmp(gaussian,'n'))
172
173         fprintf('pump spectrum:\nspecified at fffpumpspectrum.m\n\n')
174
175     end
176
177     fprintf('pulse duration:\n%6.3f ps\n\n', tau)
178
179     fprintf('spectral width of pump light:\n%5.2f nm\n\n', Deltalambdap.*1000)
180
181     fprintf('crystal:\n%s\n\n', crystal)
182
183     if (strcmp(crystal,'KTP'))
184
185         fprintf('optic axis of KTP crystal:\n%s\n\n', KTPoptax)
186
187     end
188
189     fprintf('crystal length:\n%4.1f mm\n\n', L./1000)
190
191     if (strcmp(opt,'Lambda'))
192
193         fprintf('temperature:\n%4.2f deg C\n\n', T)
194
195     elseif (strcmp(opt,'T'))
196
197         fprintf('poling periodicity:\n%6.2f um\n\n', Lambda)
198
199     end
200
201     fprintf('parameter to be optimised for QPM:\n%s\n\n', opt)
202
203     fprintf('_____________________________________________________\n\n')
204
205     answer=input('enter c to change input parameters or return to proceed: ', 's');
206     end
207
208 end
209
210 % input wavelengths to be handed over to fffQPM ('ps' = pump and signal):
211 inputWLs='ps';
212
213 clc;
214
215 % printing all inputs:
216 fprintf('\n________your input parameters_____________________________\n\n')
217
```

```
218     fprintf('pump, signal and idler wavelength:\nlambda_p = %6.1f nm\nlambda_s = %6.1f nm\nlambda_i = %6.1f
            nm\n\n', lambdap.*1000,lambdas.*1000,lambdai.*1000)
219
220     fprintf('downconversion:\ntype %s: %s --> %s + %s\n\n', Type,polp,pols,poli)
221
222     if (strcmp(gaussian,'y'))
223
224         fprintf('pump spectrum:\ngaussian\n\n')
225
226     elseif (strcmp(gaussian,'n'))
227
228         fprintf('pump spectrum:\nspecified at fffpumpspectrum.m\n\n')
229
230     end
231
232     fprintf('pulse duration:\n%6.3f ps\n\n', tau)
233
234     fprintf('spectral width of pump light:\n%5.2f nm\n\n', Deltalambdap.*1000)
235
236     fprintf('crystal:\n%s\n\n', crystal)
237
238     if (strcmp(crystal,'KTP'))
239
240         fprintf('optic axis of KTP crystal:\n%s\n\n', KTPoptax)
241
242     end
243
244     fprintf('crystal length:\n%4.1f mm\n\n', L./1000)
245
246     if (strcmp(opt,'Lambda'))
247
248         fprintf('temperature:\n%4.2f deg C\n\n', T)
249
250     elseif (strcmp(opt,'T'))
251
252         fprintf('poling periodicity:\n%6.2f um\n\n', Lambda)
253
254     end
255
256     fprintf('parameter to be optimised for QPM:\n%s\n\n', opt)
257
258
259 fprintf('________your results_____________________________________\n')
260
261
262 %_________________QPM condition output and plot_____________________________________________
263
264     if (strcmp(opt,'Lambda'))
265
266         % find root of Delta_k(Lambda):
267         [Lambda0,outrange,m,Lambdastart,Lambdaend]=fffrootfinderQPM(opt,lambdap,lambdas,pol,crystal,KTPoptax
                ,Lambda,T,m);
268
269         % if root of Lambda is not within specified range:
270         if (outrange==1)
271
272             fprintf('\nLambda_0 seems to be out of scanned range ([%i,%i] um).\nthis makes all further
                    calculations pointless!\nyou might wanna check your inputs or adjust the scanning range.\n\
                    n', Lambdastart,Lambdaend)
273
274             %_____wide range plot of mismatch vs. periodicity_____________________________
275
276             Lambda_var=linspace(1,20000,1000);
277
278             Deltakm=fffQPM(inputWLs,lambdap,lambdas,pol,crystal,KTPoptax,Lambda_var,T,m);
279
280             subplot(1,2,1)
281             plot(Lambda_var,Deltakm,'linewidth',2)
282             xlim([1,20000])
283             h=get (gcf, 'currentaxes');
284             set(h,'fontweight','bold','fontsize',9,'linewidth',2);
285             grid on;
286             title(['\Delta k_m (\Lambda), m=',num2str(m)],'fontweight','bold','fontsize',12)
287             xlabel('\Lambda [\mum]','fontweight','bold','fontsize',12)
288             ylabel('\Delta k_m [\mum^{-1}]','fontweight','bold','fontsize',12)
289
290             Deltakm=fffQPM(inputWLs,lambdap,lambdas,pol,crystal,KTPoptax,Lambda_var,T,-m);
291
292             subplot(1,2,2)
293             plot(Lambda_var,Deltakm,'linewidth',2)
294             xlim([1,20000])
295             h=get (gcf, 'currentaxes');
296             set(h,'fontweight','bold','fontsize',9,'linewidth',2);
297             grid on;
```

```
298             title(['\Delta k_m (\Lambda), m=',num2str(-m)],'fontweight','bold','fontsize',12)
299             xlabel('\Lambda [\mum]','fontweight','bold','fontsize',12)
300             ylabel('\Delta k_m [\mum^{-1}]','fontweight','bold','fontsize',12)
301
302             return
303
304         end
305
306         answer='c';
307
308         % optional change of QPM order m, in case of Lambda < 5um:
309         while (Lambda0<5 && strcmp(answer,'c'))
310
311             fprintf('\ncrystal periodicity required for QPM:\n%7.3f um\n\n' ,Lambda0)
312             fprintf('Lambda_0 is less than 5 um.\nwanna change the QPM order? currently: m=%i.\n', m)
313
314             answer=input('enter c if you want to change m, otherwise return: ' ,'s');
315
316             if (strcmp(answer,'c'))
317
318                 m=input('enter new QPM order: ');
319
320                 [Lambda0,outrange,m,Lambdastart,Lambdaend]=fffrootfinderQPM(opt,lambdap,lambdas,pol,crystal,
                        KTPoptax,Lambda,T,m);
321
322             else
323
324                 fprintf('\n')
325                 answer='nothanks';
326
327             end
328
329         end
330
331         %_________phase mismatch vs. periodicity_____________________________________________
332
333         Lambda_var=linspace(Lambda0-Lambda0*0.5,Lambda0+Lambda0*0.5,10000);
334
335         Deltakm=fffQPM(inputWLs,lambdap,lambdas,pol,crystal,KTPoptax,Lambda_var,T,m);
336
337         subplot(2,2,1);
338         plot(Lambda_var,Deltakm,'linewidth',2)
339         xlim([Lambda0-Lambda0*0.5,Lambda0+Lambda0*0.5])
340         h=get (gcf, 'currentaxes');
341         set(h,'fontweight','bold','fontsize',9,'linewidth',2);
342         grid on;
343         title('QPM condition','fontweight','bold','fontsize',12)
344         xlabel('\Lambda [\mum]','fontweight','bold','fontsize',12)
345         ylabel('\Delta k_m [\mum^{-1}]','fontweight','bold','fontsize',12)
346
347
348         %_________signal intensity vs. periodicity_____________________________________________
349
350         Deltakm=fffQPM(inputWLs,lambdap,lambdas,pol,crystal,KTPoptax,Lambda_var,T,m);
351
352         I=(sin(Deltakm.*L/2)./(Deltakm.*L/2)).^2;
353
354         % figure
355         subplot(2,2,2)
356         plot(Lambda_var,I,'linewidth',2)
357         h=get (gcf, 'currentaxes');
358         set(h,'fontweight','bold','fontsize',9,'linewidth',2)
359         grid on;
360         axis([Lambda0-0.5,Lambda0+0.5,0,1])
361         title('output intensity vs. periodicity','fontweight','bold','fontsize',12)
362         xlabel('\Lambda [\mum]','fontweight','bold','fontsize',12)
363         ylabel('I_{rel}','fontweight','bold','fontsize',12)
364
365         Lambda=Lambda0; % for later use in T-lambda-plot
366
367
368     elseif (strcmp(opt,'T'))
369
370         % find root of Delta_k(T):
371         [T0,outrange,m,Tstart,Tend]=fffrootfinderQPM(opt,lambdap,lambdas,pol,crystal,KTPoptax,Lambda,T,m);
372
373
374         answer2='c';
375
376         while (outrange==1)
377
378             fprintf('\nT_0 seems to be out of scanned range ([%i,%i] deg C).\nthis makes all further
                    calculations pointless!\nmaybe there is more than just one root within the scanned range.\
                    nyou might wanna adjust the scanning range or change the QPM order (currently: m=%i).\n',
```

```
                Tstart,Tend,m)
379
380             %_____wide range plot of mismatch vs. temperature_____________________________
381
382             T_var=linspace(-270,500,1000);
383
384             Deltakm=fffQPM(inputWLs,lambdap,lambdas,pol,crystal,KTPoptax,Lambda,T_var,m);
385
386             subplot(1,2,1)
387             plot(T_var,Deltakm,'linewidth',2)
388             h=get (gcf, 'currentaxes');
389             set(h,'fontweight','bold','fontsize',9,'linewidth',2)
390             grid on;
391             xlim([-300,1000])
392             title(['\Delta k_m (\Lambda), m=',num2str(m)],'fontweight','bold','fontsize',12)
393             xlabel('T [deg C]','fontweight','bold','fontsize',12)
394             ylabel('\Delta k_m [\mum^{-1}]','fontweight','bold','fontsize',12)
395
396             Deltakm=fffQPM(inputWLs,lambdap,lambdas,pol,crystal,KTPoptax,Lambda,T_var,-m);
397
398             subplot(1,2,2)
399             plot(T_var,Deltakm,'linewidth',2)
400             h=get (gcf, 'currentaxes');
401             set(h,'fontweight','bold','fontsize',9,'linewidth',2)
402             grid on;
403             xlim([-300,1000])
404             title(['\Delta k_m (\Lambda), m=',num2str(-m)],'fontweight','bold','fontsize',12)
405             xlabel('T [deg C]','fontweight','bold','fontsize',12)
406             ylabel('\Delta k_m [\mum^{-1}]','fontweight','bold','fontsize',12)
407
408             answer2=input('enter c to change m or return to quit program: ' ,'s');
409
410             if (strcmp(answer2,'c'))
411
412                 m=input('enter new QPM order: ');
413
414                 [T0,outrange,m,Tstart,Tend]=fffrootfinderQPM(opt,lambdap,lambdas,pol,crystal,KTPoptax,Lambda
                        ,T,m);
415
416             else
417
418                 fprintf('\n')
419                 return
420
421             end
422
423         end
424
425         %_________phase mismatch vs. temperature_____________________________________________
426
427         T_var=linspace((T0-0.75*abs(T0)),(T0+0.75*abs(T0)),1000);
428
429         Deltakm=fffQPM(inputWLs,lambdap,lambdas,pol,crystal,KTPoptax,Lambda,T_var,m);
430
431         subplot(2,2,1);
432         plot(T_var,Deltakm,'linewidth',2)
433         h=get (gcf, 'currentaxes');
434         set(h,'fontweight','bold','fontsize',9,'linewidth',2)
435         grid on;
436         xlim([(T0-0.75*abs(T0)),(T0+0.75*abs(T0))])
437         title('QPM condition','fontweight','bold','fontsize',12)
438         xlabel('T [deg C]','fontweight','bold','fontsize',12)
439         ylabel('\Delta k_m [\mum^{-1}]','fontweight','bold','fontsize',12)
440
441
442         %_________signal intensity vs. temperature_____________________________________________
443
444         Deltakm=fffQPM(inputWLs,lambdap,lambdas,pol,crystal,KTPoptax,Lambda,T_var,m);
445
446         I=(sin(Deltakm.*L/2)./(Deltakm.*L/2)).^2;
447
448         % figure
449         subplot(2,2,2)
450         plot(T_var,I,'linewidth',2)
451         h=get (gcf, 'currentaxes');
452         set(h,'fontweight','bold','fontsize',9,'linewidth',2)
453         grid on;
454         axis([(T0-0.75*abs(T0)),(T0+0.75*abs(T0)),0,1])
455         title('output intensity vs. temperature','fontweight','bold','fontsize',12)
456         xlabel('T [deg C]','fontweight','bold','fontsize',12)
457         ylabel('I_{rel}','fontweight','bold','fontsize',12)
458
459         T=T0;
460
```

```
461     end
462
463
464
465 %_____________________print results (I): L_0/T_0, m_____________________________________________
466
467 if (strcmp(opt,'Lambda'))
468
469     fprintf('\ncrystal periodicity required for QPM:\n%7.3f um\n\n' ,Lambda0)
470
471 elseif (strcmp(opt,'T'))
472
473     fprintf('\ntemperature required for QPM:\n%6.2f deg C\n\n' ,T0)
474
475 end
476
477 fprintf('QPM order:\n%i\n\n' ,m)
478
479
480 %_____________________signal, idler vs. temperature at fixed pump_____________________________
481
482 % set signal wavelength to be optimised by fffrootfinderQPM:
483 opt='lambdas';
484
485 Trange=50;
486
487 T_var=linspace((T-Trange),(T+Trange),100);
488
489 lambdas0=zeros(1,numel(T_var));
490 lambdai0=zeros(1,numel(T_var));
491
492 for (j=1:numel(T_var))
493
494     % find root of Delta_k (lambda_s) for each T
495     [lambdas0(j),outrange,m,lambdasstart,lambdasend]=fffrootfinderQPM(opt,lambdap,lambdas,pol,crystal,
          KTPoptax,Lambda,T_var(j),m);
496
497     % calculate idler wavelength corresponding to root lambda_s_0:
498     lambdai0(j)=1/(1/lambdap-1./lambdas0(j));
499
500 end
501
502 % figure
503 subplot(2,2,4)
504 h=plot(T_var,lambdas0.*1000,T_var,lambdai0.*1000);
505 set(h(1),'linewidth',2);
506 set(h(2),'linewidth',2);
507 h=get (gcf, 'currentaxes');
508 set(h,'fontweight','bold','fontsize',9,'linewidth',2)
509 grid on;
510 xlim([(T-Trange),(T+Trange)])
511 title('temperature dependence of signal/idler wavelength at fixed pump','fontweight','bold','fontsize',12)
512 xlabel('T [deg C]','fontweight','bold','fontsize',12)
513 ylabel('\lambda [nm]','fontweight','bold','fontsize',12)
514 legend('signal','idler')
515
516
517
518 %_____________________pump spectrum_____________________________________________________________
519
520 lambdaprange=0.009;
521 lambdap_var_free=linspace((lambdap0-lambdaprange),(lambdap0+lambdaprange),250);     % lambda_p as free
       parameter (used only for plot)
522
523 % set pump wavelength as input parameter for fffpumpspectrum:
524 inputWLsPS='pump';
525
526 % calculate pump amplitude:
527 mu_pump_plot=fffpumpspectrum(inputWLsPS,lambdap_var_free,lambdas,lambdai,gaussian,lambdap0,Deltalambdap);
528
529 % figure
530 subplot(2,2,3)
531 plot(lambdap_var_free.*1000,mu_pump_plot,'linewidth',2)
532 h=get (gcf, 'currentaxes');
533 set(h,'fontweight','bold','fontsize',9,'linewidth',2)
534 grid on;
535 axis([(lambdap0-lambdaprange)*1000,(lambdap0+lambdaprange)*1000,0,1])
536 title('pump spectrum','fontweight','bold','fontsize',12)
537 xlabel('\lambda_p [nm]','fontweight','bold','fontsize',12)
538 ylabel('I_{rel}','fontweight','bold','fontsize',12)
539
540
541
542 % range and step size of signal and idler wavelengths:
```

```
lambdasrange=0.015;
lambdairange=lambdasrange;
resolution=200;

% create array of values for signal and idler wavelengths used as free parameters for following calculations
    :
lambdas_var=linspace((lambdas-lambdasrange),(lambdas+lambdasrange),resolution);
lambdai_var=linspace((lambdai-lambdairange),(lambdai+lambdairange),resolution);

[xx,yy]=meshgrid(lambdas_var,lambdai_var);

% calculation of pump intensity for every pair of signal and idler wavelengths:
inputWLsPS='si';
mu_pump=fffpumpspectrum(inputWLsPS,lambdap,xx,yy,gaussian,lambdap0,Deltalambdap);


% calculation of phase-mismatch for every pair of signal and idler wavelengths:
inputWLs='si';
[Deltakm,alpha]=fffQPM(inputWLs,xx,yy,pol,crystal,KTPoptax,Lambda,T,m);

% calculation of crystal length w.r. to temperature:
L_of_T=L*(1+alpha*(T-25));

% calculation of phase-match intensity for every pair of signal and idler wavelengths:
psi_PM=(sin(Deltakm.*L_of_T/2)./(Deltakm.*L_of_T/2));


figure

%_________________pump intensity_____________________________________________________

% figure
subplot(3,3,1)
pcolor(lambdas_var.*1000,lambdai_var.*1000,mu_pump.^2)
axis([(lambdas-lambdasrange),(lambdas+lambdasrange),(lambdai-lambdairange),(lambdai+lambdairange)].*1000, '
    square')
h=get (gcf, 'currentaxes');
set(h,'fontweight','bold','fontsize',9,'linewidth',2)
shading('interp')
title('pump intensity','fontweight','bold','fontsize',12)
xlabel('\lambda_s [nm]','fontweight','bold','fontsize',12)
ylabel('\lambda_i [nm]','fontweight','bold','fontsize',12)

%_________________PM intensity_____________________________________________________

% figure
subplot(3,3,4)
pcolor(lambdas_var.*1000,lambdai_var.*1000,psi_PM.^2)
axis([(lambdas-lambdasrange),(lambdas+lambdasrange),(lambdai-lambdairange),(lambdai+lambdairange)].*1000, '
    square')
h=get (gcf, 'currentaxes');
set(h,'fontweight','bold','fontsize',9,'linewidth',2)
shading('interp')
title('QPM intensity','fontweight','bold','fontsize',12)
xlabel('\lambda_s [nm]','fontweight','bold','fontsize',12)
ylabel('\lambda_i [nm]','fontweight','bold','fontsize',12)


%_________________intensity vs. signal and idler WL including pump spectrum_____________

% figure
subplot(3,3,7)
pcolor(lambdas_var.*1000,lambdai_var.*1000,mu_pump.^2+psi_PM.^2);
axis([(lambdas-lambdasrange),(lambdas+lambdasrange),(lambdai-lambdairange),(lambdai+lambdairange)].*1000, '
    square')
h=get (gcf, 'currentaxes');
set(h,'fontweight','bold','fontsize',9,'linewidth',2)
shading('interp')
title('pump intensity + QPM intensity','fontweight','bold','fontsize',12)
xlabel('\lambda_s [nm]','fontweight','bold','fontsize',12)
ylabel('\lambda_i [nm]','fontweight','bold','fontsize',12)



%_________________schmidt number and purity_____________________________________________

lambdasrangeJSI=0.009;
lambdairangeJSI=lambdasrangeJSI;
resolutionJSI=300;

lambdas_var=linspace((lambdas-lambdasrangeJSI),(lambdas+lambdasrangeJSI),resolutionJSI);
lambdai_var=linspace((lambdai-lambdairangeJSI),(lambdai+lambdairangeJSI),resolutionJSI);

[xx,yy]=meshgrid(lambdas_var,lambdai_var);
```

```
623
624 inputWLsPS='si';
625 mu_pump=fffpumpspectrum(inputWLsPS,lambdap,xx,yy,gaussian,lambdap0,Deltalambdap);
626
627 [Deltakm,alpha]=fffQPM(inputWLs,xx,yy,pol,crystal,KTPoptax,Lambda,T,m);
628 L_of_T=L*(1+alpha*(T-25));
629 psi_PM=(sin(Deltakm.*L_of_T/2)./(Deltakm.*L_of_T/2));
630
631 % calculation of joint spectral intensity for every pair of signal and idler wavelengths:
632 JSI=(mu_pump.*psi_PM).^2;
633
634 % singular value decomposition of z:
635 [U,D,V_dagger]=svd(JSI);
636
637 % normalisation of diagonal matrix:
638 D_norm=D/sqrt(trace(D^2));
639
640 % purity:
641 P=trace(D_norm^4);
642
643 % schmidt number:
644 K=1/P;
645
646
647 fprintf('spectral purity of signal and idler:\n%5.3f\n\n', P)
648
649 fprintf('schmidt number of joint intensity distribution:\n%5.3f\n\n', K)
650
651
652 if (strcmp(readorenter,'f')==0)
653
654     %_____________signal and idler spectra_____________________________________________
655
656     %_____________integration over intensity w.r. to lambda_s for each lambda_i__________
657
658     intensity_vs_signal=zeros(1,numel(lambdas_var));
659
660     for (i=1:numel(lambdas_var))
661
662         % integrate intensity over idler wavelength for fixed signal wavelength:
663         intensity_for_each_idler=0;
664         for (j=1:numel(lambdai_var))
665
666             inputWLsPS='si';
667             mu_pump=fffpumpspectrum(inputWLsPS,lambdap,lambdas_var(i),lambdai_var(j),gaussian,lambdap0,
                    Deltalambdap);
668
669             [Deltakm,alpha]=fffQPM(inputWLs,lambdas_var(i),lambdai_var(j),pol,crystal,KTPoptax,Lambda,T,m);
670             L_of_T=L*(1+alpha*(T-25));
671             psi_PM_vs_s=(sin(Deltakm.*L_of_T/2)./(Deltakm.*L_of_T/2));
672
673             JSI_vs_idler=(mu_pump.*psi_PM_vs_s).^2;
674
675             intensity_for_each_idler = intensity_for_each_idler + JSI_vs_idler;
676
677         end
678
679             intensity_vs_signal(i)=intensity_for_each_idler;
680
681     end
682
683     % evaluation of maximal intensity for rescaling of spectral function:
684     intensity_max_s=max(intensity_vs_signal);
685
686     % rescaling of spectral function to fit into JSI plot:
687     intensity_vs_signal_calibrated_axes=intensity_vs_signal./max(intensity_vs_signal).*(lambdairangeJSI
            .*1000)+(lambdai-lambdairangeJSI).*1000;
688
689
690     %_____________FWHM_s_____________________________________________________________
691
692     intensity_minus_halfmax_s  = abs(intensity_vs_signal-intensity_max_s./2);
693     intensity_minus_halfmax1_s = intensity_minus_halfmax_s(1:floor(numel(intensity_minus_halfmax_s)./2));
694     intensity_minus_halfmax2_s = intensity_minus_halfmax_s(numel(intensity_minus_halfmax_s)/2:numel(
            intensity_minus_halfmax_s));
695
696     index1_s = find(intensity_minus_halfmax1_s == min(intensity_minus_halfmax1_s));
697     index2_s = find(intensity_minus_halfmax2_s == min(intensity_minus_halfmax2_s));
698     index2_s = index2_s + floor(numel(intensity_minus_halfmax_s)./2);
699
700     lambda_s_FWHM1=lambdas_var(index1_s);
701     lambda_s_FWHM2=lambdas_var(index2_s);
702
703     FWHM_s=lambda_s_FWHM2-lambda_s_FWHM1;
```

```
704
705     Deltalambdas=FWHM_s/(2*sqrt(2*log(2)));
706
707
708
709     %_____________integration over intensity w.r. to lambda_s for each lambda_i__________
710
711     intensity_vs_idler=zeros(1,numel(lambdai_var));
712
713     for (i=1:numel(lambdai_var))
714
715         intensity_for_each_signal=0;
716         for (j=1:numel(lambdas_var))
717
718             inputWLsPS='si';
719             mu_pump=fffpumpspectrum(inputWLsPS,lambdap,lambdas_var(i),lambdai_var(j),gaussian,lambdap0,
                    Deltalambdap);
720
721             [Deltakm,alpha]=fffQPM(inputWLs,lambdas_var(j),lambdai_var(i),pol,crystal,KTPoptax,Lambda,T,m);
722             L_of_T=L*(1+alpha*(T-25));
723             psi_PM_vs_i=(sin(Deltakm.*L_of_T/2)./(Deltakm.*L_of_T/2));
724
725             JSI_vs_signal=(mu_pump.*psi_PM_vs_i).^2;
726
727             intensity_for_each_signal = intensity_for_each_signal + JSI_vs_signal;
728
729         end
730
731             intensity_vs_idler(i)=intensity_for_each_signal;
732
733     end
734
735     intensity_max_i=max(intensity_vs_idler);
736
737     intensity_vs_idler_calibrated_axes=intensity_vs_idler./max(intensity_vs_idler).*(lambdasrangeJSI.*1000)
            +(lambdas-lambdasrangeJSI).*1000;
738
739
740     %_____________FWHM_i_____________________________________________________________________
741
742     intensity_minus_halfmax_i  = abs(intensity_vs_idler-intensity_max_i./2);
743     intensity_minus_halfmax1_i = intensity_minus_halfmax_i(1:floor(numel(intensity_minus_halfmax_i)./2));
744     intensity_minus_halfmax2_i = intensity_minus_halfmax_i(numel(intensity_minus_halfmax_i)/2:numel(
            intensity_minus_halfmax_i));
745
746     index1_i = find(intensity_minus_halfmax1_i == min(intensity_minus_halfmax1_i));
747     index2_i = find(intensity_minus_halfmax2_i == min(intensity_minus_halfmax2_i));
748     index2_i = index2_i + floor(numel(intensity_minus_halfmax_i)./2);
749
750     lambda_i_FWHM1=lambdas_var(index1_i);
751     lambda_i_FWHM2=lambdas_var(index2_i);
752
753     FWHM_i=lambda_i_FWHM2-lambda_i_FWHM1;
754
755     Deltalambdai=FWHM_i/(2*sqrt(2*log(2)));
756
757     %_____________print results (II): signal and idler widths_____________________________
758
759     fprintf('FWHM and gaussian width of signal spectrum:\n%5.2f nm, %5.2f nm\n\n' ,FWHM_s.*1000,Deltalambdas
            .*1000)
760
761     fprintf('FWHM and gaussian width of idler spectrum:\n%5.2f nm, %5.2f nm\n\n' ,FWHM_i.*1000,Deltalambdai
            .*1000)
762
763 end
764
765 %_________________joint spectral intensity_____________________________________________
766
767 % figure
768 subplot(1,2,2)
769 pcolor(lambdas_var.*1000,lambdai_var.*1000,JSI)
770 colorbar ();
771 axis([(lambdas-lambdasrangeJSI),(lambdas+lambdasrangeJSI),(lambdai-lambdairangeJSI),(lambdai+lambdairangeJSI
        )].*1000, 'square')
772 h=get (gcf, 'currentaxes');
773 set(h,'fontweight','bold','fontsize',9,'linewidth',2)
774 shading('interp')
775 title('joint spectral intensity','fontweight','bold','fontsize',12)
776 xlabel('\lambda_s [nm]','fontweight','bold','fontsize',12)
777 ylabel('\lambda_i [nm]','fontweight','bold','fontsize',12)
778
779
780 if (strcmp(readorenter,'f')==0)
781
```

```
782     hold on;
783
784     h=plot(lambdas_var.*1000,intensity_vs_signal_calibrated_axes,'w',intensity_vs_idler_calibrated_axes,
            lambdai_var.*1000,'w');
785     set(h(1),'linewidth',2);
786     set(h(2),'linewidth',2);
787
788     hold off;
789
790 end
791
792
793
794 %_________________optitional additional plots_____________________________________________
795
796 fprintf('\ni can offer more plots, if you want:\n\nfigure a:\n(1) intensity vs. signal and idler wavelength
        at fixed monochromatic pump,\n(2) a wide range plot of the QPM intensity band for varying pump,\n(3)
        and a 3D plot of the QPM spectrum.\n\nfigure b:\n(1) purity vs. pump width,\n(2) purity vs. crystal
        length,\n(3) purity vs. pump width and crystal length.\n\nenter a to see figure a,\nb to see figure b,\
        nab to see both figures,\nor return to end program: ');
797
798 moreplots=input('', 's');
799
800 fprintf('\n')
801
802 if (strcmp(moreplots,'a') || strcmp(moreplots,'ab'))
803
804     figure
805
806     %_____________3D plot of JSI_____________________________________________________________
807
808     % figure
809     subplot(2,2,2);
810     surf(lambdas_var.*1000,lambdai_var.*1000,JSI)
811     axis([(lambdas-lambdasrangeJSI),(lambdas+lambdasrangeJSI),(lambdai-lambdairangeJSI),(lambdai+
            lambdairangeJSI)].*1000, 'square')
812     h=get (gcf, 'currentaxes');
813     set(h,'fontweight','bold','fontsize',9,'linewidth',2)
814     shading('interp')
815     title('joint spectral intensity','fontweight','bold','fontsize',12)
816     xlabel('\lambda_s [nm]','fontweight','bold','fontsize',12)
817     ylabel('\lambda_i [nm]','fontweight','bold','fontsize',12)
818     zlabel('I_{rel}','fontweight','bold','fontsize',12)
819
820
821
822     %_____________intensity vs. signal and idler wavelength at fixed pump_________________
823
824     lambdasrange=0.016;
825     lambdairange=lambdasrange;
826
827     lambdas_var=linspace((lambdas-lambdasrange),(lambdas+lambdasrange),400);
828     lambdai_var=linspace((lambdai-lambdairange),(lambdai+lambdairange),400);
829
830     inputWLs='ps';
831     Deltakm=fffQPM(inputWLs,lambdap,lambdas_var,pol,crystal,KTPoptax,Lambda,T,m);
832     Is=(sin(Deltakm.*L/2)./(Deltakm.*L/2)).^2;
833
834     inputWLs='pi';
835     Deltakm=fffQPM(inputWLs,lambdap,lambdai_var,pol,crystal,KTPoptax,Lambda,T,m);
836     Ii=(sin(Deltakm.*L/2)./(Deltakm.*L/2)).^2;
837
838     % figure
839     subplot(2,2,3);
840     plot(lambdas_var.*1000,Is,'linewidth',2)
841     axis([(lambdas-lambdasrange).*1000,(lambdas+lambdasrange).*1000,0,1])
842     h=get (gcf, 'currentaxes');
843     set(h,'fontweight','bold','fontsize',9,'linewidth',2)
844     grid on;
845     title('intesity vs. \lambda_s at fixed \lambda_p and \lambda_i','fontweight','bold','fontsize',12)
846     xlabel('\lambda_s [nm]','fontweight','bold','fontsize',12)
847     ylabel('I_{rel}','fontweight','bold','fontsize',12)
848
849     % figure
850     subplot(2,2,4);
851     plot(lambdai_var.*1000,Ii,'linewidth',2)
852     axis([(lambdai-lambdairange).*1000,(lambdai+lambdairange).*1000,0,1])
853     h=get (gcf, 'currentaxes');
854     set(h,'fontweight','bold','fontsize',9,'linewidth',2)
855     grid on;
856     title('intesity vs. \lambda_i at fixed \lambda_p and \lambda_s','fontweight','bold','fontsize',12)
857     xlabel('\lambda_i [nm]','fontweight','bold','fontsize',12)
858     ylabel('I_{rel}','fontweight','bold','fontsize',12)
859
```

```
860
861
862     %_____________intensity vs. signal and idler wavelengths - wide range_____________
863
864     lambdasrange=5;
865     lambdairange=lambdasrange;
866     resolution=300;
867
868     lambdas_var=linspace((lambdap+0.1),lambdasrange,resolution);
869     lambdai_var=linspace((lambdap+0.1),lambdairange,resolution);
870
871     [xx,yy]=meshgrid(lambdas_var,lambdai_var);
872
873     inputWLs='si';
874     [Deltakm,alpha]=fffQPM(inputWLs,xx,yy,pol,crystal,KTPoptax,Lambda,T,m);
875     L_of_T=L*(1+alpha*(T-25));
876     psi_PM=(sin(Deltakm.*L_of_T/2)./(Deltakm.*L_of_T/2));
877
878     % figure
879     subplot(2,2,1)
880     pcolor(lambdas_var.*1000,lambdai_var.*1000,psi_PM.^2);
881     axis([(lambdap+0.1),(lambdasrange),(lambdap+0.1),(lambdairange)].*1000, 'square')
882     h=get (gcf, 'currentaxes');
883     set(h,'fontweight','bold','fontsize',9,'linewidth',2)
884     shading('interp')
885     title('QPM intensity','fontweight','bold','fontsize',12)
886     xlabel('\lambda_s [nm]','fontweight','bold','fontsize',12)
887     ylabel('\lambda_i [nm]','fontweight','bold','fontsize',12)
888
889 end
890
891 if (strcmp(moreplots,'b') || strcmp(moreplots,'ab'))
892
893     figure
894
895     %_____________purity plot_____________________________________________________
896
897     resolutionPurity=100;
898
899     lambdas_var=linspace((lambdas-lambdasrangeJSI),(lambdas+lambdasrangeJSI),resolutionPurity);
900     lambdai_var=linspace((lambdai-lambdairangeJSI),(lambdai+lambdairangeJSI),resolutionPurity);
901
902     [xx,yy]=meshgrid(lambdas_var,lambdai_var);
903
904     inputWLs='si';
905
906     L_min=1000;
907     L_max=50000;
908     L_var=linspace(L_min,L_max,resolutionPurity);
909
910     Deltalambdap_min=0.00001;
911     Deltalambdap_max=0.005;
912     Deltalambdap_var=linspace(Deltalambdap_min,Deltalambdap_max,resolutionPurity);
913
914
915     %_____________purity vs. crystal length for fixed pump width_____________________
916
917     P_of_L=zeros(1,numel(L_var));
918
919     for (i=1:numel(L_var))
920
921         inputWLsPS='si';
922         mu_pump=fffpumpspectrum(inputWLsPS,lambdap,xx,yy,gaussian,lambdap0,Deltalambdap);
923
924         [Deltakm,alpha]=fffQPM(inputWLs,xx,yy,pol,crystal,KTPoptax,Lambda,T,m);
925         L_var(i)=L_var(i).*(1+alpha.*(T-25));
926         psi_PM=(sin(Deltakm.*L_var(i)/2)./(Deltakm.*L_var(i)/2));
927
928         JSI=(mu_pump.*psi_PM).^2;
929
930         [U,D,V_dagger]=svd(JSI);
931         D_norm=D./sqrt(trace(D^2));
932
933         P_of_L(i)=trace(D_norm^4);
934
935     end
936
937     % find index of L_var, for which P is maximal:
938     index_L_P_max  = find(P_of_L==max(P_of_L));
939
940     % find L_var, for which P is maximal:
941     L_for_P_max_mm = L_var(index_L_P_max)./1000;
942
943     % maximal P for fixed width and varying length:
```

```
944       P_of_L_max     = P_of_L(index_L_P_max);
945
946
947       xdummy0to1     = 0:0.1:1;
948       constant_L     = (xdummy0to1-xdummy0to1)+L_of_T./1000;
949       constant_L_opt = (xdummy0to1-xdummy0to1)+L_for_P_max_mm;
950
951       % figure
952       subplot(2,2,1)
953       h=plot(L_var./1000,P_of_L,constant_L,xdummy0to1,'-',constant_L_opt,xdummy0to1,'-');
954       set(h(1),'linewidth',2);
955       grid on;
956       axis([L_min./1000,L_max./1000,0,1])
957       h=get (gcf, 'currentaxes');
958       set(h,'fontweight','bold','fontsize',9,'linewidth',2)
959       title(['purity vs. crystal length at \Delta \lambda_p=', num2str(Deltalambdap*1000) ,' nm'],'fontweight'
              ,'bold','fontsize',12)
960       xlabel('L [mm]','fontweight','bold','fontsize',12)
961       ylabel('P','fontweight','bold','fontsize',12)
962       legend('P','current L','optimal L')
963
964
965
966       %_____________purity vs. pump width for fixed crystal length_________________________
967
968       P_of_D=numel(1,numel(Deltalambdap_var));
969       for (i=1:numel(Deltalambdap_var))
970
971           inputWLsPS='si';
972           mu_pump=fffpumpspectrum(inputWLsPS,lambdap,xx,yy,gaussian,lambdap0,Deltalambdap_var(i));
973
974           [Deltakm,alpha]=fffQPM(inputWLs,xx,yy,pol,crystal,KTPoptax,Lambda,T,m);
975           L_of_T=L.*(1+alpha.*(T-25));
976           psi_PM=(sin(Deltakm.*L_of_T/2)./(Deltakm.*L_of_T/2));
977
978           JSI=(mu_pump.*psi_PM).^2;
979
980           [U,D,V_dagger]=svd(JSI);
981           D_norm=D./sqrt(trace(D^2));
982
983           P_of_D(i)=trace(D_norm^4);
984
985       end
986
987       % find index of Deltalambdap_var, for which P is maximal:
988       index_D_P_max  = find(P_of_D==max(P_of_D));
989
990       % find Deltalambdap_var, for which P is maximal:
991       D_for_P_max_nm = Deltalambdap_var(index_D_P_max).*1000;
992
993       % maximal P for fixed length and varying width:
994       P_of_D_max     = P_of_D(index_D_P_max);
995
996       % translate width for maximal P into pulse duration:
997       tau_for_P_max=sqrt(log(2)/2)*lambdap0.^2./(pi*3e8*D_for_P_max_nm)*1e9;
998
999
1000      constant_D     = (xdummy0to1-xdummy0to1)+Deltalambdap.*1000;
1001      constant_D_opt = (xdummy0to1-xdummy0to1)+D_for_P_max_nm;
1002
1003      % figure
1004      subplot(2,2,3)
1005      h=plot(Deltalambdap_var.*1000,P_of_D,constant_D,xdummy0to1,'-',constant_D_opt,xdummy0to1,'-');
1006      set(h(1),'linewidth',2);
1007      grid on;
1008      axis([Deltalambdap_min.*1000,Deltalambdap_max.*1000,0,1])
1009      h=get (gcf, 'currentaxes');
1010      set(h,'fontweight','bold','fontsize',9,'linewidth',2)
1011      title(['purity vs. pump width at Lambda=', num2str(L_mm) ,' mm'],'fontweight','bold','fontsize',12)
1012      xlabel('\Delta \lambda_p [nm]','fontweight','bold','fontsize',12)
1013      ylabel('P','fontweight','bold','fontsize',12)
1014      legend('P','current \Delta \lambda_p','optimal \Delta \lambda_p')
1015
1016
1017      fprintf('crystal length for best purity at pump width %5.2f nm/pulse duration %6.3f ps:\n%4.1f mm (P
              =%5.3f)\n\n', Deltalambdap*1000,tau,L_for_P_max_mm,P_of_L_max)
1018
1019      fprintf('pump width and pulse duration for best purity at crystal length %4.1f mm:\n%5.2f nm, %6.3f ps (
              P=%5.3f)\n\n', L_mm,D_for_P_max_nm,tau_for_P_max,P_of_D_max)
1020
1021
1022      %_____________purity vs. pump width and crystal length_________________________________
1023
1024
```

```
    for (i=1:numel(Deltalambdap_var))

        for (j=1:numel(L_var))

            inputWLsPS='si';
            mu_pump=fffpumpspectrum(inputWLsPS,lambdap,xx,yy,gaussian,lambdap0,Deltalambdap_var(i));

            [Deltakm,alpha]=fffQPM(inputWLs,xx,yy,pol,crystal,KTPoptax,Lambda,T,m);
            L_var(j)=L_var(j).*(1+alpha.*(T-25));
            psi_PM=(sin(Deltakm.*L_var(j)/2)./(Deltakm.*L_var(j)/2));

            JSI=(mu_pump.*psi_PM).^2;

            [U,D,V_dagger]=svd(JSI);
            D_norm=D./sqrt(trace(D^2));

            P(i,j)=trace(D_norm^4);

        end

    end

    % figure
    subplot(1,2,2)
    pcolor(Deltalambdap_var.*1000,L_var./1000,P)
    colorbar ();
    axis([Deltalambdap_min.*1000,Deltalambdap_max.*1000,L_min./1000,L_max./1000], 'square')
    h=get (gcf, 'currentaxes');
    set(h,'fontweight','bold','fontsize',9,'linewidth',2)
    shading('interp')
    title('purity vs. pump width and crystal length','fontweight','bold','fontsize',12)
    xlabel('\Delta \lambda_p [nm]','fontweight','bold','fontsize',12)
    ylabel('L [mm]','fontweight','bold','fontsize',12)

    hold on;

    constant_L=(Deltalambdap_var-Deltalambdap_var)+L_of_T./1000;
    constant_D=(L_var-L_var)+Deltalambdap.*1000;

    plot(Deltalambdap_var.*1000,constant_L,'-w',constant_D,L_var./1000,'-w')
    axis([Deltalambdap_min.*1000,Deltalambdap_max.*1000,L_min./1000,L_max./1000], 'square')

    hold off;

end
```

## B.2 QPMinputs

```
%%%%%%%%%%%%%%%% ENTER YOUR INPUT PARAMETERS %%%%%%%%%%%%%%%%%%%%%%%%%%%%%%%%%%%%%%%%%%%%

%_________________pump and signal wavelength [nm]_____________________________________

lambdap_nm=775;
lambdas_nm=2*lambdap_nm;

%_________________pump, signal and idler polarisation ('o' or 'e')_____________________

polp='e';
pols='o';
poli='e';

%_________________gaussian pump? ('y' or 'n')_____________________________________________

gaussian='y';

    %_____________choose pulse duration ('t') or gaussian width ('w') as input___________

    timeorwidth='t';

        %_________pulse duration [ps]_____________________________________________________

        tau=0.25;

        %_________spectral width of pump [nm]_____________________________________________

        Deltalambdap_nm=1.5;

%_________________crystal type ('KTP' or 'LN')_____________________________________________

crystal='KTP';

```

```
35      %_____________KTP optic axis ('z' or 'y')_____________________________________________
36
37      KTPoptax='y';
38
39  %_________________crystal length [mm]_____________________________________________________
40
41  L_mm=4.6;
42
43  %_________________parameter to be optimised for QPM ('Lambda' or 'T')_____________________
44
45  opt='Lambda';
46
47      %_____________poling periodicity [um]_____________________________________________
48
49      Lambda=46.11;
50
51      %_____________temperature [deg C]_____________________________________________________
52
53      T=50;
54
55  %_________________QPM order_____________________________________________________________
56
57  m=1;
58
59
60  %%%%%%%%%%%%%%%%%%%%%%%%%%%%%%%%%%%%%%%%%%%%%%%%%%%%%%%%%%%%%%%%%%%%%%%%%%%%%%%%%%%%%%%%
61
62
63
64
65
66
67  lambdap=lambdap_nm./1000;
68  lambdas=lambdas_nm./1000;
69  lambdap0=lambdap;
70
71  if (strcmp(timeorwidth,'t'))
72
73      Deltalambdap=sqrt(log(2)/2)*lambdap.^2./(pi*3e8*tau)*1e6;
74
75  else
76
77      Deltalambdap=Deltalambdap_nm./1000;
78      tau=sqrt(log(2)/2)*lambdap.^2./(pi*3e8*Deltalambdap)*1e6;
79
80  end
81
82  L=L_mm.*1000;
83
84  lambdai=1/(1/lambdap-1/lambdas);
85
86  pol=[polp,pols,poli];
87
88  if (strcmp(pol,['o','o','o']) || strcmp(pol,['e','e','e']))
89
90      Type='0';
91
92  elseif (strcmp(pol,['o','e','e']) || strcmp(pol,['e','o','o']))
93
94      Type='I';
95
96  elseif (strcmp(pol,['o','o','e']) || strcmp(pol,['o','e','o']) || strcmp(pol,['e','o','e']) || strcmp(pol,['
        e','e','o']))
97
98      Type='II';
99
100 end
```

## B.3 fffQPM

```
1   function [Deltakm,alpha] = fffQPM(inputWLs,lambda1,lambda2,pol,crystal,KTPoptax,Lambda,T,m)
2
3
4   if (strcmp(inputWLs,'ps'))
5
6       lambdap=lambda1;
7       lambdas=lambda2;
8
9       lambdai=1./(1./lambdap-1./lambdas);
10
11  elseif (strcmp(inputWLs,'pi'))
12
```

```
13      lambdap=lambda1;
14      lambdai=lambda2;
15
16      lambdas=1./(1./lambdap-1./lambdai);
17
18  elseif (strcmp(inputWLs,'si'))
19
20      lambdas=lambda1;
21      lambdai=lambda2;
22
23      lambdap=1./(1./lambdas+1./lambdai);
24
25  end
26
27  lambda1=lambdap;
28  lambda2=lambdas;
29  lambda3=lambdai;
30
31
32  % reference temperature:
33  TR=25;
34
35  if (strcmp(crystal,'LN'))
36
37  A1z=5.35583;
38  A2z=0.100473;
39  A3z=0.20692;
40  A4z=100;
41  A5z=128.806;
42  A6z=1.5334e-2;
43  B1z=4.629e-7;
44  B2z=3.862e-8;
45  B3z=0.89e-8;
46  B4z=2.657e-5;
47
48  A1y=4.9048;
49  A2y=0.11775;
50  A3y=0.21802;
51  A4y=0;
52  A5y=0;
53  A6y=0.027153;
54  B1y=2.1429e-8;
55  B2y=2.2314e-8;
56  B3y=2.9671e-8;
57  B4y=0;
58
59  % thermal extension coefficients in x-direction:
60  alpha0=13.3e-6;
61  alpha1=9.7e-9;
62
63  % temperature parameter:
64  F=fffF(T);
65
66  % k chosen to propagate along x-axis (due to QPM considerations)
67  % ==> n_ord=n_y (=n_x)
68  % ==> n_opt=n_z
69
70  nord1=fffsellmeierLN(lambda1,A1y,A2y,A3y,A4y,A5y,A6y,B1y,B2y,B3y,B4y,F);
71  % notation: "nord1" --> refractive index along ordinary axis for wavelength lambda_1
72
73  nopt1=fffsellmeierLN(lambda1,A1z,A2z,A3z,A4z,A5z,A6z,B1z,B2z,B3z,B4z,F);
74  % notation: "nopt1" --> index along optic (extraordinary) axis for wavelength lambda_1
75
76  nord2=fffsellmeierLN(lambda2,A1y,A2y,A3y,A4y,A5y,A6y,B1y,B2y,B3y,B4y,F);
77  nopt2=fffsellmeierLN(lambda2,A1z,A2z,A3z,A4z,A5z,A6z,B1z,B2z,B3z,B4z,F);
78
79  nord3=fffsellmeierLN(lambda3,A1y,A2y,A3y,A4y,A5y,A6y,B1y,B2y,B3y,B4y,F);
80  nopt3=fffsellmeierLN(lambda3,A1z,A2z,A3z,A4z,A5z,A6z,B1z,B2z,B3z,B4z,F);
81
82
83  elseif (strcmp(crystal,'KTP'))
84
85      % koenig and wong, 2004
86      A1y=2.09930;
87      A2y=0.922683;
88      A3y=0.0467695;
89      A4y=0;
90      A5y=0;
91      A6y=0.0138408;
92
93      % % fan, huang et al., 1987
94      % A1y=2.19229;
95      % A2y=0.83547;
96      % A3y=0.04970;
```

```
97      % A4y=0;
98      % A5y=0;
99      % A6y=0.01621;
100
101     % fradkin, arie et al., 1999
102     A1z=2.12725;
103     A2z=1.18431;
104     A3z=5.14852e-2;
105     A4z=0.6603;
106     A5z=100.00507;
107     A6z=9.68956e-3;
108
109     ay10=6.2897e-6;
110     % notation: "ay10" --> a0 component for n1 in y direction
111
112     ay11=6.3061e-6;
113     ay12=-6.0629e-6;
114     ay13=2.6486e-6;
115
116     ay20=-0.14445e-8;
117     ay21=2.2244e-8;
118     ay22=-3.5770e-8;
119     ay23=1.3470e-8;
120
121     az10=9.9587e-6;
122     az11=9.9228e-6;
123     az12=-8.9603e-6;
124     az13=4.1010e-6;
125
126     az20=-1.1882e-8;
127     az21=10.459e-8;
128     az22=-9.8136e-8;
129     az23=3.1481e-8;
130
131     % thermal extension coefficients in x-direction:
132     alpha0=6.7e-6;
133     alpha1=11e-9;
134
135 if (strcmp(KTPoptax,'y'))
136
137     % k chosen to propagate along x-axis
138     % ==> n_ord=n_z (although higher non-linearity for n_ext=n_z!! --> would result in too small L,
            therefore higher QPM order.)
139     % ==> n_opt=n_y
140
141         % n ordinary for wavelength of first photon (T-independent!!):
142         nord_lambda1=fffsellmeierKTP(lambda1,A1z,A2z,A3z,A4z,A5z,A6z);
143
144         nz11=fffnpoly(az10,az11,az12,az13,lambda1);
145         nz21=fffnpoly(az20,az21,az22,az23,lambda1);
146         % notation: "ny21" --> n2 for first photon polarised in z direction
147
148         % temperature dependent portion of refractive index:
149         Deltan1=fffDeltan(nz11,nz21,T,TR);
150
151     % n ordinary for wavelength of 1st photon (T-dependent!!):
152     nord1=nord_lambda1+Deltan1;
153
154         nopt_lambda1=fffsellmeierKTP(lambda1,A1y,A2y,A3y,A4y,A5y,A6y);
155         ny11=fffnpoly(ay10,ay11,ay12,ay13,lambda1);
156         ny21=fffnpoly(ay20,ay21,ay22,ay23,lambda1);
157         Deltan1=fffDeltan(ny11,ny21,T,TR);
158     nopt1=nopt_lambda1+Deltan1;
159
160         nord_lambda2=fffsellmeierKTP(lambda2,A1z,A2z,A3z,A4z,A5z,A6z);
161         nz12=fffnpoly(az10,az11,az12,az13,lambda2);
162         nz22=fffnpoly(az20,az21,az22,az23,lambda2);
163         Deltan2=fffDeltan(nz12,nz22,T,TR);
164     nord2=nord_lambda2+Deltan2;
165
166         nopt_lambda2=fffsellmeierKTP(lambda2,A1y,A2y,A3y,A4y,A5y,A6y);
167         ny12=fffnpoly(ay10,ay11,ay12,ay13,lambda2);
168         ny22=fffnpoly(ay20,ay21,ay22,ay23,lambda2);
169         Deltan2=fffDeltan(ny12,ny22,T,TR);
170     nopt2=nopt_lambda2+Deltan2;
171
172         nord_lambda3=fffsellmeierKTP(lambda3,A1z,A2z,A3z,A4z,A5z,A6z);
173         nz13=fffnpoly(az10,az11,az12,az13,lambda3);
174         nz23=fffnpoly(az20,az21,az22,az23,lambda3);
175         Deltan3=fffDeltan(nz13,nz23,T,TR);
176     nord3=nord_lambda3+Deltan3;
177
178         nopt_lambda3=fffsellmeierKTP(lambda3,A1y,A2y,A3y,A4y,A5y,A6y);
179         ny13=fffnpoly(ay10,ay11,ay12,ay13,lambda3);
```

```
180         ny23=fffnpoly(ay20,ay21,ay22,ay23,lambda3);
181         Deltan3=fffDeltan(ny13,ny23,T,TR);
182     nopt3=nopt_lambda3+Deltan3;
183
184
185     elseif (strcmp(KTPoptax,'z'))
186
187     % n_ord=n_y
188     % n_opt=n_z
189
190         nord_lambda1=fffsellmeierKTP(lambda1,A1y,A2y,A3y,A4y,A5y,A6y);
191         ny11=fffnpoly(ay10,ay11,ay12,ay13,lambda1);
192         ny21=fffnpoly(ay20,ay21,ay22,ay23,lambda1);
193         Deltan1=fffDeltan(ny11,ny21,T,TR);
194     nord1=nord_lambda1+Deltan1;
195
196         nopt_lambda1=fffsellmeierKTP(lambda1,A1z,A2z,A3z,A4z,A5z,A6z);
197         nz11=fffnpoly(az10,az11,az12,az13,lambda1);
198         nz21=fffnpoly(az20,az21,az22,az23,lambda1);
199         Deltan1=fffDeltan(nz11,nz21,T,TR);
200     nopt1=nopt_lambda1+Deltan1;
201
202         nord_lambda2=fffsellmeierKTP(lambda2,A1y,A2y,A3y,A4y,A5y,A6y);
203         ny12=fffnpoly(ay10,ay11,ay12,ay13,lambda2);
204         ny22=fffnpoly(ay20,ay21,ay22,ay23,lambda2);
205         Deltan2=fffDeltan(ny12,ny22,T,TR);
206     nord2=nord_lambda2+Deltan2;
207
208         nopt_lambda2=fffsellmeierKTP(lambda2,A1z,A2z,A3z,A4z,A5z,A6z);
209         nz12=fffnpoly(az10,az11,az12,az13,lambda2);
210         nz22=fffnpoly(az20,az21,az22,az23,lambda2);
211         Deltan2=fffDeltan(nz12,nz22,T,TR);
212     nopt2=nopt_lambda2+Deltan2;
213
214         nord_lambda3=fffsellmeierKTP(lambda3,A1y,A2y,A3y,A4y,A5y,A6y);
215         ny13=fffnpoly(ay10,ay11,ay12,ay13,lambda3);
216         ny23=fffnpoly(ay20,ay21,ay22,ay23,lambda3);
217         Deltan3=fffDeltan(ny13,ny23,T,TR);
218     nord3=nord_lambda3+Deltan3;
219
220         nopt_lambda3=fffsellmeierKTP(lambda3,A1z,A2z,A3z,A4z,A5z,A6z);
221         nz13=fffnpoly(az10,az11,az12,az13,lambda3);
222         nz23=fffnpoly(az20,az21,az22,az23,lambda3);
223         Deltan3=fffDeltan(nz13,nz23,T,TR);
224     nopt3=nopt_lambda3+Deltan3;
225
226 end
227
228
229 end
230
231 % periodicity including thermal extension:
232 alpha=alpha0+alpha1.*(T-TR);
233 Lambda=Lambda.*(1+alpha.*(T-TR));
234
235 %_________________type 0_____________________________________________________________________
236
237 if (strcmp(pol,['e','e','e']))
238
239     n1=nopt1;
240     n2=nopt2;
241     n3=nopt3;
242
243 elseif (strcmp(pol,['o','o','o']))
244
245     n1=nord1;
246     n2=nord2;
247     n3=nord3;
248
249 %_________________type I_____________________________________________________________________
250
251 elseif (strcmp(pol,['e','o','o']))
252
253     n1=nopt1;
254     n2=nord2;
255     n3=nord3;
256
257 elseif (strcmp(pol,['o','e','e']))
258
259     n1=nord1;
260     n2=nopt2;
261     n3=nopt3;
262
263 %_________________type II____________________________________________________________________
```

```
264
265 elseif (strcmp(pol,['e','o','e']))
266
267     n1=nopt1;
268     n2=nord2;
269     n3=nopt3;
270
271 elseif (strcmp(pol,['e','e','o']))
272
273     n1=nopt1;
274     n2=nopt2;
275     n3=nord3;
276
277 elseif (strcmp(pol,['o','o','e']))
278
279     n1=nord1;
280     n2=nord2;
281     n3=nopt3;
282
283 elseif (strcmp(pol,['o','e','o']))
284
285     n1=nord1;
286     n2=nopt2;
287     n3=nord3;
288
289 end
290
291 % phase mismatch w.o. periodic poling:
292 Deltak=fffDeltak(lambda1,lambda2,lambda3,n1,n2,n3);
293
294 % phase mismatch including periodic poling:
295 Deltakm=Deltak-2*pi*m./Lambda;
296
297 return
298 end
299
300 %_________________Delta k_____________________________________________________
301
302 function [Deltak] = fffDeltak(lambda1,lambda2,lambda3,n1,n2,n3)
303
304 Deltak=2*pi*(n1./lambda1-n2./lambda2-n3./lambda3);
305
306 return
307 end
308
309 %_________________F parameter__________________________________________________
310
311 function [F] = fffF(T)
312
313 F=(T-24.5).*(T+570.82);
314
315 return
316 end
317
318 %_________________sellmeier equation for LN_____________________________________
319
320 function [n] = fffsellmeierLN(lambda,A1,A2,A3,A4,A5,A6,B1,B2,B3,B4,F)
321
322 n=(A1+B1*F+(A2+B2*F)./(lambda.^2-(A3-B3*F).^2)+(A4+B4*F)./(lambda.^2-A5)-A6*lambda.^2).^(1/2);
323
324 return
325 end
326
327 %_________________temp. indep. sellmeier equation for KTP_____________________
328
329 function [n] = fffsellmeierKTP(lambda,A1,A2,A3,A4,A5,A6)
330
331 n=(A1+A2./(1-A3./lambda.^2)+A4./(1-A5./lambda.^2)-A6.*lambda.^2).^(1/2);
332
333 return
334 end
335
336 %_________________polynomial n_____________________________________________
337
338 function [npoly] = fffnpoly(a0,a1,a2,a3,lambda)
339
340     npoly=a0+a1./lambda+a2./lambda.^2+a3./lambda.^3;
341
342 return
343 end
344
345 %_________________Delta n_____________________________________________________
346
347 function [Deltan] = fffDeltan(n1,n2,T,TR)
```

```
348
349     Deltan=n1*(T-TR)+n2*(T-TR).^2;
350
351 return
352 end
353
354
355 % sellmeier equations for n_z in LN:
356 % jundt. temperature-dependent sellmeier equation for the index of refraction, n_e, in congruent lithium
        niobate. optics letters, 1997.
357
358 % sellmeier equations for n_y in LN:
359 % edwards and lawrence. a temperature-dependent dispersion equation for congruently grown lithium niobate.
        optical and quantum electronics, 1984.
360
361 % thermal extension of LN:
362 % pignatiello, de rosa et al. measurement of the thermal expansion coefficients of ferroelectric crystals by
         a moire interferometer. optics communications, 2007.
363
364 % sellmeier equation for n_y in KTP:
365 % koenig and wong. extended phase matching of second-harmonic generation in periodically poled KTiOPO4 with
        zero group-velocity mismatch. applied physics letters, 2004
366
367 % or: sellmeier equation for n_y in KTP:
368 % fan, huang et al. second harmonic generation and accurate index of refraction measurement in flux-grown
        KTiOPO4. applied optics, 1987
369
370 % sellmeier equation for n_z in KTP:
371 % fradkin, arie, et al. tunable midinfrared source by difference frequency generation in bulk periodically
        poled KTiOPO44. applied physics letters, 1999
372
373 % temperature dependence (ay10,..., ny11,..., npoly, Deltan) of KTP indices and thermal extension of KTP:
374 % emanueli and arie. temperature-dependent dispersion equations for KTiOPO4 and KTiOAsO4. applied optics,
        2003
```

## B.4 fffrootfinderQPM

```
1  function [x0,outrange,m,xstart,xend] = fffrootfinderQPM(opt,lambda1,lambda2,pol,crystal,KTPoptax,Lambda,T,m)
2
3
4  inputWLs='ps';
5
6  tol=1e-9;
7
8  outrange=0;
9
10
11 if (strcmp(opt,'Lambda') || strcmp(opt,'T'))
12
13     if (strcmp(opt,'Lambda'))
14
15         xstart = 1;
16         xend   = 20000;
17         xmid   = (xend+xstart)/2;
18
19         ystart = fffQPM(inputWLs,lambda1,lambda2,pol,crystal,KTPoptax,xstart,T,m);
20         yend   = fffQPM(inputWLs,lambda1,lambda2,pol,crystal,KTPoptax,xend,T,m);
21         ymid   = fffQPM(inputWLs,lambda1,lambda2,pol,crystal,KTPoptax,xmid,T,m);
22
23         if (sign(ystart).*sign(yend)~=-1)
24
25             m=-m;
26
27             ystart = fffQPM(inputWLs,lambda1,lambda2,pol,crystal,KTPoptax,xstart,T,m);
28             yend   = fffQPM(inputWLs,lambda1,lambda2,pol,crystal,KTPoptax,xend,T,m);
29             ymid   = fffQPM(inputWLs,lambda1,lambda2,pol,crystal,KTPoptax,xmid,T,m);
30
31             if (sign(ystart).*sign(yend)~=-1)
32
33                 outrange=1;
34                 x0=xmid;
35                 m=-m;
36                 return
37
38             end
39
40         end
41
42         i=0;
43
44         while (abs(ymid)>tol)
45
```

```
46              i=i+1;
47
48              if (sign(ystart).*sign(ymid)==-1)
49
50                  xend=xmid;
51
52              elseif (sign(ymid).*sign(yend)==-1)
53
54                  xstart=xmid;
55
56              end
57
58              xmid   = (xend+xstart)/2;
59              ystart = fffQPM(inputWLs,lambda1,lambda2,pol,crystal,KTPoptax,xstart,T,m);
60              yend   = fffQPM(inputWLs,lambda1,lambda2,pol,crystal,KTPoptax,xend,T,m);
61              ymid   = fffQPM(inputWLs,lambda1,lambda2,pol,crystal,KTPoptax,xmid,T,m);
62
63          end
64
65          x0=xmid;
66
67
68      elseif (strcmp(opt,'T'))
69
70          xstart = 0;
71          xend   = 300;
72          xmid   = (xend+xstart)/2;
73
74          ystart = fffQPM(inputWLs,lambda1,lambda2,pol,crystal,KTPoptax,Lambda,xstart,m);
75          yend   = fffQPM(inputWLs,lambda1,lambda2,pol,crystal,KTPoptax,Lambda,xend,m);
76          ymid   = fffQPM(inputWLs,lambda1,lambda2,pol,crystal,KTPoptax,Lambda,xmid,m);
77
78          if(sign(ystart).*sign(yend)~=-1)
79
80              m=-m;
81
82              ystart = fffQPM(inputWLs,lambda1,lambda2,pol,crystal,KTPoptax,xstart,T,m);
83              yend   = fffQPM(inputWLs,lambda1,lambda2,pol,crystal,KTPoptax,xend,T,m);
84              ymid   = fffQPM(inputWLs,lambda1,lambda2,pol,crystal,KTPoptax,xmid,T,m);
85
86              if (sign(ystart).*sign(yend)~=-1)
87
88                  outrange=1;
89                  x0=xmid;
90                  m=-m;
91                  return
92
93              end
94
95          end
96
97          i=0;
98
99          while (abs(ymid)>tol)
100
101             i=i+1;
102
103             if (sign(ystart).*sign(ymid)==-1)
104
105                 xend=xmid;
106
107             elseif (sign(ymid).*sign(yend)==-1)
108
109                 xstart=xmid;
110
111             end
112
113             xmid   = (xend+xstart)/2;
114             ystart = fffQPM(inputWLs,lambda1,lambda2,pol,crystal,KTPoptax,Lambda,xstart,m);
115             yend   = fffQPM(inputWLs,lambda1,lambda2,pol,crystal,KTPoptax,Lambda,xend,m);
116             ymid   = fffQPM(inputWLs,lambda1,lambda2,pol,crystal,KTPoptax,Lambda,xmid,m);
117
118         end
119
120         x0=xmid;
121
122         end
123
124
125 elseif (strcmp(opt,'lambdas'))
126
127     xstart = lambda2-0.05;
128     xend   = lambda2+0.05;
129     xmid   = (xend+xstart)/2;
```

```
130
131     ystart = fffQPM(inputWLs,lambda1,xstart,pol,crystal,KTPoptax,Lambda,T,m);
132     yend   = fffQPM(inputWLs,lambda1,xend,pol,crystal,KTPoptax,Lambda,T,m);
133     ymid   = fffQPM(inputWLs,lambda1,xmid,pol,crystal,KTPoptax,Lambda,T,m);
134
135     if (sign(ystart).*sign(yend)~=-1)
136
137         outrange=1;
138         x0=xmid;
139         return
140
141     end
142
143     i=0;
144
145     while (abs(ymid)>tol)
146
147         i=i+1;
148
149         if (sign(ystart).*sign(ymid)==-1)
150
151             xend=xmid;
152
153         elseif (sign(ymid).*sign(yend)==-1)
154
155             xstart=xmid;
156
157         end
158
159         xmid   = (xend+xstart)/2;
160         ystart = fffQPM(inputWLs,lambda1,xstart,pol,crystal,KTPoptax,Lambda,T,m);
161         yend   = fffQPM(inputWLs,lambda1,xend,pol,crystal,KTPoptax,Lambda,T,m);
162         ymid   = fffQPM(inputWLs,lambda1,xmid,pol,crystal,KTPoptax,Lambda,T,m);
163
164     end
165
166     x0=xmid;
167
168 end
169
170
171 return
172 end
```

## B.5 fffpumpspectrum

```
1  function [mu_pump] = fffpumpspectrum(inputWLsPS,lambdap_var,lambdas,lambdai,gaussian,lambdap0,Deltalambdap)
2
3
4  if (strcmp(inputWLsPS,'si'))
5
6      lambdap_var=1./(1./lambdas+1./lambdai);
7
8  end
9
10
11 if (strcmp(gaussian,'y'))
12
13     mu_pump=exp(-(lambdap_var-lambdap0).^2./(2.*Deltalambdap.^2));
14
15 elseif (strcmp(gaussian,'n'))
16
17     % in order for the calculations to make sense, please express your self-defined pulse shape in terms of
           lambdap0 and Deltalambdap and make sure that it's normalised.
18
19     lambdap01=lambdap0+0.0004;
20     lambdap02=lambdap0-0.0008;
21
22     Deltalambdap1=Deltalambdap*0.1933;
23     Deltalambdap2=Deltalambdap*0.20556;
24
25     mu1=exp(-(lambdap_var-lambdap01).^2/(2*Deltalambdap1^2))*0.72;
26     mu2=exp(-(lambdap_var-lambdap02).^2/(2*Deltalambdap2^2));
27
28     mu_pump=mu1+mu2;
29
30 end
31
32 return
33
34 end
```

## B.6 readmeQPM

```
%%%%%%%%%%%%%%%%%% THANKS FOR USING QPMoptics! %%%%%%%%%%%%%%%%%%%%%%%%%%%%%%%%%%%%%%%%


This program was created with support of the Austrian Institute of Technology, Department Digital Safety and Security (AIT, DSS). Feel free to use it, change it, share and distribute it. Please do neither pay for it nor try to sell it.

The program was developed using GNU octave but it can just as well be executed by Matlab.

If you find a way to improve the program or if you just want to share your opinion, please don't hesitate to contact me under fabian.laudenbach.fl@ait.ac.at .

Best regards,
Fabian Laudenbach



%%%%%%%%%%%%%%%%%%%%%%%%%%%%%%%%%%%%%%%%%%%%%%%%%%%%%%%%%%%%%%%%%%%%%%%%%%%%%%%%%%%%%%%%%%%%


Some remarks on the usage of this program:

%_____________________________________________________________________________________________

Make sure that the following files are all contained in one folder (the prefix 'fff' in a file's name indicates an external function called by 'QPMoptics'):

    # QPMoptics.m
    # QPMinputs.m
    # fffQPM.m
    # fffrootfinderQPM.m
    # fffpumpspectrumQPM.m

%_____________________________________________________________________________________________

Legend of occurring physical variables:

    # lambda_p, lambda_s, lambda_i : pump, signal and idler wavelength [um]
    # polp, pols, poli             : pump, signal and idler polarisation ('o' for ordinary, 'e' for extraordinary)
    # Type                         : SPDC type ('0', 'I' or 'II')
    # tau                          : FWHM of laser-pulse duration [ps]
    # Deltalambdap                 : Gaussian width of pump laser spectrum [um]
    # crystal                      : periodically poled crystal ('KTP' for potassium titanyl phosphate, 'LN' for lithium niobate)
    # KTPoptax                     : optic axis of KTP crystal ('z' or 'y'; default: 'y')
    # L                            : crystal length [um]
    # Lambda                       : poling periodicity Lambda [um]
    # T                            : temperature [deg C]
    # m                            : quasi-phase-matching order
    # alpha                        : thermal expansion coefficient
    # Deltakm                      : phase mismatch [um]
    # Deltalambdas, Deltalambdai   : Gaussian width of signal and idler output [um]
    # mu_pump                      : pump envelope amplitude
    # psi_PM                       : phase-matching envelope amplitude
    # I                            : phase-matching envelope intensity
    # JSI                          : joint spectral intensity
    # K                            : Schmidt number
    # P                            : spectral purity of signal and idler output

    (Unless denoted otherwise (e.g. lambdas_nm, L_mm), all variables describing a length (wavelength, spectral width, phase mismatch, crystal length, periodicity) are understood in micrometers.)

%_____________________________________________________________________________________________

Some of the calculations within this program are very extensive and consume a lot of computing time. This is especially the case for

    # the evaluation of the output spectra: can be skipped by entering 'f' right after the program was started,
    # the evaluation of spectral purity with respect to spectral pump width and crystal length: can be abbreviated by increasing the step-size, i.e. decreasing the variable 'resolutionPurity' in the file QPMoptics.m .

%_____________________________________________________________________________________________

Note that some calculations only make sense as long as the joint spectral intensity (JSI) is confined within the specified range of signal and idler output, i.e. as long as the JSI doesn't exceed the plot axes. Otherwise the following problems will occur:

```

```
68      # The evaluation of the output spectra will produce the error message, "QPMoptics: A(I): index out of
            bounds;...".
69      # The displayed values for Schmidt number and spectral purity will make no sense and should not be taken
            seriously.
70
71      In order to confine the JSI within the plot, you may increase the signal and idler range by adjusting
            the variables 'lambdasrangeJSI' and 'lambdairangeJSI'.
72
73  %_____________________________________________________________________________________________
```

# Bibliography


[1] JA Armstrong, N Bloembergen, J Ducuing, and PS Pershan. Interactions between light waves in a nonlinear dielectric. *Physical Review*, 127(6):1918, 1962.

[2] CH Bennett and G Brassard. 1984 quantum cryptography: Public key distribution and coin tossing proc. ieee. In *Proc. Conf. Comput. Syst. Signal Process*, pages 175–179, 1992.

[3] Charles H Bennett and Stephen J Wiesner. Communication via one-and two-particle operators on einstein-podolsky-rosen states. *Physical review letters*, 69(20):2881, 1992.

[4] Dik Bouwmeester, Jian-Wei Pan, Klaus Mattle, Manfred Eibl, Harald Weinfurter, and Anton Zeilinger. Experimental quantum teleportation. *Nature*, 390(6660):575–579, 1997.

[5] AV Burlakov, MV Chekhova, DN Klyshko, SP Kulik, AN Penin, YH Shih, and DV Strekalov. Interference effects in spontaneous two-photon parametric scattering from two macroscopic regions. *Physical Review A*, 56(4):3214, 1997.

[6] Marc Busse. Entanglement in open quantum systems. Master's thesis, Ludwig-Maximilians-Universität München, May 2006.

[7] David Deutsch and Richard Jozsa. Rapid solution of problems by quantum computation. *Proceedings of the Royal Society of London. Series A: Mathematical and Physical Sciences*, 439(1907):553–558, 1992.

[8] JH Eberly. Schmidt analysis of pure-state entanglement. *Laser physics*, 16(6):921–926, 2006.

[9] GJ Edwards and M Lawrence. A temperature-dependent dispersion equation for congruently grown lithium niobate. *Optical and quantum electronics*, 16(4):373–375, 1984.

[10] Shai Emanueli and Ady Arie. Temperature-dependent dispersion equations for $KTiOPO_4$ and $KTiOAsO_4$. *Applied optics*, 42(33):6661–6665, 2003.

[11] K Fradkin, A Arie, A Skliar, and G Rosenman. Tunable midinfrared source by difference frequency generation in bulk periodically poled ktiopo4. *Applied physics letters*, 74(7):914–916, 1999.

[12] Thomas Gerrits, Martin J Stevens, Burm Baek, Brice Calkins, Adriana Lita, Scott Glancy, Emanuel Knill, Sae Woo Nam, Richard P Mirin, Robert H Hadfield, et al. Generation of degenerate, factorizable, pulsed squeezed light at telecom wavelengths. *Optics express*, 19(24):24434–24447, 2011.

[13] CK Hong, ZY Ou, and Leonard Mandel. Measurement of subpicosecond time intervals between two photons by interference. *Physical Review Letters*, 59(18):2044, 1987.

[14] Rui-Bo Jin, Ryosuke Shimizu, Isao Morohashi, Kentaro Wakui, Masahiro Takeoka, Shuro Izumi, Takahide Sakamoto, Mikio Fujiwara, Taro Yamashita, Shigehito Miki, et al. Efficient generation of twin photons at telecom wavelengths with 2.5 ghz repetition-rate-tunable comb laser. *Scientific reports*, 4, 2014.

[15] Rui-Bo Jin, Ryosuke Shimizu, Kentaro Wakui, Hugo Benichi, and Masahide Sasaki. Widely tunable single photon source with high purity at telecom wavelength. *Optics express*, 21(9):10659–10666, 2013.

[16] Rui-Bo Jin, Kentaro Wakui, Ryosuke Shimizu, Hugo Benichi, Shigehito Miki, Taro Yamashita, Hirotaka Terai, Zhen Wang, Mikio Fujiwara, and Masahide Sasaki. Nonclassical interference between independent intrinsically pure single photons at telecommunication wavelength. *Physical Review A*, 87(6):063801, 2013.

[17] Dieter H Jundt. Temperature-dependent sellmeier equation for the index of refraction, $n_e$, in congruent lithium niobate. *Optics Letters*, 22(20):1553–1555, 1997.

[18] Friedrich König and Franco NC Wong. Extended phase matching of second-harmonic generation in periodically poled ktiopo4 with zero group-velocity mismatch. *Applied physics letters*, 84(10):1644–1646, 2004.

[19] Rodney Loudon. *The Quantum Theory of Light*. Oxford University Press, 2000.

[20] Peter J. Mosley. *Generation of Heralded Single Photons in Pure Quantum States*. PhD thesis, Hertford College, Oxford, 2007.

[21] Peter J Mosley, Jeff S Lundeen, Brian J Smith, and Ian A Walmsley. Conditional preparation of single photons using parametric downconversion: a recipe for purity. *New Journal of Physics*, 10(9):093011, 2008.

[22] Jian-Wei Pan, Dik Bouwmeester, Harald Weinfurter, and Anton Zeilinger. Experimental entanglement swapping: Entangling photons that never interacted. *Physical Review Letters*, 80(18):3891, 1998.

[23] F Pignatiello, M De Rosa, P Ferraro, S Grilli, P De Natale, A Arie, and S De Nicola. Measurement of the thermal expansion coefficients of ferroelectric crystals by a moiré interferometer. *Optics communications*, 277(1):14–18, 2007.

[24] A Poppe, A Fedrizzi, R Ursin, H Böhm, T Lörunser, O Maurhardt, M Peev, M Suda, Ch Kurtsiefer, H Weinfurter, et al. Practical quantum key distribution with polarization entangled photons. *Optics Express*, 12(16):3865–3871, 2004.

[25] Peter E Powers. *Fundamentals of nonlinear optics*. CRC Press, 2011.

[26] Malvin Carl Teich and Saleh Bahaa E. A. *Fundamentals of photonics*. John Wiley & Sons, 2007.

[27] Alexander Treiber, Andreas Poppe, Michael Hentschel, Daniele Ferrini, Thomas Lorünser, Edwin Querasser, Thomas Matyus, Hannes Hübel, and Anton Zeilinger. A fully automated entanglement-based quantum cryptography system for telecom fiber networks. *New Journal of Physics*, 11(4):045013, 2009.

[28] Alfred B U'Ren, Christine Silberhorn, Reinhard Erdmann, Konrad Banaszek, Warren P Grice, Ian A Walmsley, and Michael G Raymer. Generation of pure-state single-photon wavepackets by conditional preparation based on spontaneous parametric downconversion. *arXiv preprint quant-ph/0611019*, 2006.

# Fabian Laudenbach

*Curriculum Vitae*

## Education

2013–2015 **Master studies physics**, *Universität Wien*, Vienna.
Specialisation: quantum optics, quantum information, quantum field theory, special and general relativity, statistical physics, scientific computing

2006–2013 **Magister-/Bachelor studies physics**, *Universität Wien*, Vienna.

## Master Thesis

title *Engineering Spectrally Pure Quantum States with SPDC using Periodically Poled Crystals and Pulsed Laser Sources*

supervisors Assoz. Prof. Dr. Philip Walther (Universität Wien)
Dr. Andreas Poppe (Austrian Institute of Technology)

funded by Austrian Institute of Technology, Department Digital Safety and Security

## Bachelor Thesis

title *Funktionalintegrale und Brown'sche Bewegung* (*Functional Integrals and Brownian Motion*)

supervisor Univ.-Prof. Dr. Jakob Yngvason

as part of Course *Praktikum Theoretische Physik*

## Scientific Work Experience

since 2014 **Quantum optics lab research**, *Austrian Institute of Technology*, Vienna.
Entangled photon sources
Single photon spectroscopy
Optical metro-access networks
Research on non-linear optics and pure quantum state generation